Dynamics of Cell Movement and Tissue Motion in Gastrulation and Micromass Cell Culture

Cheng Cui

Submitted to the faculty of the University Graduate School
in partial fulfillment of the requirements
for the degree of
Doctor of Philosophy
in the Department of Physics
Indiana University
July, 2005

Accepted by the Graduate Faculty, Indiana University, in partial fulfillment of the requirements for the degree of Doctor of Philosophy.

James A. Glazier, Ph.D.

Sima Setayeshgar, Ph.D.

Santiago D. Schnell, Ph.D.

Joseph B. Duffy, Ph.D.

July, 2005

To my parents, sister, Yupeng and my son, Runzhe.

Acknowledgements

This dissertation is by far the most significant scientific accomplishment in my life and it would have been impossible without the people who supported me and believed in me.

Most of all I would like to thank my advisor, Prof. James A. Glazier, not only for his guidance of my research work, but also for his patience and kindness.

Special thanks to Prof. Cornelis Weijer at the Wellcome Trust Biocenter, Dundee, Scotland and Prof. Stuart A. Newman at New York Medical College, who provided opportunities for me to work in their labs.

I would also like to thank all our group members, especially Dr. Roeland Merks, and Mr. Kun Chen for providing help with Monte Carlo simulations and Dr. Tilmann Glimm at Emory University for helpful discussions on data analysis of cell movement in micromass cell culture.

Finally, I thank my wife, Yupeng Liu, who gives me support all the time, and my son, Runzhe, who brings me happiness and inspiration.

This work has been supported in part by grants NSF IBN-0083653 and NASA NAG 2-1619.

Abstract

This dissertation studies the dynamics of cell and tissue motion in two biological situations: early gastrulation of the chick embryo and chondrogenic condensation in micromass culture of embryonic chick limb cells.

Analysis of epiblast cell movement during primitive-streak formation showed that epiblast cells move in two large-scale, counter-rotating streams that merge at the site of streak formation. Within each stream, epiblast cells move little relative to their neighbors. Our studies with the cell-cycle inhibitor *aphidicolin* have shown that cell division enables the epiblast to expand, causes the circular flow patterns and drives streak formation. Application of the Rho-kinase inhibitor Y27632 did not inhibit streak initiation but resulted in abnormal streak extension, suggesting that the initial stages of streak formation do not rely on signaling through the planar-polarity pathway.

Analysis of mesenchymal cell movement during chondrogenic condensation in micromass culture of embryonic chick limb cells using phase-contrast microscopy revealed that cells in the condensation centers have small contact areas with their substrate and move faster, while cells outside of the condensation centers have larger substrate contact areas and move slower. Fitting cells with ellipses,

which show the elongation directions of the cells, showed no correlation between the cells' directions of elongation and movement, which indicates that cells in micromass culture move passively, being pushed around and deformed by neighboring cells. We propose that changes in the interaction between cells and their substrate because of ECM deposition underneath the cells cause the speed and contact-area changes in the condensation centers.

Contents

Acknowledgements v

Abstract vi

1 Introduction 1

1.1 Embryogenesis and Pattern Formation 1

1.2 Genetic and Generic Mechanisms 2

1.3 The Chick Embryo as an Experimental Model 3

1.4 Dynamics of Cell and Tissue Motion During Morphogenesis: The Main Themes and Results of this Dissertation 7

2 Cell and Tissue Movement During Gastrulation of Chick Embryos 11

2.1 Primitive-Streak Formation During Chick Embryo Gastrulation: An Introduction 12

2.1.1 Blastoderm, Specification of Dorso-Ventral and Antero-Posterior Axes and Hypoblast Formation 12

2.1.2 The Posterior Marginal Zone and Induction of the Primitive Streak 14

2.1.3 Elongation and Regression of the Primitive Streak 17
2.2 Materials and Methods 20
2.2.1 Embryo Culturing Technique 20
2.2.2 Cell Tracking Using the Carbocyanine Dye, DiI and Time-Lapse Microscopy 21
2.2.3 Application of Aphidicolin and the Rho-kinase Inhibitor Y27632 24
2.2.4 Removal and Rotation of the Hypoblast 24
2.2.5 High Magnification Imaging of Cultured Embryos 25
2.2.6 8'Bromo-deoxy-Uridine Incorporation and Immuno-Histochemistry 25
2.2.7 Image Analysis 27
2.3 Results 27
2.3.1 Tissue-Movement Patterns During Streak Formation . . 28
2.3.2 Tissue-Movement Patterns During Streak Extension . . . 28
2.3.3 Optical-Flow Detection of Movement Patterns in Bright-field Images 30
2.3.4 Streak Formation and Elongation Require Active Motion of Cells Both at the Base and Tip of the Streak 32
2.3.5 The Role of Cell Division in Streak Formation 35
2.3.6 Removal and Rotation of the Hypoblast 41
2.4 Discussion 41
2.4.1 Streak Formation Involves Large-Scale, Active Tissue Flows 41
2.4.2 Cell Division is Necessary for, but Does Not Drive, Streak Formation 45
2.4.3 A More 'Complete' Fate Map of Cells in the Epiblast . . 46

2.4.4 Possible Mechanisms Underlying Streak Formation . . . 48
2.5 Acknowledgement . . . 50

3 Cell Movement in Micromass Cell-Culture 51

3.1 Limb Development in the Chick Embryo and Its Relation to Micromass Culture: An Introduction . . . 51
3.1.1 Embryonic Chick Limb Development . . . 51
3.1.2 Micromass Cell-Culture and *in vitro* Study of Cartilage Condensation During Embryonic Limb Development . . . 57
3.2 Materials and Methods . . . 64
3.2.1 Cell-Culture . . . 64
3.2.2 Microscopy and Image Acquisition . . . 65
3.2.3 Image Processing and Data Analysis . . . 66
3.2.4 Flatness of Distributions . . . 68
3.3 Experimental Results . . . 69
3.3.1 Cell Movement and Deformation . . . 69
3.3.2 Decrease in Cell-Substrate Contact Area . . . 69
3.3.3 Bulk Cell Movement . . . 71
3.3.4 Cells Velocities and Orientations . . . 71
3.3.5 Cell Deformation, Cell Movement and Elongation Direction 77
3.3.6 Auto-Correlation of Velocities . . . 82
3.3.7 Temporal Angular Correlation . . . 82
3.3.8 Spatial Velocity Correlation . . . 84
3.3.9 Condensation Centers . . . 86
3.3.10 Relative Cell Velocities . . . 89

3.3.11 Cell Velocities 92
3.3.12 Condensation-Center Radius 92
3.3.13 Changes in Cell Diffusion Rates 96
3.3.14 Directed Cell Movement 98
3.4 Discussion 101
3.4.1 Cell Behavior Changes in Time 101
3.4.2 Possible Mechanisms 103
3.4.3 Cell Diffusion and Haptotaxis 104

4 Whole-Mount Culture of Chick Embryos Between HH Stages 13 and 22 **107**

4.1 Introduction 108
4.2 Experimental Procedures and Results 108
4.2.1 Protocol for Preparing Agar-Albumen Culture Dishes . . 110
4.2.2 Protocol for Preparing Cultured Chick Embryos 112
4.3 Discussion 115
4.3.1 Advantages of the EEC Method Compared to Other Methods 115
4.3.2 Larger Filter-Paper Rings Allow Cultured Embryos to Live Longer 116
4.3.3 Is Dorsal Side Up, or Ventral Side Up Better? 117
4.4 Conclusion 119

5 Transplantation of Embryonic Chick Limbs **120**

5.1 Introduction 120
5.2 Experimental Protocols for Limb Grafting 121

5.2.1 Prepare Cultured Chick Embryos as Hosts 121
5.2.2 Explant Chick Limb Buds from Donor Embryos and Graft to the Host's Flank 121
5.2.3 Advantages of Grafting Chick Limb Buds to the Flanks of Earlier-Stage Hosts 123
5.3 Application: Chick Limb Buds Grafted to Both Flanks of a Host 124
5.3.1 Motivation and Introduction 124
5.3.2 Transplantation of Limbs with AER Removed 127
5.4 Conclusion 128

6 Conclusions and Suggestions for Future Work 129
6.1 Gastrulation 130
6.1.1 Initiation of the Primitive Streak 130
6.1.2 Primitive-Streak Elongation 130
6.1.3 Individual Cell Movement in the Epiblast 131
6.2 Embryonic Limb Development 132
6.3 *In vivo* Electroporation 133

A Experimental Protocols 137
A.1 Chick Whole-Embryo Culture Using a Filter-Paper Carrier . . . 137
A.1.1 Protocol for Preparing Agar-Albumen Culture Dishes . . 137
A.1.2 Protocol for Preparing EC Cultures 138
A.2 Protocol for Whole-Mount BrdU Incorporation 140
A.2.1 Solutions 141
A.2.2 Procedures 143
A.2.3 Special Notes 145

A.3 Protocol for Micromass Chick Limb Cell-Cultures 146
A.3.1 Materials and Instruments 146
A.3.2 Media 147
A.3.3 Procedures 149
A.3.4 Special Notes 152

References **154**

List of Figures

1.1 Life cycle of the chicken. 8

2.1 Blastoderm development of chick embryo. 13

2.2 Three models for the origin of the primitive streak. 15

2.3 EC culture of a developing chick embryo at different times. . . . 22

2.4 A typical chick embryo injected with DiI. 23

2.5 The experimental setup for incubating embryo cultures on the microscope stage. 26

2.6 Diagram of the metal chamber holding the embryo culture for high-magnification observations. 26

2.7 Tracks of tissue movement in a chick embryo cultured from HH stage 1. 29

2.8 Tracks of tissue movement in an embryo beginning at HH stage 3. 31

2.9 Velocity-vector fields of cells in the embryo during primitive-streak formation. 33

2.10 Velocity-vector fields of cells in a chick embryo during primitive-streak elongation. 34

2.11 Inhibition of streak extension by local inhibition of actin polymerization. 36

2.12 Spatial distribution of cells in S phase during early gastrulation. 39
2.13 Inhibition of cell movement in the presence of aphidicolin. . . . 40
2.14 Embryo with hypoblast removed. 42
2.15 Embryos with hypoblast rotated or removed. 43
3.1 Cross-section of the embryonic chick hind-limb field at two developmental stages. 53
3.2 A molecular model of embryonic chick limb initiation. 54
3.3 Embryonic limb development in chick. 55
3.4 Progress-zone model. 60
3.5 Two models of developing limbs. 61
3.6 Sonic hedgehog is expressed at the posterior margin of the limb bud. 62
3.7 A-P axis specification of the embryonic chick limb: a morphogen model. 63
3.8 Digitization of images of a chick-leg embryonic mesenchymal micromass cell-culture. 67
3.9 Cell fitting with an ellipse. 70
3.10 Trajectories of 17 cells over 8 hours in micromass cell-culture. . 70
3.11 Average surface area of cells as a function of time. 72
3.12 Trajectory of the average center-of-mass of all analyzed cells in image set II. 73
3.13 Average speed of cell movement at different times in image set II. 74
3.14 Distribution of cell movement directions. 75
3.15 Cumulative probability distribution (*CPD*) of cell movement directions. 76

3.16 Average cell eccentricities at different times in image set II. . . . 78
3.17 Distribution of eccentricities of fitting ellipses for 92 cells in 25 images from image set II. 79
3.18 Histogram of the angles between the eccentricity vectors $\vec{e}$ and the velocity vectors $\vec{v}$. 80
3.19 Cumulative probability distribution (*CPD*) of angles between the eccentricity vectors $\vec{e}$ and the velocity vectors $\vec{v}$. 81
3.20 Temporal auto-correlation of the velocity *vs.* time interval t for cells in image set I. 83
3.21 Temporal angular correlation of the velocity *vs.* time interval t for cells in image set I. 85
3.22 Spatial auto-correlation of velocities. 87
3.23 Exponential fit of spatial correlation averaged over frames 1 through 24. 88
3.24 Color map of average cell surface area for cells in image set II. . 90
3.25 Color map of average cell speed for cells in image set II. 91
3.26 Average speed of cells (left y axis) and number of cells per bin (right y axis) as a function of average cell surface area. 93
3.27 Histograms of speeds. 94
3.28 Concentric bands centered at the center of condensation (330, 200) with a band width of 50 pixels. 95
3.29 Cell flux towards the center of condensation and average cell speed as a function of distance from the center of condensation. 97
3.30 Mean-squared displacement between 0 and 240 minutes. 99
3.31 Mean-squared displacement between 240 and 480 minutes. . . . 100

3.32 Kinetic ratio ($<\vec{v}>^2$ / $<\vec{v}^2>$) in micromass cell-culture of embryonic (HH stage 25) chick-leg mesenchymal cells. 102
3.33 Mean-squared displacement of all cells, cells inside the condensation center all the time and cells outside the condensation center all the time. 106
4.1 Extended EC (*EEC*) culture of a chick embryo. 109
4.2 Extended EC culture of chick embryo with larger filter-paper ring. 118
5.1 Flank transplantation of an embryonic chick limb. 125
5.2 Two limbs from donors at HH stage 20 transplanted to a host at HH stage 15. 126
6.1 *In vivo* electroporation of a quail embryo. 134
A.1 Filter paper ring and 35 mm dish with substrate. 140
A.2 Embryo culture dishes are kept in a 245 x 245 mm Bio-Assay square dish with moistened tissue lining the base. 140

List of Tables

3.1 The two digitized image sets of cell movements during micromass culture of embryonic (HH stage 25) chick-leg mesenchymal cells. 68

3.2 Counts of cells moving into the FOV for image set II. 71

Chapter 1

Introduction

1.1 Embryogenesis and Pattern Formation

One of the major characteristics of living organisms is the high degree of order of their constituent parts, which takes form especially during early stages of embryonic development. Embryo development in all species follows the same pattern: first the developmental axes are laid down, then cells differentiate to perform different functions at different places. During this differentiation stage, *pattern*, the particular arrangement of organells, cells, tissues, or organs, emerges and is faithfully repeated in each individual. Developmental biology seeks to understand the mechanisms guiding the formation of patterns during embryogenesis.

1.2 Genetic and Generic Mechanisms

The ability of each individual species to maintain its developmental patterns comes from the replication from one generation to the next of genetic information encoded in DNA, which provides the blueprint for these patterns. Since the discovery of the double-stranded structure of DNA in 1953 and of how the genetic information duplicates faithfully and passes to offspring, many people have believed that genetic mechanisms fully determine pattern formation during embryonic development. During this period, the study of physical or *generic* principles of pattern formation during embryonic development has lagged behind genomic approaches, despite some remarkable advances, such as the *reaction-diffusion* (*RD*) mechanisms which Turing proposed in 1952 [114], Steinberg's statement of the *differential adhesion hypothesis* (*DAH*) in 1963 [102], Wolpert's *positional information hypothesis* [123] and Keller's studies of convergence and extension [56]. Two reasons may explain this slow progress. First, the study of molecular and genetic mechanisms between 1950-1990 advanced so fast that, by itself, it seemed to promise explanations of the principles of developmental biology. Biologists became so gene-oriented that they concentrated on finding new genes, expression patterns and pathways of particular genes and on the effects of knocking-out and overexpressing genes. The second reason was the pervasive belief that understanding of pattern formation would come from improved information about smaller and smaller parts of whole organisms. People became more interested in investigating sub-cellular-level mechanisms, and neglected mechanisms at cellular or tissue levels.

Only recently (after 1990), have increasing numbers of biologists realized

that *morphogenesis* (changes of form in early embryos) is not merely a sequence of genetic events, but a process in which generic mechanisms play an equally important role, and that meaningful organization and application of knowledge at the molecular level requires understanding general principles at the cellular and tissue levels. Physicists and biologists are now enhancing their cooperation and we are witnessing the establishment of interdisciplinary biology and bioinformatics programs in major universities around the world. Most researchers today, not only physicists and biologists, but those from computer science, bioengineering, information technology and many other fields, share the belief that understanding the principles of developmental biology requires an integrated and cooperative approach, which combines the skills of scientists from all these related fields.

1.3 The Chick Embryo as an Experimental Model

Although people have studied a wide variety of species, for both historical and practical reasons, a relatively small number of organisms provide most of our knowledge about animal development. Sea urchins and frogs were the main animals experimental biologists used at the beginning of the 20th century and *Xenopus* is still in use, because its developing embryos are easy to obtain, sufficiently large and robust enough for experimental manipulations. Among invertebrates, people use the fruit fly *Drosophila* and the nematode worm *Caenorhabditis elegans* as models, because we know a great deal about their developmental genetics and they are easy to modify genetically.

Among vertebrates, people use *Xenopus*, mice, chicks and zebrafish as mod-

els. Each has its own advantages. In the 1980s, the frog *Xenopus laevis* became a very popular model because its large eggs allow direct injection of DNA constructs into the fertilized egg and the embryo does not increase in volume during early stages of development. Most importantly, compared to mouse, which is also a common model, assessing the phenotypic consequences of genetic, chemical, or surgical manipulation of the developing *Xenopus* embryo is quick and easy. Mice are popular models to study gene function during morphogenesis and embryogenesis primarily because of their similarity to humans [87].

Chick embyros, because they are easy to obtain, manipulate and monitor during development, have been popular models for a much longer time (more than 2000 years), since Aristotle opened chicken eggs daily to examine progressive stages of embryogenesis [1]. Interestingly, until well into the 19th century, people used chicken embryos at different stages to support either the theories of preformation (which held that the adult is preformed in miniature from the time of fertilization or even earlier and just grows homogeneously) and epigenesis (which holds that the embryo increases in complexity as it develops). As experimental tools advanced, starting with simple microscopes in the 17th century, chicken embryos provided increasing insights into development. For example, in the 1670s, Malpighi confirmed the theory that arteries and veins connected to each other via capillary vessels. He also discovered the neural groove (neural tube) and somites and that the heart began to beat before blood started to form [109].

The development of techniques to label cells with dyes, to culture chick embryos for long periods and to graft parts of embryos onto different locations in the same or other host embryos, allowed great advances in embryology. An

early landmark advance was Gräper's 1929 discovery using labeled cells and time-lapse movies, of movement during gastrulation [45]. In 1930, 6 years after Spemann's experiments on frog embryos, which identified organizing centers, Waddington showed that the early endoderm (which we now call *hypoblast*) could influence the direction of the primitive streak and that *Hensen's node* (*HN*) is the amniote organizer [109]. Bellairs, in 1953, found that the definitive (gut) endoderm arises from the epiblast through dorso-ventral (*D-V*) cell migration through the primitive streak during gastrulation [6]. Saunders' pioneering work on chick-limb development used grafting and transplantation to define the *zone of polarizing activity* (*ZPA*) and the *apical ectodermal ridge* (*AER*) as important signaling regions directing limb development [93, 94]. In the 1970s the quail-chick chimera technique enabled researchers to follow the migration and differentiation of cell populations in intact embryos [25], which confirmed the migration of neural-crest cells which His discovered in chick embryos in 1868 [109].

Chick embryo experiments have led researchers to propose many major developmental concepts:

Induction: In *induction*, certain pieces of embryonic tissue (called *organizers*) can influence the differentiation of cells or tissues nearby. Induction was first discovered in frog embryos and later confirmed in chick embryos [108].

Regulation: In 1960 Spratt cut a chick embryo at Hamburger & Hamilton (*HH*) stage [49] 1 into several pieces and showed that every fragment with at least 50,000 cells could form its own primitive streak, demonstrating the plasticity of chick embryo development [101].

Left-right asymmetry: Researchers first discovered in chick embryos the set of genes, Activin receptor IIa, Sonic hedgehog (*Shh*), and cNR-1 (related to the mouse gene Nodal) which regulates the left-right asymmetry in vertebrates [69].

Migration of neural-crest cells: Le Douarin first revealed the migration and development of neural-crest cells by grafting quail embryo fragments into chick embryos, allowing tracking of the quail cells [26]. Le Douarin showed that the neural-crest cells migrate from the dorsal edges of the neural tube to give rise to a wide variety of tissues, ranging from pigment cells to the bones of the skull.

Development of somites: The somites give rise to both axial muscles and the muscle-cell precursors which migrate into the limb. Studies using chick embryos showed that oscillating cycles of gene expression precede somite formation [85].

Limb development: Studies on chick embryos have provided much of the knowledge we have on limb development. In 1948 Saunders did the two most important experiments, which identified the developing limb's two organizing centers: he showed that removal of the *AER* resulted in truncation of the developing limb, and that grafting the posterior limb edge, the *ZPA*, onto the anterior of the limb resulted in the development of additional digits [93].

In summary, the main reason for the special role of the chick embryo in pre-1980s developmental biology is that, as a warm-blooded vertebrate, it is a

model for 'higher' animals, while being easier to culture and manipulate than the mouse embryo.

However, from 1980 to 2000, the difficulty of genetically manipulating chick embryos, reduced their attractiveness as models. Most molecular studies were limited to analysis of gene expression and phenotype in normal and manipulated embryos (at different developmental stages), where manipulations included transplantation of organizing tissues, such as *posterior-marginal-zone* (*PMZ*) cells during gastrulation and AER cells in developing chick limbs [93] and introducing beads soaked with different drugs or growth factors [92].

Only recently have four major technical advances revived the role of chick embryos as models and given chick embryos a brighter future in the study of morphogenesis [109]: the introduction of new methods for gain- and loss-of-function and promoter analyses by *in-ovo* electroporation [65], the isolation of embryonic stem (*ES*) cells [83], the development of new methods for producing transgenics, and the sequencing of the chicken genome [52].

1.4 Dynamics of Cell and Tissue Motion During Morphogenesis: The Main Themes and Results of this Dissertation

One of the important characteristics of morphogenesis is dramatic, coordinated cell and tissue movement, which gives rise to patterns and eventually a functional embryo. Our research concentrated on cell movement during early *gastrulation* and complex pattern formation during *limb formation* in developing

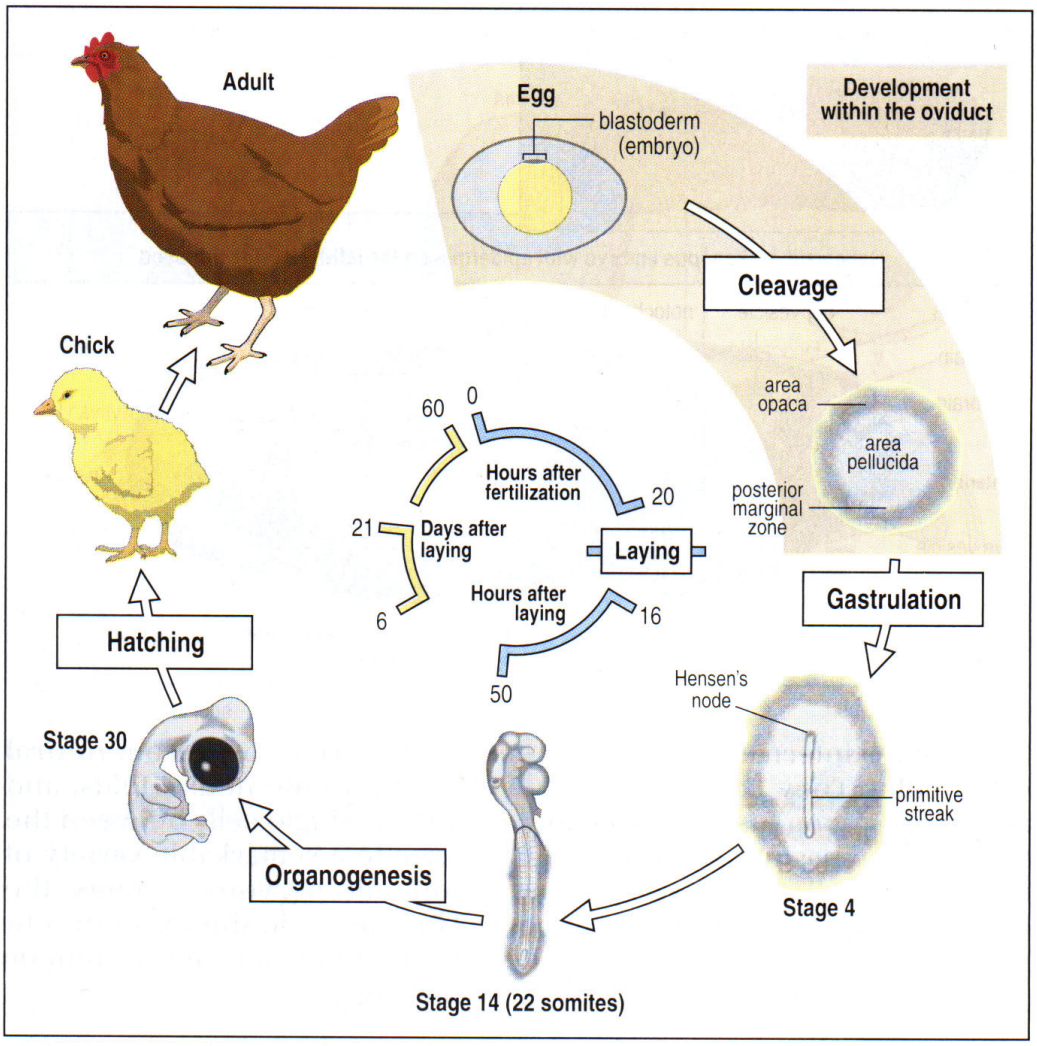

Figure 1.1: Life cycle of the chicken. We discuss cell and tissue movements during gastrulation in chapter 2 and cell movement in micromass cell-cultures of embryonic chick limb-bud cells, which form during organogenesis, in chapter 3. Adapted from figure 2.11 in *Principles of Development, second edition* by Wolpert, 1998 [124].

chick embryos. We then used these experimental results to reveal the underlying generic mechanisms governing the formation of different patterns.

We tried to understand how the primitive streak forms and elongates along the midline of the blastoderm during gastrulation in the chick embryo. In chapter 2, we discuss the patterns of tissue flow underlying the formation of the primitive streak. We analyzed time-lapse sequences of bright-field images to extract the tissue-velocity field and used DiI labeling of small groups of cells to show that epiblast cells move in two large-scale, counter-rotating streams, which merge at the site of streak formation. Despite the large-scale tissue flows, individual cells appear to move little relative to their neighbors. We also found that the streak elongates in both the anterior and posterior directions. We then treated the embryo with two drugs, latrunculin B, which inhibits actin polymerization and aphidicolin, which prevent cells from dividing. We found that local application of latrunculin B at the streak tip immediately terminated anterior extension of the streak tip, but did not prevent posterior elongation of the streak, which therefore must have a different driving mechanism. Inhibition of actin polymerization, and hence active cell migration, at the base of the streak completely inhibited streak formation, implying that movement of cells into the base of the forming streak is crucial for extension. We also found that aphidicolin at concentrations that completely block cell-cycle progression, permits initial streak formation, but arrests development during extension. We then studied cell-division patterns at different developmental stages and found that cells divide at roughly the same rate throughout the epiblast before the primitive streak forms. Division then decreases in the central epiblast and incipient streak and increases at the boundary between the *area pellucida* and

the *area opaca* during elongation. Our analysis suggests that cell division is critical to allow the epiblast to expand in peripheral areas, maintaining the cell-flow pattern that supplies the streak with cells from the lateral epiblast, but that division does not drive the observed tissue flow or streak formation.

We also tried to understand how the cartilage derived from the initially homogeneous mesenchymal cells in the chick limb bud forms the pattern of one piece of cartilage in the upper arm, two pieces of cartilage in the lower arm and three clusters of digital cartilage in the hand (five in humans and mice). Chapter 3 presents studies of cell movement during chondrogenic condensation over a period of 8 hours in a high-density cell-culture of developing chick-limb precartilage mesenchyme, using phase-contrast microscopy and video-based cell tracking. Statistical analysis showed that precartilage cells random walk with a persistence time of less than four minutes. We characterized the size of a condensation center and found that early in the culture period, cells inside the center have smaller surface contact areas with their substrate than cells outside the center. In agreement with predictions of a simple haptotaxis model, inside a condensation, directions of elongation and cell movement are uncorrelated, indicating that cells primarily move passively, being pushed around and deformed by neighboring cells' movements and deformations, while cells just outside the condensation center tend to migrate towards the center. In contrast to a classical haptotaxis model, however, cells within the condensation center move significantly faster than cells outside the center. These results suggest that the cell-extracellular matrix (*ECM*) interaction mediating condensation is highly dynamic.

Chapter 2

Cell and Tissue Movement During Gastrulation of Chick Embryos

During gastrulation, the three germ layers, *ectoderm*, *mesoderm* and *endoderm* develop from the blastula. In chick embryos, gastrulation begins with the induction of the primitive streak, followed by its elongation and regression. During elongation and regression, cells in the epiblast move towards the primitive streak, ingress in a dorso-ventral direction through it, differentiate and form mesoderm and ectoderm. Our research on this subject concentrates on the induction and elongation of the primitive streak and its relationship to coordinated cell movement and division.

2.1 Primitive-Streak Formation During Chick Embryo Gastrulation: An Introduction

2.1.1 Blastoderm, Specification of Dorso-Ventral and Antero-Posterior Axes and Hypoblast Formation

The cleavage of the chick embryo happens when the egg is still in the hen's oviduct. During cleavage, the embryonic cells divide at a high rate into several thousand cells. These cells form a single-cell layer of *blastodisc*, called *blastoderm* on top of the yolk (figure 2.1). At the center of the blastoderm is the *area pellucida*, while the margin of the *area pellucida* is the *area opaca*, which appears opaque because of contact with the yolk (page 36-37 in [124]).

The contact between the blastoderm and the yolk specifies the *dorso-ventral* (*D-V*) axis, where the side of the blastoderm facing the yolk is the *ventral* side. Inverting the pH gradient or membrane potential across the blastoderm can reverse some characteristics of the chick blastoderm along the D-V axis [104]. While in the oviduct, the yolk contacting the cell blastoderm has lower density and the blastoderm sits on top of the yolk. After the egg shell forms, the egg rotates so that the blastoderm and the yolk tilt in the gravitational field, with that part of the blastoderm contacting the yolk which has lowest density still uppermost. This part of the blastoderm will become the posterior end of the future embryo [12, 63, 124].

Figure 2.1 shows that a second layer of cells called the *hypoblast*, forms underneath the epiblast. Additional hypoblast cells move to the posterior at prestreak stages X-XII (Eyal-Giladi and Kochav staging [31]), making the posterior region

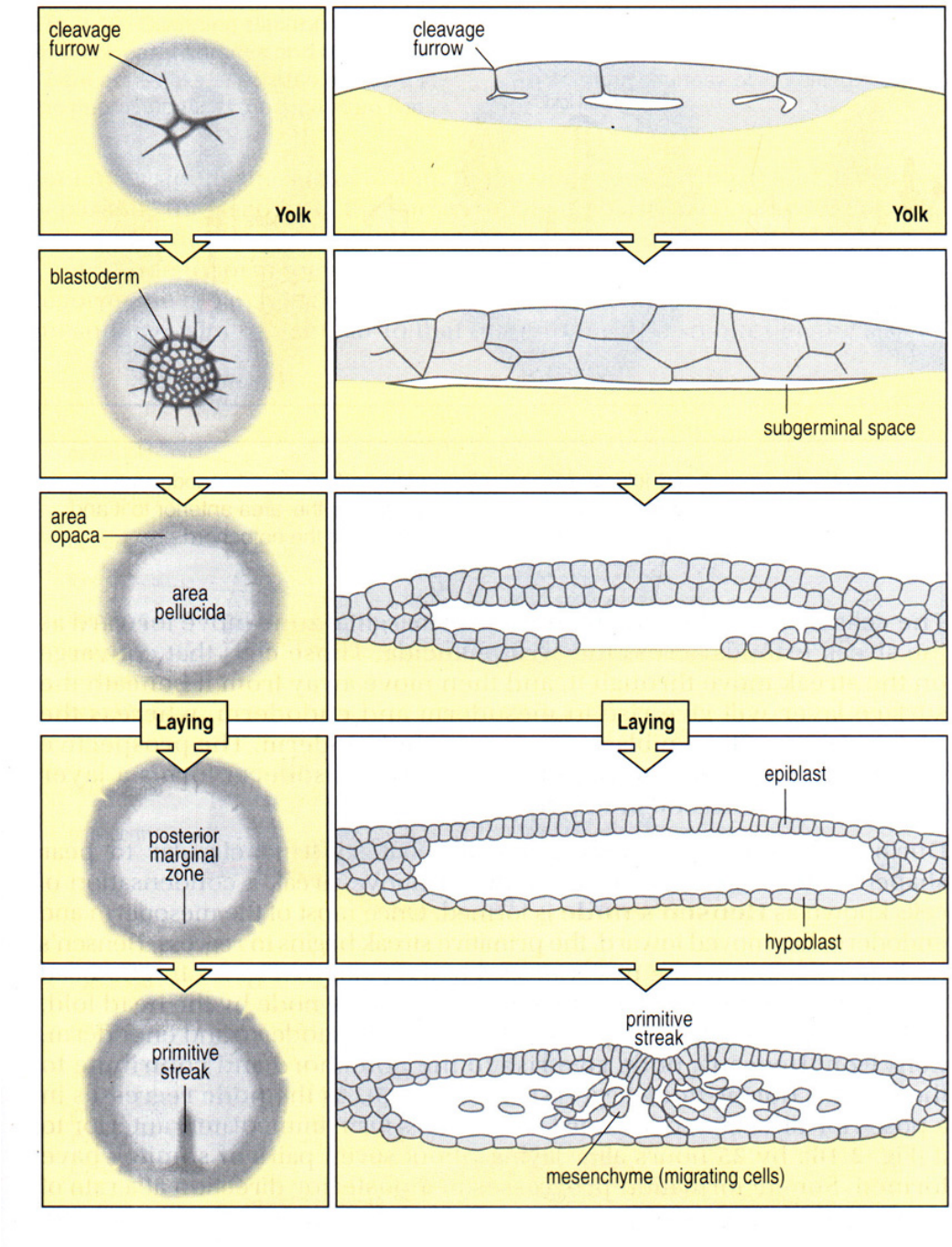

Figure 2.1: Blastoderm development in the chick embryo. Adapted from figure 2.12 in *Principles of Development, second edition* by Wolpert, 1998 [124].

of the blastoderm darker under bright-field microscopy. Fate mapping studies have shown that only cells in the epiblast, not those in the hypoblast, contribute to the chick embryo. However, the hypoblast is important in initiation of the primitive streak [10, 9] and activation of epiblast gene expression [62].

2.1.2 The Posterior Marginal Zone and Induction of the Primitive Streak

One fascinating feature of embryo development in amniotes, such as reptiles, birds and mammals, is the formation of the primitive streak, which serves as the initiation site for gastrulation. A small population of cells in a special region of the posterior end of the marginal zone, the *posterior marginal zone* (*PMZ*), which separates the *area pellucida* from the *area opaca*, can induce epiblast cells anterior to this special population to form a primitive streak. PMZ cells express several proteins, including Activin [76], Vg1 [10, 96, 97], Wnt8c [53, 96, 97], and Chordin [110], which mediate their inducing activity. Before gastrulation begins, transplanting the PMZ to another region in the marginal zone can induce an ectopic primitive streak. Implantation of a COS-cell aggregate (a cell line derived from the African green monkey and used for transfection and cloning experiments) overexpressing proteins typical of the PMZ has the same effect [99].

Even though the molecular mechanisms by which these factors induce epiblast cells to differentiate into primitive-streak precursor cells are still not clear, people have proposed three models (figure 2.2) for the origins of the cells that give rise to the initial primitive streak.

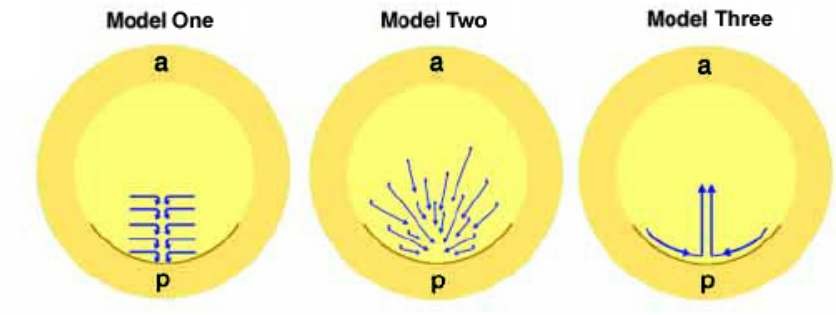

Figure 2.2: Three models for the origins of the cells that give rise to the initial primitive streak. **a** and **p** denote anterior and posterior ends of the blastoderm (yellow disk) respectively. The arc represents Koller's sickle. The light yellow region is the *area pellucida* and the dark yellow region is the *area opaca*. Model One - generalized epiblast migration [5]. Model Two - Stern and Canning model [105]. Model Three - Eyal-Giladi model [32]. See text for details on these three models. Adapted from figure 1 of [119].

In the first model, epiblast cells migrate from lateral regions towards the midline, where they ingress to form the primitive streak [5]. In 1990, based on experiments labeling cells which express HNK-1, an immunoreactive epitope commonly present in both primitive-streak cells and a subpopulation of the epiblast, Stern and Canning proposed a second model, in which some sparsely-distributed cells in the epiblast are predetermined to become primitive-streak cells [105]. These special epiblast cells delaminate from the epiblast layer into the cavity underneath and migrate towards the posterior end of the blastoderm in response to the chemo-attractant factors the cells in the PMZ secrete [105, 106]. Eyal-Giladi *et al.* [32] used grafting of fluorescent-dye-marked blastodermal segments, and Wei and Mikawa [119] used retroviral and DiI cell tracking to test Stern's model. Both found that the precursor cells of the initial primitive streak reside in the posterior region of the epiblast. Eyal-Giladi proposed a third model, that factors that cells in the PMZ secrete act directly on adjacent epiblast cells and induce them to form the initial primitive streak. This model differs from Stern and Canning's model of primitive-streak initiation, in that only the cells in the posterior region, not sparsely-distributed cells throughout the epiblast, contribute to the primitive streak.

All these investigators used fate mapping techniques, in which they labeled cells at particular positions with fluorescent tags to locate the primitive-streak precursor cells, then looked for these tagged cells after a period of incubation, normally 4-8 hours. The shortcoming of this method is that the investigators could not monitor cell or tissue movement during primitive-streak formation 'dynamically' (in real time). Another constraint on their experiments was that each of their fate-mapping regions was only a portion of the epiblast, because

they could only follow a single group of cells per experiment (or at most two groups of cells using double labeling).

2.1.3 Elongation and Regression of the Primitive Streak

The primitive-streak precursor cells accumulate in the posterior region of the epiblast, anterior to the PMZ, forming a triangular shape. After a few hours of incubation, the primitive streak changes its shape from a triangle to a rod extending from the posterior margin of the epiblast anteriorly along the midline of the epiblast. The primitive streak continues to elongate anteriorly until it reaches a length of 70-80% of the extension of the epiblast, after which it starts to regress. In the mean time, epiblast cells lateral to the primitive streak migrate towards the streak, ingress through it and differentiate into mesoderm and endoderm cells. After the primitive streak regresses back to the posterior margin all three germ layers, ectoderm (epiblast), mesoderm and endoderm, have taken their correct relative positions and the embryo is ready for the next stage of development.

The elongation of the primitive streak of the amniote embryo mimics the antero-posterior (A-P) body-axis elongation in nonamniotes, particular that of amphibian gastrulation. In amphibian gastrulation the *convergence and extension* mechanism, in which lateral cells intercalate towards the midline of the embryo, largely accomplishes the A-P elongation of the body axis. Since cells do not divide and cell volume does not change [56, 57, 122], this body-axis elongation of the amphibian embryo results in a longer but narrower configuration. However, in gastrulation of chick embryos and other amniotes, the primi-

tive streak not only extends anteriorly, but tissue volume increases several-fold. The composition of the primitive streak is also dynamic, since epiblast cells continue to migrate towards the streak and ingress through it. Studies of cell division have shown that cells in both the lateral epiblast and the primitive streak actively proliferate with a mitotic index of about 2-4 hours [91, 119]. The differences between the elongation of the primitive streak in chick embryos and the elongation of the A-P body axis in amphibian embryos suggest that their elongation mechanisms may differ.

By fate tracing cells in a fluorescently-labeled graft of the latero-posterior region of the epiblast into unlabeled epiblast, Eyal-Giladi *et al.* found that precursor cells first migrate towards the midline, then move anteriorly towards the center of the embryonic disc [32]. However, we still know neither why the cells move in this pattern, nor what forces drive the cell and tissue movement. Cells in the PMZ might secrete chemoattractant factors to attract neighboring cells to move towards the midline. Later, the PMZ cells might send different, chemorepulsive factors, or the streak-precursor cells might differentiate and react chemorepulsively to the originally chemoattractant factors. Either mechanism could induce the streak-precursor cells' anterior movement. Even though chemotactic factors have not been identified in early stages of primitive-streak morphogenesis, such factors (FGF4 and FGF8) do induce positive and negative chemotaxis, controlling cell movement in later stages of chick-embryo gastrulation [125]. Alternatively, the force driving cell migration might come from other regions of the epiblast, such as the local differences in proliferation rates in gastrulating rabbit embryos [115]. If cells in one region of the epiblast divide faster than cells in surrounding regions and offspring cells grow to normal cell

size, in order to maintain the single cell layer of the epiblast during gastrulation, the cells in this region will tend to expand laterally, pushing cells in surrounding regions. The epiblast-cell layer, as a continuous sheet, transmits the pushing force to other regions in the epiblast far from the region where cells divide at a higher rate.

Wei *et al.* [119] and Lawson *et al.* [68] proposed another model for the extension of the primitive streak. Lawson *et al.* found that DiI-labeled streak-precursor cells in regions lateral to the streak gave rise to arrays of labeled cells that extended along the primitive streak in later stages (HH stages 4 to 5), implying that cell intercalate. Wei *et al.* investigated cell shapes by staining cells' actin-containing adherens belts with phalloidin, and measured the orientations of the cell-division cleavage planes by looking at the orientation of DAPI-stained metaphase chromosome plates. They found no apparent elongation of cell shapes along the A-P axis in any area of the blastodisc (including the primitive streak) but the primitive-streak cells were smaller than non-primitive-streak epiblast cells. They also found that about 50% of metaphase cells in the primitive streak had their plane of cell division perpendicular to the A-P axis, compared to less than 20% of non-primitive-streak epiblast cells. They proposed that oriented cell division in the primitive streak caused its elongation. Concha *et al.* [16] and Gong *et al.* [43] have made similar observations of preferred orientations of cell-division cleavage planes during zebrafish-embryo gastrulation. Together, these studies show that the formation and elongation of the primitive streak involves cell intercalation, oriented cell division and active cell proliferation.

This chapter describes our experiments on gastrulating chick embryos, which

quantitatively characterized cell and tissue movement in the epiblast using specialized image-processing techniques to extract local, flow-velocity fields from time-lapse sequences of brightfield images of early chick development. We also tracked several small groups of DiI-labeled cells in the epiblast during streak development. These measurements confirmed and extended earlier observations of large-scale, circular tissue flows in the epiblast [45]. An analysis of cell-division patterns showed that cycling cells distribute more or less randomly throughout the early epiblast, but later localize to the boundary region (everywhere in the interface region) between the *area pellucida* and *area opaca*, suggesting that the cell-division pattern could affect local cell displacements. Arresting cells in S phase by applying the DNA-polymerase inhibitor aphidicolin caused severe developmental defects, but did not inhibit the induction of the primitive streak. Our work (in this chapter) suggests that cell division is important to the elongation of the primitive streak, but that the induction of the primitive streak does not require cell division.

2.2 Materials and Methods

2.2.1 Embryo Culturing Technique

We incubated fertilized white Leghorn eggs (High Sex × Rhode Island Red; Winter Farm, Thirplow, Herts, UK) at 37°C for 0-8 hours to obtain embryos between Eyal-Giladi and Kochav stage X and HH stage 1 [31, 49]. We cultured the embryos using the EC culture technique [13] described in section A.1. We usually cultured the embryos ventral side up on an agar-albumen substrate in

35 mm Petri dishes, because we took images using an inverted microscope. Figure 2.3 shows pictures of such an embryo (cultured at HH stage 2) 22, 31, 51 and 71 hours after initiation of culture.

After the primitive streak forms, the embryo blastoderm seems to adhere to the vitelline membrane better than in younger embryos. The problem with younger embryos (eggs incubated less than 6 hours) is that the blastoderm slips off the vitelline membrane when washing the yolk off the embryo with simple saline (a step in the protocol, section A.1). So washing requires great care.

Extra yolk cells can cause problems during DiI injection and imaging. Using fine-tip forceps we removed any extra floating yolk cells on top of the *area pellucida* to improve our view of the *area pellucida* when injecting DiI and imaging.

2.2.2 Cell Tracking Using the Carbocyanine Dye, DiI and Time-Lapse Microscopy

We used the carbocyanine dye 1,1'-dioctadecyl-3,3,3',3'-tetramethyl indocarbocyanine perchlorate (Molecular Probes) (*DiI*) to label small groups of cells. We diluted a 2.5% stock of DiI in ethanol 1:10 in 0.3M sucrose at 45°C and backloaded the solution into a micropipette made by pulling a 1 mm glass capillary in a vertical micropipette puller (Sutter P-30). We then injected the diluted DiI solution into the epiblast layer at different locations in the embryo by inserting the pipette tip into the epiblast and applying air pressure to the micropipette. Figure 2.4 shows a typical embryo after injection, with the groups of labeled cells shown as green dots. Normally each labeled group had 10-30 cells.

We put the culture into a warm (37°C), humid, black chamber installed on

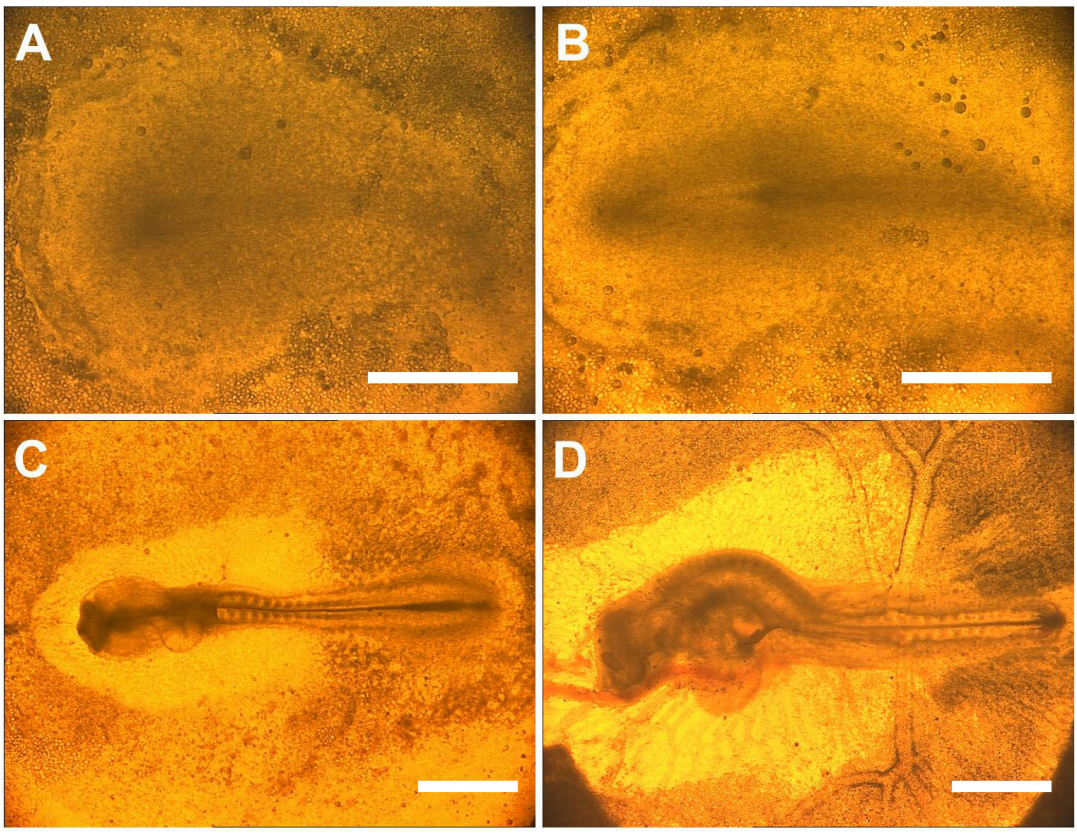

Figure 2.3: Images of a developing chick embryo at different times during EC culture. A) 22 hours, B) 31 hours, C) 51 hours and D) 71 hours after initiation of culture. The embryo was at HH stage 2 at the beginning of culture. The white scale bars in all four panels represent 1 mm. The anterior direction of the embryo is to the left in each panel.

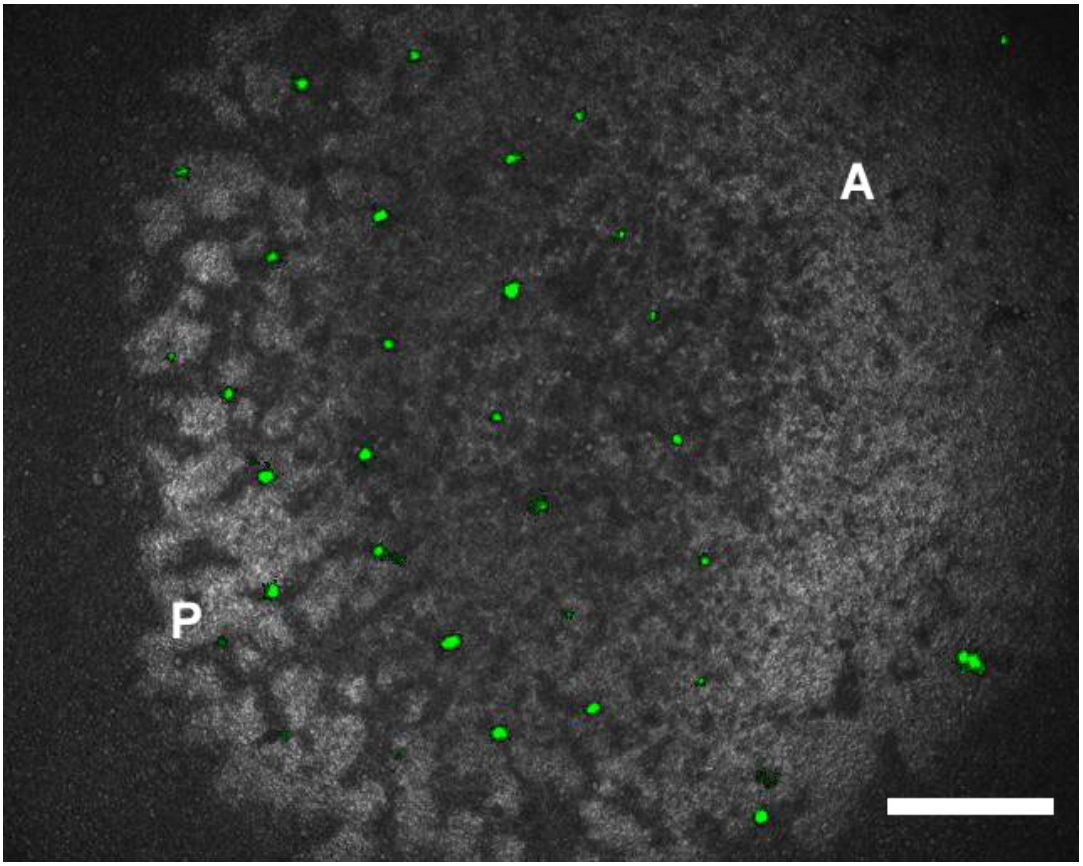

Figure 2.4: A typical chick embryo injected with DiI at different locations (shown as green dots) of the *area pellucida*. Respectively, "A" and "P" represent the anterior and posterior boundaries of the *area pellucida*, the light region in the center. The posterior region of the *area pellucida* is darker than the anterior region of the *area pellucida* because more hypoblast cells are present in the posterior region. The white scale bar represents 500 μm.

the stage of an inverted microscope (Zeiss Axiovert 135TV) and incubated it for 12-15 hours (figure 2.5 shows the experimental setup). At the same time, we took both fluorescent and brightfield images using a CCD camera (Hamamatsu 4770) every 4 minutes and then processed and combined them into continuous movies using Matlab and QuickTime.

2.2.3 Application of Aphidicolin and the Rho-kinase Inhibitor Y27632

We applied solutions of aphidicolin (to block cell division) and Rho-kinase inhibitor Y27632 (to block the Wnt-mediated planar-polarity signaling pathway and convergent extension [74, 118]) of different concentrations (10 μM, 50 μM and 100 μM) to the top of the cultured chick embryos (with ventral side up in culture) after DiI injection. As a control, we treated other embryos with the same volume of PBS. We recorded both brightfield and fluorescent movies of the aphidicolin-treated embryos (see section 2.2.2) and processed the images to calculate the cell trajectories (see sections 2.3.1 through 2.3.3).

2.2.4 Removal and Rotation of the Hypoblast

We incubated fertile eggs for 8-20 hours and cultured the embryos in Petri dishes using the EC culturing technique we describe in section A.1. We removed the hypoblast layer in two ways. When the embryo was young (incubated around 10 hours), its hypoblast layer was loose and easy to break apart. Using a hair loop, or simply forceps, we could break and remove the hypoblast. When the embryo was older (incubated more than 20 hours), its hypoblast layer was stiffer and

remained a single sheet when removed. We used a tungsten needle fixed to a holder and moved the cultured embryo under the dissecting microscope so that the tungsten needle cut the connecting region between the hypoblast and the *area opaca*. We then removed the whole sheet of hypoblast using forceps. We injected DiI into the epiblast layer of some embryos with the hypoblast layer removed and recorded both brightfield and fluorescent images.

To rotate the hypoblast layer, we incubated eggs for more than 15 hours and cultured the embryos in EC cultures. We cut the hypoblast layers using the method we described above. However, instead of removing the hypoblast layer from the embryos, we used forceps to rotate them by a certain angle (normally 90° or 180°) and replace them on the embryos. We then put the embryo cultures back in the incubator and observed the embryos' development.

2.2.5 High Magnification Imaging of Cultured Embryos

When observing cell movements at high magnification, the objective lens must be very close to the cultured embryo because of the short working distance of the high magnification 40x objective lens. We used a specially-constructed metal chamber to culture the embryo, as figure 2.6 illustrates.

2.2.6 8'Bromo-deoxy-Uridine Incorporation and Immuno-Histochemistry

We incubated eggs for 8 hours at 38°C to HH stage 1. We transferred the embryos to EC cultures and incubated them with 100 μl of 10 μM 8'Bromo-

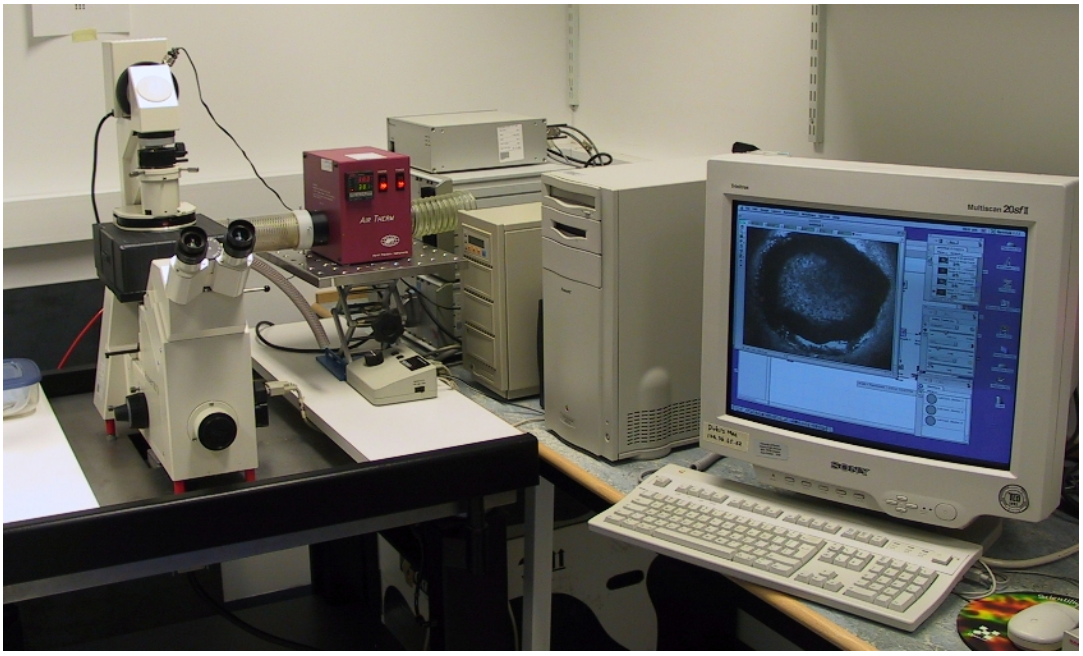

Figure 2.5: The experimental setup for incubating the chick-embryo cultures on the microscope stage.

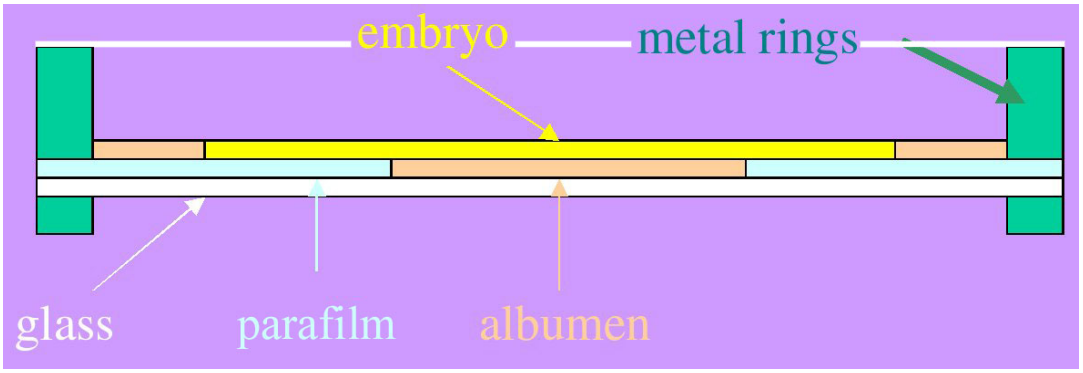

Figure 2.6: Diagram of the metal chamber holding the embryo culture for high-magnification observations. The embryo sits on top of a thin layer of albumen over a coverglass so that the objective lens can approach close to the embryo from below. The top cover of the metal chamber is a removable plastic Petri-dish lid. The diameter of the metal chamber is about 35 mm.

deoxy-Uridine (*BrdU*[1]) in PBS for 2 hours [119]. To block S-phase progression, we treated the embryos with aphidicolin (20 μl of 10 μM solution, or 10 μl of 100 μM solution). We followed the protocol in section A.2 to stain for BrdU incorporation. Finally, we mounted the stained embryos on slides in 50 mM TRIS/HCl (pH 7.5) containing 80% glycerine.

2.2.7 Image Analysis

We calculated cell trajectories from the information in successive time-lapse fluorescent images using custom-written Matlab programs. We extracted the velocity-vector fields using a dedicated C++ program, which calculates the information flow for every pixel in the image and displays it in various ways [98].

2.3 Results

To analyze tissue movements during streak formation quantitatively we processed time series of brightfield images of developing chick embryos in EC culture to obtain velocity-vector fields for the entire *area pellucida*. We combined these measurements with DiI labeling and tracking of small groups of cells in the *area pellucida*. We then used tracking algorithms (comparing a small block in one frame of one image to blocks in a larger search region in the next frame of the image using spatial correlations) to visualize and measure the movement of these cells before and during primitive-streak formation and extension.

[1] PHarMingen Cat. No. 2420KC.

2.3.1 Tissue-Movement Patterns During Streak Formation

We injected DiI to label and track small groups of cells at multiple locations in each embryo. In experiments starting at HH stage 1 or younger, a few hours before the primitive streak became visible as an optically dense structure (figure 2.7), these labeled groups of cells revealed two large-scale, counter-rotating tissue flows in the epiblast, which merged at the site where the primitive streak was going to form.

As panel (A) of figure 2.7 shows, two relatively still areas that did not coincide with any particular morphological structures or known cell types formed the centers of both counter-rotating flows. Our DiI labeling experiments showed little relative cell movement, despite large-scale cell displacement: the cells within each labeled group stayed close together. Closer inspection of the groups of labeled cells revealed that cells from individual groups split into several closely-spaced smaller subunits, but we could not determine whether these splits were due to adjacent cells moving apart or cells dividing, or both.

2.3.2 Tissue-Movement Patterns During Streak Extension

Using the same method (DiI labeling and tracking), we investigated how cells and tissues move during streak extension. Our experiments showed that once the streak formed, the *area-pellucida* cells laterally adjacent to the primitive streak moved towards the midline in a direction perpendicular to the streak. Figure 2.8 shows that after merging into the primitive streak, these cells then

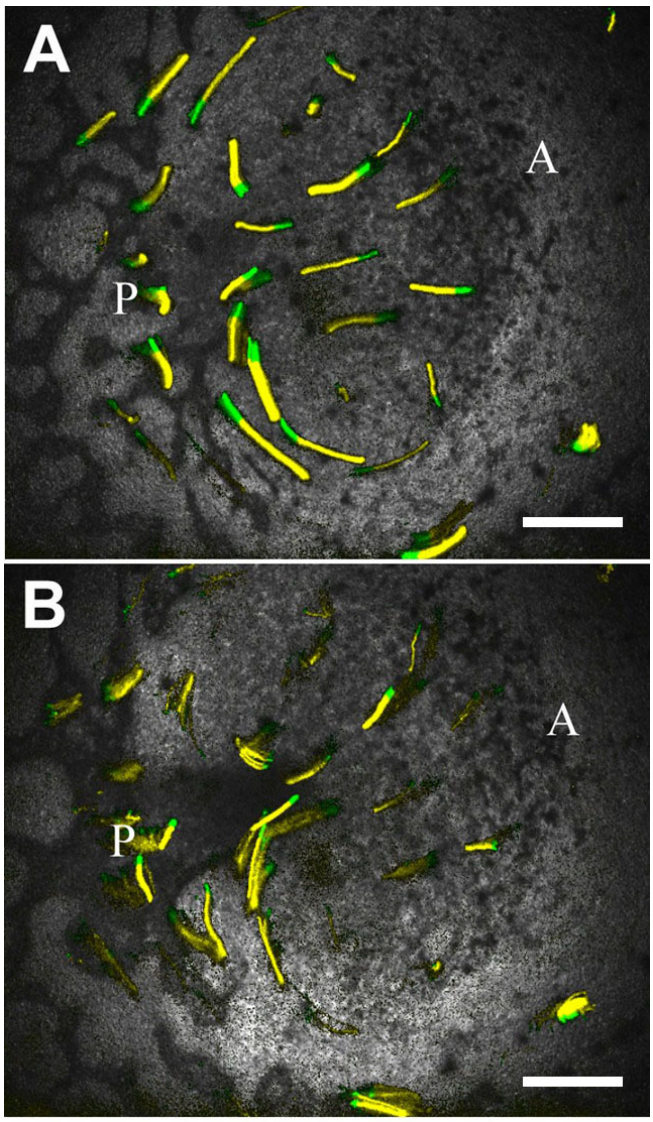

Figure 2.7: Tracks of tissue movement in a chick embryo cultured from HH stage 1. We labeled small groups of cells in the *area pellucida* with DiI and recorded both brightfield and fluorescence images at 4 minute intervals. We then merged the fluorescence images to generate tracks of tissue movement and overlaid these tracks on a brightfield image. The tracks show movements of labeled cells during the 160 minutes prior to the overlaid brightfield images, while the green heads of the tracks show movement of labeled cells in the 40 minutes before the brightfield image, indicating the movement direction. We took the brightfield images, (A) 160 minutes after the start of time-lapse movie recording, (B) 480 minutes after the start of the time-lapse movie recording. Letters "A" and "P" in panels (A) and (B) represent the anterior and posterior directions respectively. The white scale bar represents 500 μm.

bifurcate into two streams that flow, either anteriorly (contributing to the anterior elongation of the primitive streak) or posteriorly (contributing to the posterior extension of the primitive streak). Thus the primitive streak's elongation is bidirectional from its initiation.

DiI labeling experiments (figures 2.7, 2.8) showed that despite large-scale cell displacements, relative cell movement during primitive-streak extension is small: the labeled patches of cells stayed together during their extensive displacements. As during streak formation (section 2.3.1), closer inspection of the groups of labeled cells revealed that cells from individual patches split up into several nearby smaller units, but did not reveal whether these splits resulted from adjacent cells moving apart or cells dividing, or both.

2.3.3 Optical-Flow Detection of Movement Patterns in Brightfield Images

Quantitative, high-resolution analysis of brightfield images of the tissue movements in the epiblast using an optical-flow detection algorithm confirmed the presence of the two counter-rotating vortices during primitive-streak formation (figure 2.9). As the images show, speeds vary from 0.1-1.5 μm/minute at different locations, with the highest speeds at the site of streak formation and the outer periphery of the vortices. The large scale and symmetry of these flow patterns is truly remarkable, cells not only moved vigorously away from the latero-posterior region near the boundary between the *area pellucida* and *area opaca* towards the site of streak formation as Gräeper described [45], but also anteriorly and laterally away from the site of streak formation, forming large-

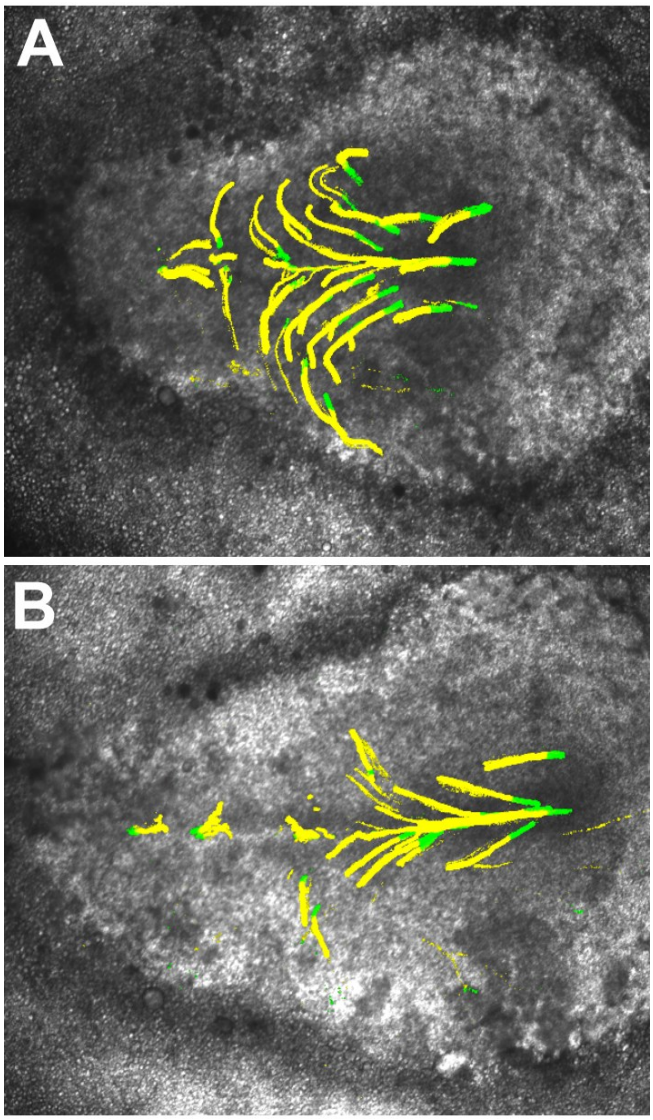

Figure 2.8: Tracks of tissue movement in an embryo beginning at HH stage 3. The tracks show movement of labeled cells in the last 160 minutes before we took the brightfield images, while the green heads of the tracks show movement of labeled cells in the last 40 minutes before the brightfield images, indicating the movement direction. We took the birghtfield images, (A) 160 minutes, (B) 480 minutes after the start of the recording.

scale closed-loop flows, which strongly resemble vortices in fluids. We observed many embryos (>60) and always found the same flow pattern.

Before the primitive streak becomes visible, the cells flowing towards the streak initiation site bifurcate into two streams that flow, either anteriorly (thus contributing to the anterior elongation of the streak) or posteriorly, indicating that the posterior extension of the streak starts during streak formation. We mark this bifurcation point with a small red box in the velocity-field figures (figure 2.9). During streak elongation this bifurcation point persists and seems to move anteriorly relative to the center of the streak, until, at the extended-streak (HH 4) stage, this point lies almost in the middle of the streak (figure 2.10), while the embryo changes from circular to pear shaped (figures 2.9, 2.10). These observations indicate a gradual increase in the rate of posterior extension relative to the rate of anterior extension. We do not know what determines this change in relative elongation rates; possibly proliferation of cells is faster in the posterior epiblast than in the central epiblast (panels (B) and (E) in figure 2.12), since elongation of the embryos did not occur in the presence of aphidicolin (figure 2.13).

2.3.4 Streak Formation and Elongation Require Active Motion of Cells Both at the Base and Tip of the Streak

The above observations demonstrate the large-scale, connected flow of the tissue around two quiescent points in the lateral part of the epiblast, but do not show which cells in the streak move actively. When we implanted a control bead at

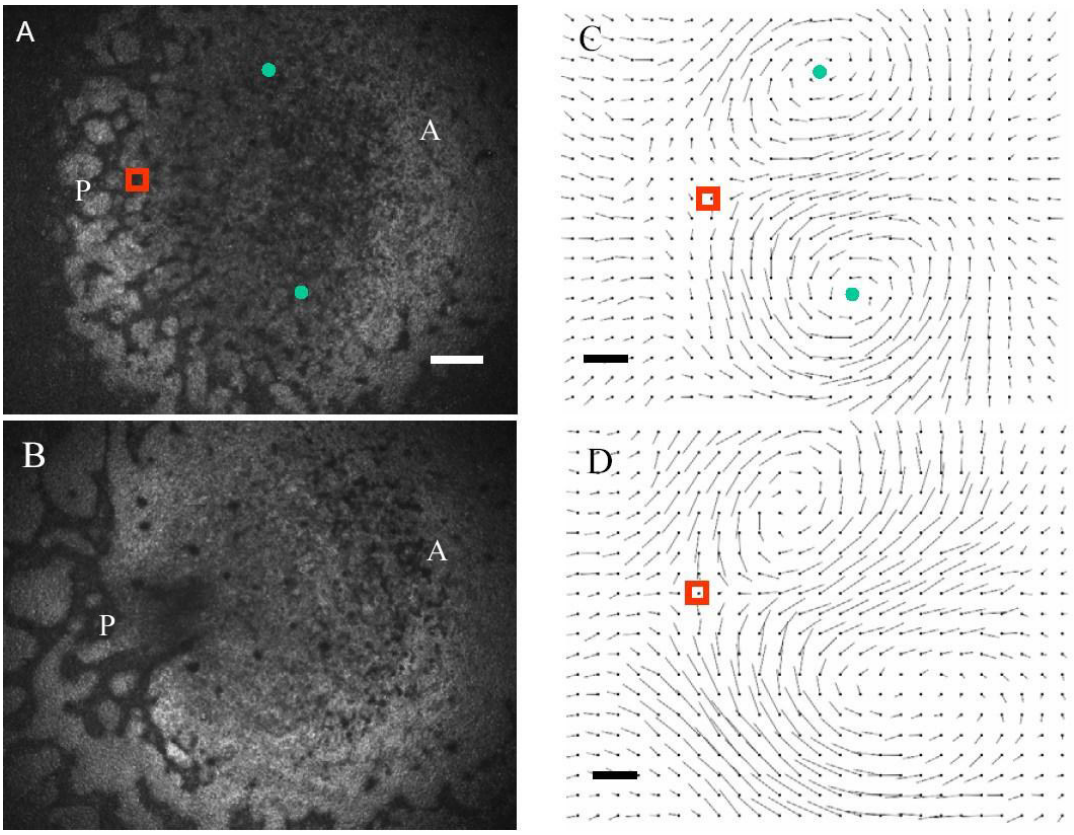

Figure 2.9: Velocity-vector fields of cells in chick embryos during primitive-streak formation. A), B) Brightfield images of the developing embryo shown in figure 2.7 at 40 minutes (before streak formation) and 320 minutes (after streak formation) after the start of recording. C), D) Corresponding velocity-vector fields calculated over the last 10 consecutive images taken at 4 minute intervals. The red boxes indicate the saddle-points where the cell flows merge and bifurcate along the A-P axis. Letters "A" and "P" represent anterior and posterior directions in (A) and (B). The green points in (A) and (C) indicate quiescent points of low flow. The white scale bar in (A) represents 500 μm in (A) and (B). The black scale bars in (C) and (D) represent a velocity of 1 μm/min.

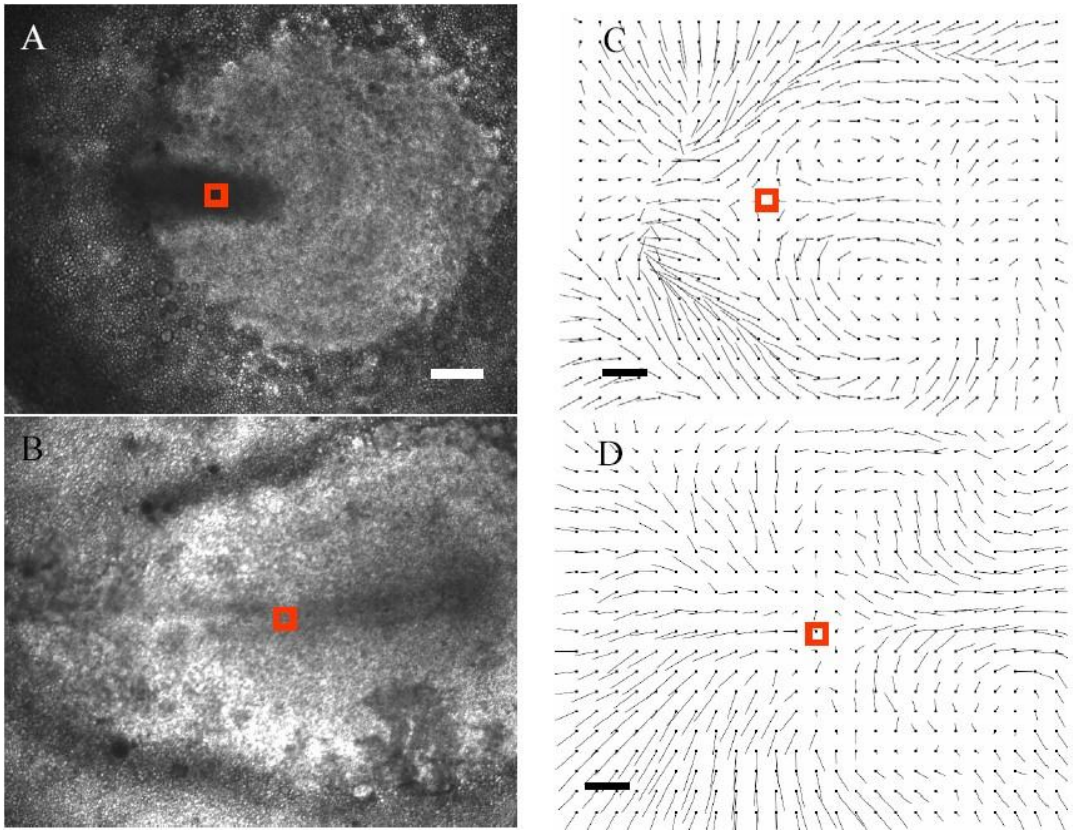

Figure 2.10: Velocity-vector fields of cells in a chick embryo during primitive-streak elongation. A), B) Brightfield images of a developing embryo at different stages (40 minutes and 600 minutes after the starting of recording). C), D) corresponding velocity-vector fields calculated over 10 consecutive images taken at 4 minute intervals. Note the change in position of the bifurcation point (red box) where the cells divide into anterior- and posterior-moving streams. The white scale bar in (A) represents 500 μm in both panels (A) and (B). The black scale bars in both panels (C) and (D) represent a velocity of 1 μm/min.

the tip of a forming streak (HH stage 2), it remained localized at the tip of the streak while the streak elongated. The streak tip pushed the bead forward and all movements were normal (panels (A), (B) and (C) in figure 2.11). So streak elongation is active and can push an inert object. How do these forces arise? We locally applied beads soaked in the actin-polymerization inhibitor Latrunculin B at various positions in the streak (figure 2.11). Slowly released from the beads, Latrunculin inhibits actin polymerization and thus active movement in cells that receive a high-enough dose. This local inhibition of movement enables us to investigate the role of active local cell movement on the elongation of the primitive streak. Putting a bead at the tip of the primitive streak immediately inhibits extension of the streak in the anterior direction, *i.e.* the tip of the streak no longer moves towards the anterior boundary of the embyro (panels (D), (E) and (F) in figure 2.11). However, the primitive streak still elongates, due to the posterior extension of the streak, as the velocity-vector field also shows (panel (F) in figure 2.11). Putting Latrunculin beads at the base of a forming streak blocks both anterior and posterior streak elongation almost completely (panels (G), (H) and (I) in figure 2.11). These observations suggest that the majority of cells that contribute to the streak must move through the posterior area of the embryo and that this movement is active and actin dependent, resulting either from cell division or crawling of cells on the basal layer.

2.3.5 The Role of Cell Division in Streak Formation

Experiments labeling individual cells with lacZ-expressing virus particles have shown that cells in the streak mostly divide with their cleavage plane perpen-

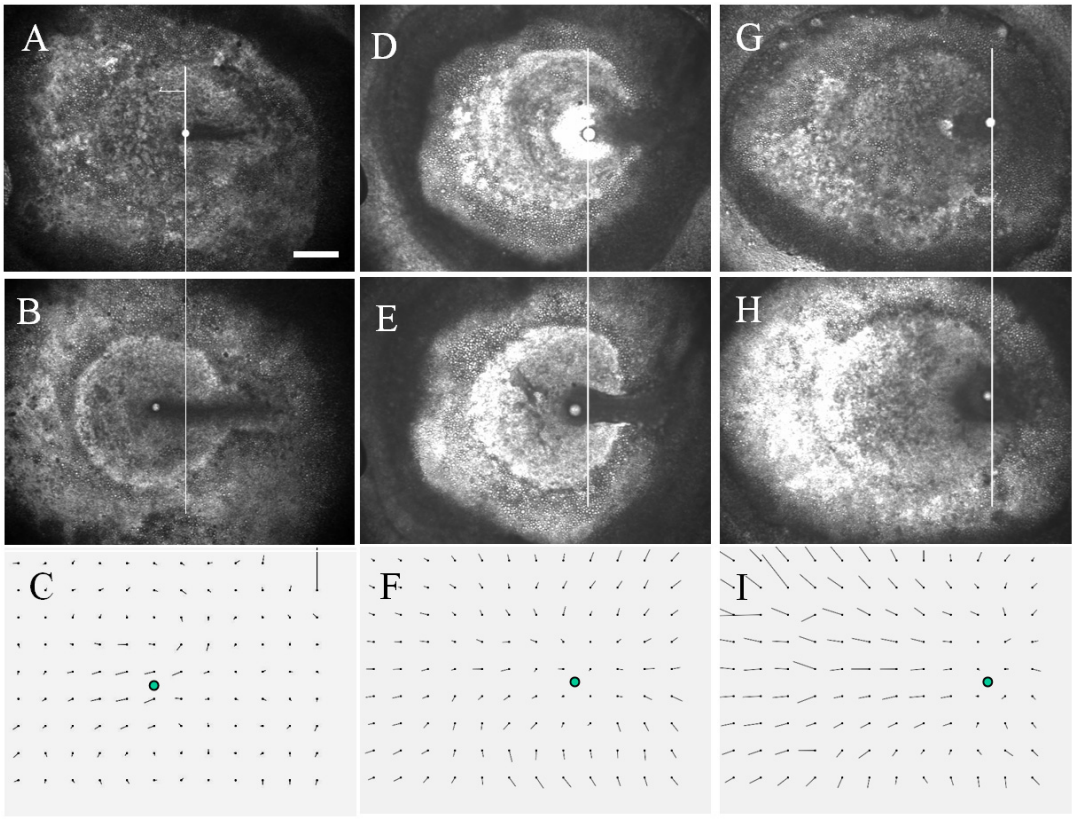

Figure 2.11: Inhibition of streak extension by local inhibition of actin polymerization. A), B), C) Movement of a central bead implanted at the tip of the streak in an HH stage 2 embryo (A) and the same embryo 6.5 hours later (B). C) Tissue velocity-vector field calculated over a 30 minute period 6-6.5 hours after implantation of the bead. D), E), F) Embryo with a bead soaked in 40 mM latrunculin implanted at the tip of the streak at the start of the experiment (D) and the same embryo 6.4 hours later (E). F) Tissue velocity-vector field calculated over a 30 minute period. G), H), I) Embryo with a latrunculin-soaked bead implanted at the base of the forming streak at the start of the experiment (G) and 6.5 hours after implantation (H). I) Tissue velocity-vector field 6-6.5 hours after implantation. Green circles in (C), (F) and (I) correspond to the positions of the beads. The white scale bar in (A) represents 500 μm and the vertical, black scale bar in (C) represents a velocity of 1 μm/min.

dicular to the direction of streak elongation [119], giving rise to strings of cells aligned along the long axis of the primitive streak. These observations led to the suggestion that oriented cell division might drive streak formation. However our observations of cell-flow patterns suggest an alternative explanation, *i.e.* that dividing cells in the streak stay interconnected and line up as a result of tissue movement rather than driving it.

Since we had little quantitative information on cell division and cell-cycle progression before streak formation and on their roles in early streak development, we decided to investigate the pattern of cell-cycle progression in more detail. We located cells in S phase using a 2 hr BrdU pulse labeling (figure 2.12). During early stages (HH 1-2) of development, the BrdU-incorporating cells in the epiblast showed no specific distribution pattern, except that slightly more cells at the very outermost edge of the blastoderm, which expands over the yolk as the embryo grows (panels (A) and (D) in figure 2.12), incorporated BrdU. In embryos labeled during the initial stages of streak formation, more cells in the anterior and lateral regions between the *area opaca* and the *area pellucida* incorporated BrdU, while fewer cells in the central region of the embryo incorporated BrdU (panels (B) and (E) in figure 2.12). To investigate whether these cell divisions form and elongate the primitive streak, we incubated embryos with the DNA-polymerase inhibitor aphidicolin, since this cell-division inhibitor, unlike most mitotic inhibitors, does not directly interfere with the cytoskeleton (which would affect the cells' motility machinery). Control points, which check for the successful replication of DNA before allowing cells to proceed into mitosis and cytokinesis, allow blocking of DNA synthesis to indirectly block cell division [75]. Incubation of the cells with aphidicolin completely in-

hibited BrdU incorporation, indicating effective cell cycle arrest (panels (C) and (F) in figure 2.12).

Analysis of tissue flow in embryos showed that at concentrations of aphidicolin that completely inhibited DNA replication, cells from the sickle region still moved towards the posterior midline, the position where the streak normally initiates. However, the primitive streak did not extend completely, causing compaction of cells and local increase in tissue density in the primitive-streak area. Cells located in the anterior and lateral parts of the *area pellucida* moved radially, directly towards the posterior pole, the site of primitive-streak formation, without following the normal, circular flow patterns (figure 2.13), resulting in a large aggregation of cells at the site of streak formation. In all these experiments the embryo tore itself apart, suggesting that the condensation of cells at the site of streak formation generates forces independent of cell division. Since cells initially aggregate at the site of streak formation in the absence of cell division, other mechanisms must drive aggregation. Our analysis suggests that increased cell division in a region between the *area opaca* and *area pellucida* is necessary for proper cell movement during the later stages of primitive-streak formation, especially during and after the half-extended streak stage, when the cells start to ingress through the streak and cells dividing in the epiblast must replace the cells that disappear at the ingression site (the midline of the primitive streak). Thus, cell division enables the epiblast to expand to compensate for the compaction of the cells in the streak and therefore is necessary for normal streak formation and to allow the embryo to grow.

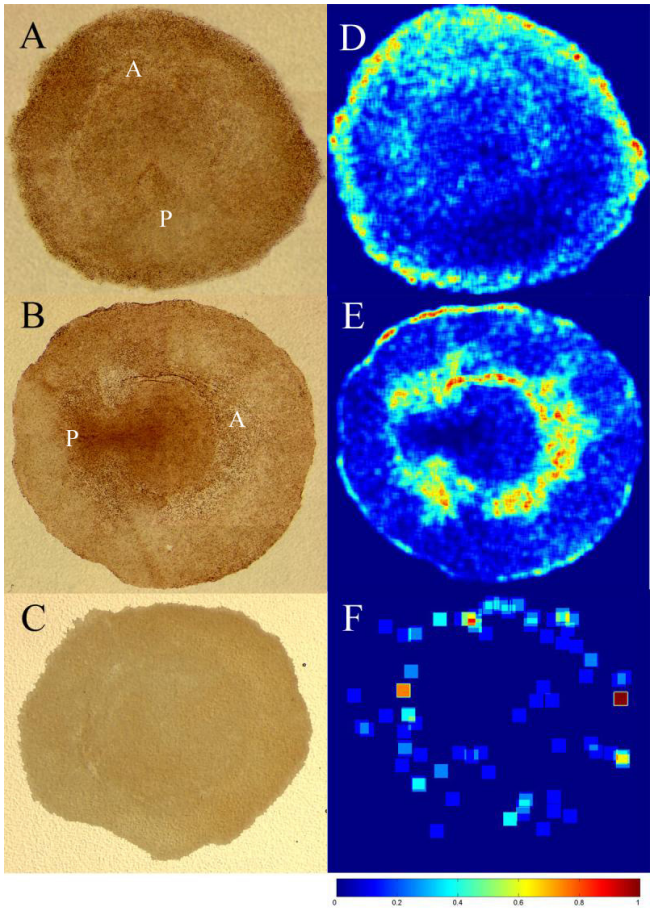

Figure 2.12: Spatial distribution of cells in S phase during early gastrulation. A) Pre-streak embryo (HH stage 1) showing uniform BrdU labeling of S-phase cells in the epiblast, with slightly more labeling at the outermost periphery of the embryo. B) HH stage 3^+ embryo showing more labeled cells in the boundary region between the *area pellucida* and *area opaca*. C) Complete inhibition of DNA synthesis in the presence of aphidicolin (10 μl, 100 μM). D)-F) The relative number of cells in S phase for images (A)-(C). We determined the number of cycling cells in each box of a 25x25 grid covering the images and displayed it as a relative color map. After aphidicolin treatment (C) BrdU incorporation effectively ceases. Smaller letters "A" and "P" in (A) and (B) indicate anterior and posterior directions repectively. The absence of cell division and the lack of a primitive streak make determining the A-P direction in embryo (C) impossible.

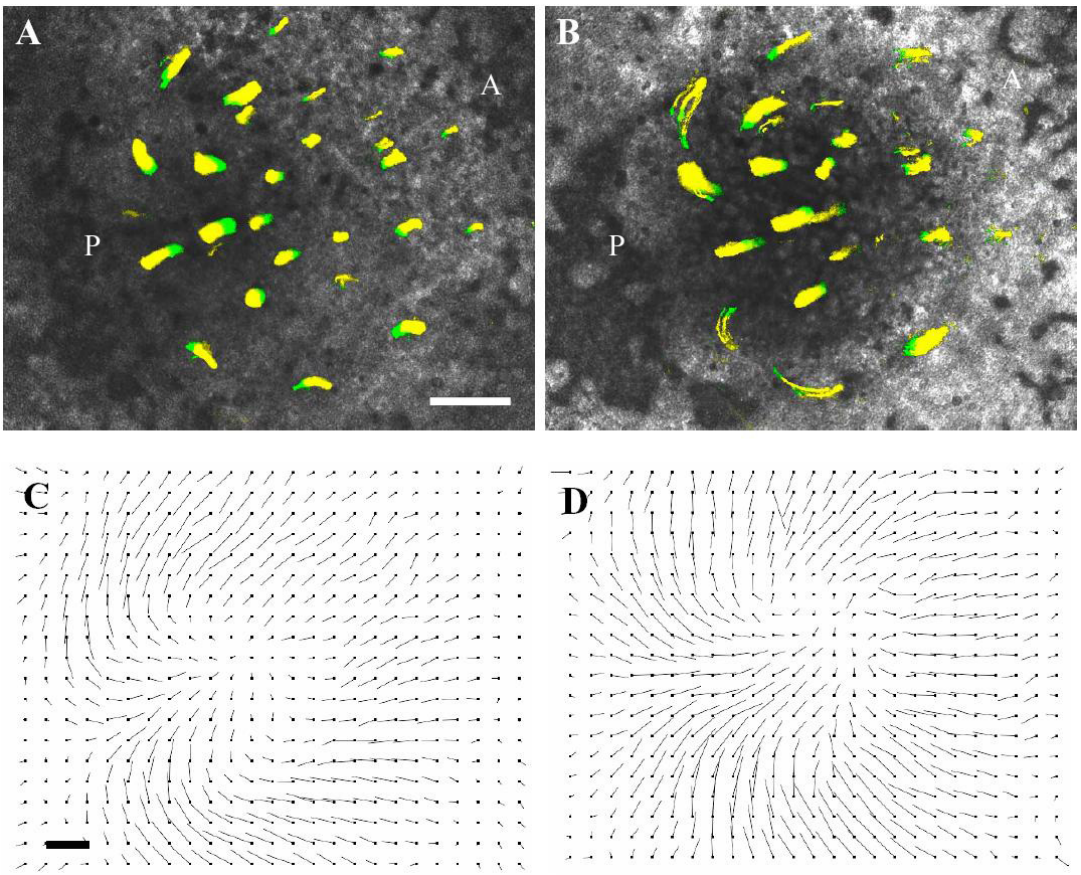

Figure 2.13: Inhibition of cell movement in the presence of aphidicolin. Trajectories of DiI-labeled cells and velocity-vector fields, showing the failure of streak formation and development in the absence of cell division. A), B) Cell-flow patterns revealed by DiI injection in embryos treated with aphidicolin. Labeled tracks show cell movement during the last 240 minutes before we took the brightfield images at 360 minutes (A) and 640 minutes (B) after the starting of recording. The green heads of the tracks show cell movement during the last 60 minutes. C), D) Velocity-vector fields calculated for the images shown in (A) and (B). The initial velocity-vector field shows that the streak starts to form but stops, since, in the absence of cell division, cells from the anterior and lateral *area pellucida* all move inward towards the center of the embryo. No cells move anteriorly, unlike in normal development (figures 2.7, 2.8, 2.9, 2.10). The white scale bar in (A) represents 500 μm. The black scale bar in (C) represents 1 μm/min.

2.3.6 Removal and Rotation of the Hypoblast

In our experiments, when we removed the hypoblast layer (from a HH stage 4 embryo), the elongation of the primitive streak stopped. However, cells continued to ingress through the groove in the middle of the primitive streak and formed another cell layer (possibly endoderm) on top of the epiblast. After the second layer formed, the primitive streak resumed elongation (figure 2.14). Thus, another cell layer on top of the epiblast is indispensable for normal embryo development, probably because the hypoblast or future endoderm layer provides an encapsulted environment and prevents the morphogens secreted by ectoderm, hypoblast or endoderm cells from diffusing away too quickly.

Our experiments on hypoblast rotation were fewer and did not yield conclusive results. Often the hypoblast, after removal, rotation and replacement, did not cover the whole bare region of the epiblast, retarding or stopping completely the embryo's development. However, primitive-streak elongation was normal in embryos that recovered from hypoblast rotation. No ectopic primitive streaks formed, nor did the forming primitive streaks bend as Eyal-Giladi and other researchers previously described [2, 9, 36] (figure 2.15).

2.4 Discussion

2.4.1 Streak Formation Involves Large-Scale, Active Tissue Flows

Our observations of cell-flow patterns do not indicate whether all or only some cells move actively. Since the cells in the epiblast form a tightly-connected

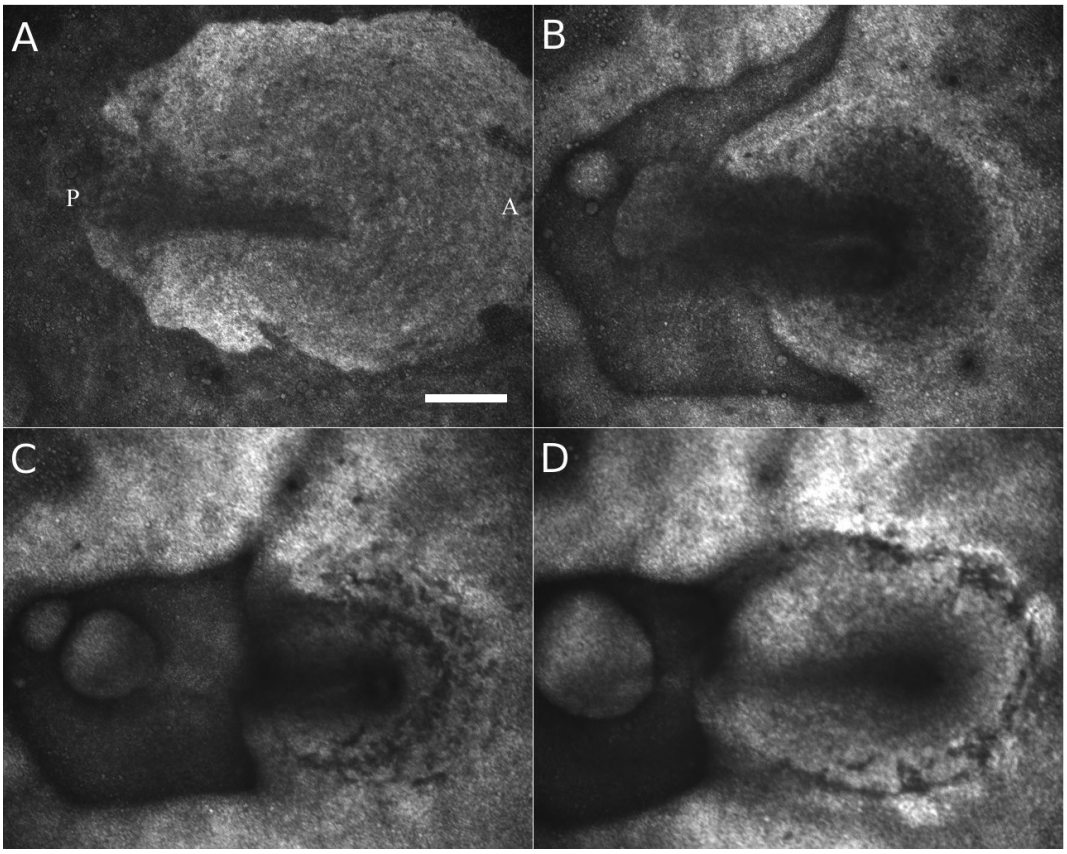

Figure 2.14: Embryo with hypoblast removed. A) 0 minutes, B) 248 minutes, C) 496 minutes, and D) 748 minutes after the time-lapse recording started. This time-lapse movie showed that soon after removal of the hypoblast, primitive-streak elongation stopped (A). However, ectodermal cells continued to ingress through the primitive streak and accumulated at the ventral side of the embryo (B) and (C). This layer of cells later became more transparent (probably because the accumulated cells reorganized into a single layer) and the primitive streak then resumed elongation (D). The white scale bar in (A) represents 500 μm.

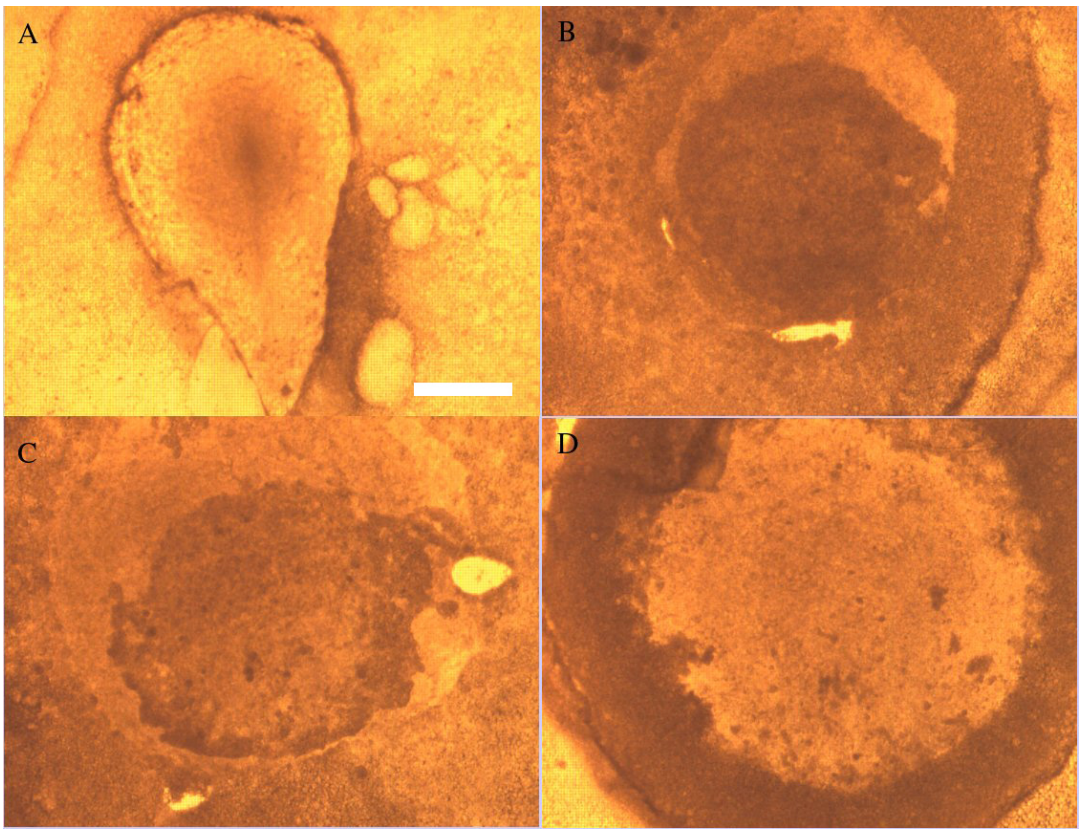

Figure 2.15: Embryos with hypoblast rotated or removed. A) We rotated the hypoblast layer in a HH stage 3 embryo by 90° counter-clockwise and incubated it for 8 hours. The embryo's primitive streak continued to elongate after hypoblast rotation. B) and C) Often after hypoblast rotation, the rotated hypoblast did not cover the whole bare region of the epiblast, causing either retarded development or death. D) An embryo with hypoblast layer removed.

epithelial sheet, local movement of one group of cells requires other cells to rearrange in order to maintain the integrity of the sheet. In this sense, cell-flow patterns very much resemble flow patterns in a fluid, where viscosity controls the interactions and flow properties. Dr. Chua at the University of Dundee, Dundee, Scotland recently showed that local inhibition of the actin cytoskeleton eliminates anterior elongation, suggesting that extension of the anterior part of the forming streak requires active migration of the cells in the streak tip (section 2.3.4). Cells in the streak tip might move up a gradient of a chemoattractant [84]. Blocking cell movement at the base of the streak, essentially at the meeting point of the bifurcating cell flows, blocks both anterior and posterior streak extension, strongly suggesting that cell flow towards the meeting point is absolutely necessary for streak formation and elongation (sections 2.3.3 and 2.3.4). The bifurcating flow pattern at the base of the streak resembles that seen during convergent extension in *Xenopus* and zebrafish embryos [42, 57]. Our analyses of brightfield images of epiblast cell movement and of the trajectories of groups of DiI-labeled cells have shown that primitive-streak formation in the chick embryo involves large-scale tissue flows including the two vortices that meet and merge along the midline at the posterior pole of the embryo (section 2.3.1). These flows do not result in large-scale cell-cell rearrangements and cells mostly keep their neighbor relationships. At the meeting point, most cells move anteriorly and a few move posteriorly before ingressing through the streak to the ventral side of the embryo. The meeting point initially lies in the posterior part of the embryo, but as the streak elongates, it moves towards the middle of the A-P axis of the streak, while the embryo changes from a circular to a pear shape (figures 2.9, 2.10). Thus in very early stages, the streak elon-

gates in both anterior and posterior directions, while in later stages, posterior elongation dominates (section 2.3.3). We do not know what determines this shift in relative elongation rates; possibly the higher proliferation rates in the posterior epiblast compared to the central epiblast (panels (B) and (E) in figure 2.12) since elongation of the embryos did not occur in presence of aphidicolin (Figure 2.13).

The cell-flow patterns during streak formation strikingly parallel movements D'Amico and Cooper recently described for nuclei in the syncytial yolk layer in early gastrulation-stage fish embryos [22]. These nuclei also form two large-scale, counter-rotating vortices flowing in a dorso-anterior direction, circulating around two quiescent lateral centers and merging at the midline of the embryo. They persist until the first somite stage. Thus, counter-rotating flows do not need active rearrangement at the cell level but can occur in a cellular syncytium, where they may either involve active transport of nuclei along the microtubule network or be driven by flows in the cytoplasm. Epiboly in fish (equivalent to epiblast movements in chick embryos) also seems to involve tissue flows directed towards the central midline, with a flow bifurcation in the anterior and posterior directions [42]. However, the extent to which these nuclear movements in the fish yolk syncytial layer resemble movements in the chick epiblast is not clear.

2.4.2 Cell Division is Necessary for, but Does Not Drive, Streak Formation

Localized or oriented cell division could locally expand the cell mass in the epiblast, displacing cells at other locations. However, our experiments with

aphidicolin showed clearly that the initial cell flows preceding streak formation occurred in the absence of cell division. A streak started to form. However, anterior and posterior extension did not complete. During streak formation (even in the presence of aphidicolin) the tissue thickens at the site of the streak, as the darkening of the structure in the brightfield images indicates. Thus, rather than cell division, the active aggregation of cells at this site (seen clearly in the tracks of DiI-labeled cells and in the velocity profile in figure 2.13), which requires the recruitment of cells from the neighboring areas of the epiblast, drives thickening. Recruitment requires the epiblast to expand in surface area, which mostly likely involves the increased cell division we observed in the boundary region between the *area opaca* and *area pellucida* (figure 2.12 in section 2.3.5). Aphidicolin inhibition of cell division prevents this expansion, so the flow of cells from anterior and lateral epiblast regions towards the location of streak formation thins and finally ruptures the epiblast. Thus cell division in the early epiblast plays an important permissive role in streak formation, expanding the surface area of the epiblast, in a functional analogue to the radial intercalation, which increases the surface area of the ectoderm during gastrulation in *Xenopus* [57]. We still must determine which signals coordinate the spatial pattern and dynamic changes of cell division during early gastrulation.

2.4.3 A More 'Complete' Fate Map of Cells in the Epiblast

Even though we do not know the function of the cell/tissue flows during primitive-streak formation, nor the exact fate of the cells in various parts of the epiblast,

our experiments and tissue-flow analysis provide clues. As previous studies showed, cells that will form the primitive streak derive from those cells just anterior to and overlaying Koller's sickle (see figure 2.2), which express many distinct genes; notably, Wnt8c, Nodal and FGF8 [14, 68]. However, our observations show that cells from the latero-posterior epiblast replace the cells of Koller's sickle that move into the primitive streak. A thin semicircle of cells at the posterior margin of the epiblast expresses ephrin-B3 [3]. Ephrin-B3 transcription restricts to the anterior primitive streak between HH stage 2 and HH stage 4, then further restricts to Hensen's node, until HH stage 10 [3, 4]. According to the fate map of the early epiblast, many of the antero-lateral, ephrin-B3-expressing cells end up in the lateral-plate mesoderm [50]. Therefore, cell flows could cause this remarkable change in gene expression, and the confinement of expression to Hensen's node could result from the more lateral cells switching off ephrin-B3 expression once they ingress through the primitive streak.

Cells anterior to Koller's sickle move anteriorly. Cells initially in the middle of the epiblast move in the anterior direction, while more lateral cells move first anteriorly then laterally to form the two rotating vortices. When we compare these movement patterns to the fate map of the epiblast, which Hatada *et al.* determined using DiI labeling at early stages of development [50] we find that anterior-moving cells join the neuro-ectoderm and surface ectoderm. The flows may also account for dynamic changes in gene expression during early development of the neural plate, *e.g.* in the expression of FGF receptors 1 and 3 [117]. Though the position of the cells in the quiescent centers of the two vortices (panels (A) and (C) in figure 2.9) does not correspond to any identi-

fied gene-expression pattern, the fate map suggests that these cells will form epidermis.

2.4.4 Possible Mechanisms Underlying Streak Formation

Major open questions regarding streak formation are: What are the cellular mechanisms which cause the cell and tissue motions which produce the primitive streak? Which signals control these mechanisms? Early streak formation could involve intercalation of cells in Koller's sickle at the base of the forming primitive streak driving bi-directional extension along the future A-P axis [58]. In *Xenopus*, convergent extension occurs in *Keller explants*, isolated pieces of dorsal tissue, even in the absence of lateral tissue [57, 116]. The Wnt-mediated, planar-polarity signaling pathway, with Rho kinase as one of its downstream targets [74] regulates convergent extension. However, our initial experiments with the Rho-kinase inhibitor Y27632 did not inhibit early streak formation, even at concentrations which inhibited streak regression [118]. Chua's latruculin experiments (section 2.3.4) showed that the streak tip has to move forward actively, so streak formation must depend on more than intercalation at the base of the streak. The planar-polarity pathway also controls the cell-cell intercalation which drives germ-band formation in *Drosophila* via preferential non-muscle-myosin-mediated contraction of cell boundaries perpendicular to the axis of extension. The pair-rule genes then control the extension of boundaries in the direction of elongation, which locally reshuffles cells and extends the germ band [8, 126]. We also tried to observe streak extension at higher magnifications to look for consistent patterns of local cell rearrangement or polarization in the

chick epiblast but did not obtain any conclusive results due to the difficulty of keeping the cells in focus during movies.

Cells could also move in response to chemo-attractants/repellents. The cells in Koller's sickle could aggregate towards the dorsal midline in response to a chemo-attractant that cells in the *PMZ* produce, resulting in aggregation at the ventral meeting point. The cells at the tip of the forming streak could then acquire the ability to respond to a gradient of another chemo-attractant, resulting in their movement towards the midline of the embryo. Alternatively, a signal coming from the base of the primitive steak could repel the cells. Possible candidate molecules include the FGFs, since all epiblast cells express both FGF receptors and some FGFs from an early stage, and since mesoderm cells chemotax to FGFs secreted by cells in the primitive streak [55, 117, 125].

In this scenario, most cells move actively, probably on a basement membrane underlying the epiblast [18], by producing cryptic lamellipodia in the direction of migration [33].

Cells in the epiblast might also respond to signals which the endoblast emits while it is replacing the hypoblast in a posterior-anterior direction. Hypoblast removal results in defective streak extension and hypoblast rotation may bend the streak [2, 9, 36] (however, our preliminary experiments on hypoblast rotation did not confirm this primitive-streak bending). Signals from the hypoblast could polarize the cells, resulting in anterior movement of cells along the midline and creating the two counter-rotating vortices lateral to the streak.

2.5 Acknowledgement

We performed all experiments related to chick gastrulation in Prof. Weijer's laboratory at the University of Dundee, Dundee, Scotland in collaboration with Dr. Yang. We analyzed the images under Prof. Glazier's supervision at the University of Notre Dame and Indiana University, Bloomington. We used Prof. Weijer's C++ software to produce the velocity maps.

Chapter 3

Cell Movement in Micromass Cell-Culture

3.1 Limb Development in the Chick Embryo and Its Relation to Micromass Culture: An Introduction

3.1.1 Embryonic Chick Limb Development

Limb development begins when the expression pattern of Homeobox genes along the somites defines the developmental limb field, inducing the *lateral plate mesoderm* (*LPM*) cells (figure 3.1) in the developmental limb field to secrete FGF10, which can, in turn, induce the ectodermal cells above the LPM to secrete FGF8 and form the *apical ectodermal ridge* (*AER*) of the limb bud (figure 3.2). According to Wolpert's *progress-zone model*, FGF8 secreted by the AER can keep

a band of underlying mesenchymal cells, in the *progress zone*, proliferating at a high rate, while the mesodermal cells outside the developmental limb field proliferate at a lower rate. This proliferation-rate difference makes the limb bud extrude from the embryo's flank and elongate in the proximo-distal (*P-D*) direction.

During limb elongation, FGF8 can induce mesenchymal cells in the posterior of the limb bud to secrete Sonic hedgehog (*Shh*) to form the *zone of polarizing activity* (*ZPA*) (panel (C) in figure 3.2). Sonic hedgehog also induces the cells at the posterior end of the AER to secrete FGF4, which together with Wnt-7a from dorsal ectodermal cells, can in turn maintain the secretion of Sonic hedgehog in the *ZPA* (panel (B) in figure 3.2).

As the limb develops, mesenchymal cells divide, migrate, and interact with each other and the surrounding ectodermal cells. Some of the mesenchymal cells in the developing limb form cartilage, which bone will later replace, in P-D order as the limb elongates. In the fore-limb, first the humerus appears, then the radius and ulna, followed by the carpals and three distinguishable digits (for chick embryos) at the very distal end of the limb (panel (C) in figure 3.3).

The embryonic chick limb has provided an excellent model of the pattern formation by which embryonic cells form the ordered spatial arrangements of differentiated tissues, particularly, how the developing chick limb becomes polarized along the P-D and the antero-posterior (*A-P*) directions. However, partly due to their importance, the mechanisms of limb patterning are controversial. Based on his studies of embryonic chick limbs in the 1960s, Wolpert proposed his *positional-information theory* of A-P and P-D pattern formation [123]. The positional-information theory states that the cells can determine their position

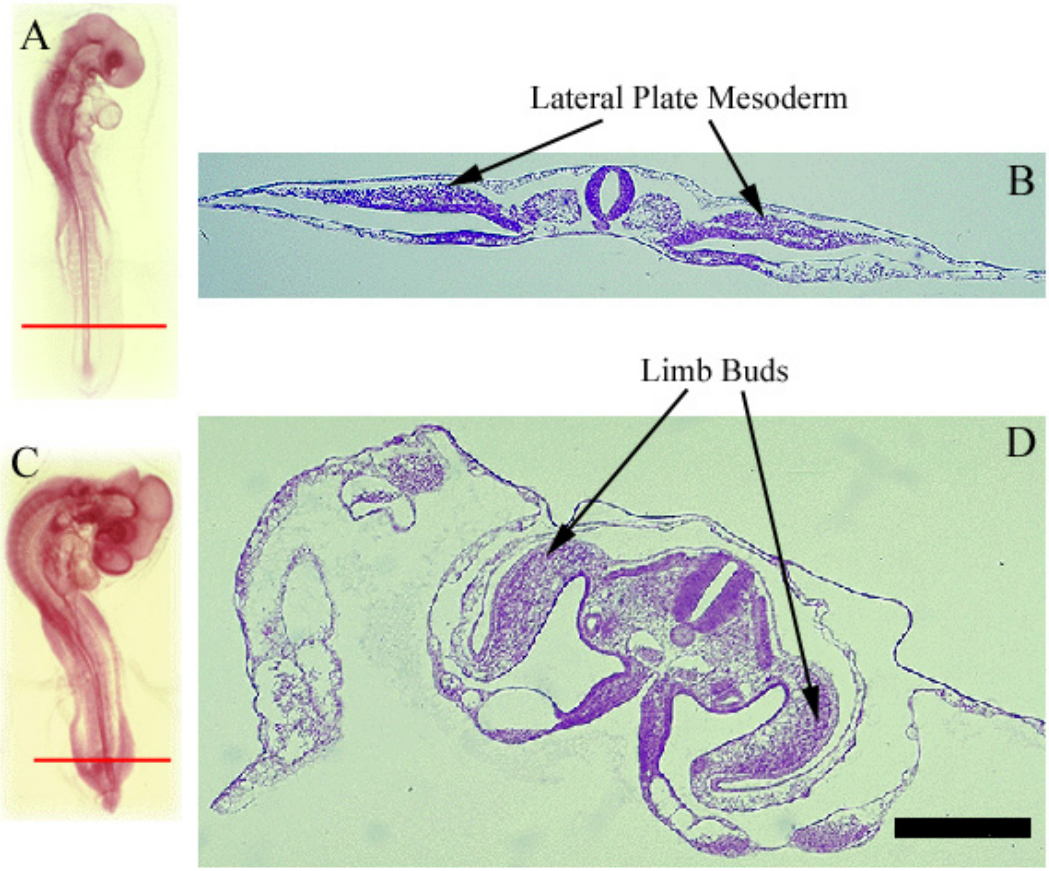

Figure 3.1: Cross-section of the embryonic chick hind-limb field at two developmental stages. A), B) HH stage 15 embryo. C), D) HH stage 18 embryo. The red lines in (A) and (C) indicate the cross-section positions. The black scale bar in (D) represents 250 μm in (B) and (D). Adapted from the Cell and Developmental Biology ONLINE! web site at http://www.uoguelph.ca/zoology/devobio/index.htm.

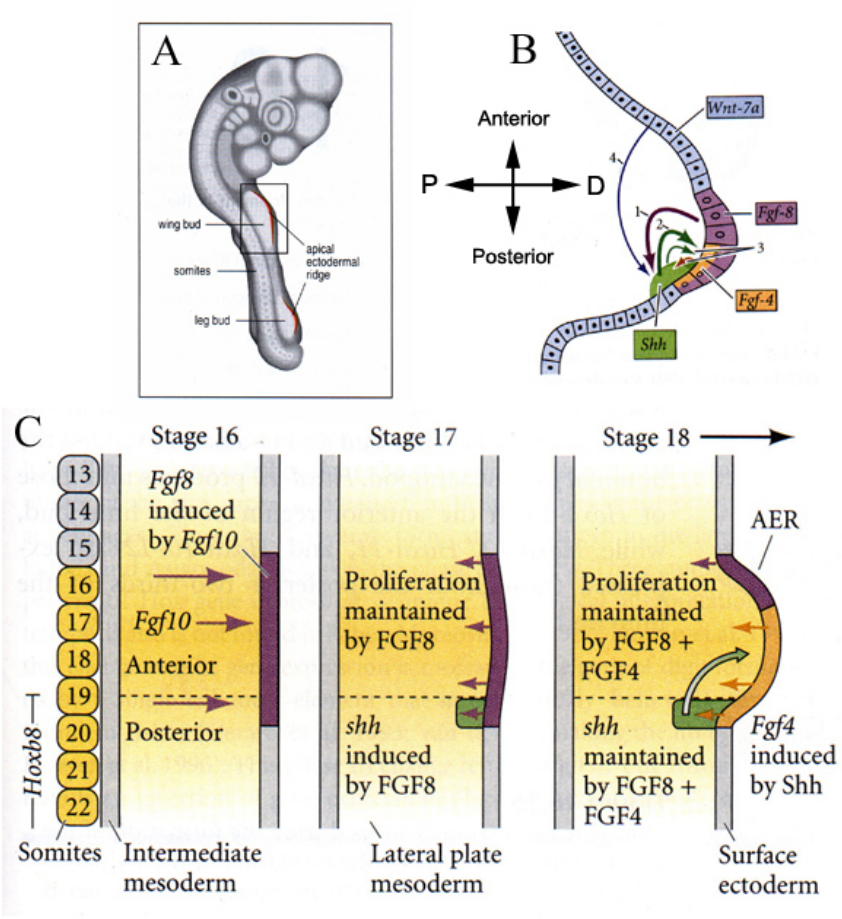

Figure 3.2: A molecular model of embryonic chick-limb initiation. The developmental limb field in panel (C) shows a detail of the black rectangle in panel (A). A) An embryo at HH stage 18 seen in side view, showing locations of limb buds and AER. The embryo is approximately 7-8 mm long. B) Antero-posterior (*A-P*) and proximo-distal (*P-D*) cross-section of a limb bud, showing ectoderm (blue), AER (purple) and ZPA (green) and the main signaling molecules. The numbers indicate the order in which the cells begin to produce these molecules. 1. The Fgf-8 secreted by the AER induces the cells at the posterior end of the limb bud (the ZPA) to produce Shh, which, in turn, induces the cells in the posterior part of the ectoderm to produce Fgf-4. The maintenace of Shh expression in the ZPA requires Fgf-4 and Wnt-7a from the ectoderm. C) Detail of the fore-limb development field, showing somite number and expression patterns and effects of key signaling molecules. See text for details. Adapted from (A): figure 10.1 in [124], and (B): figure 18.8 in [41]; (C): figure 18.10 in [41].

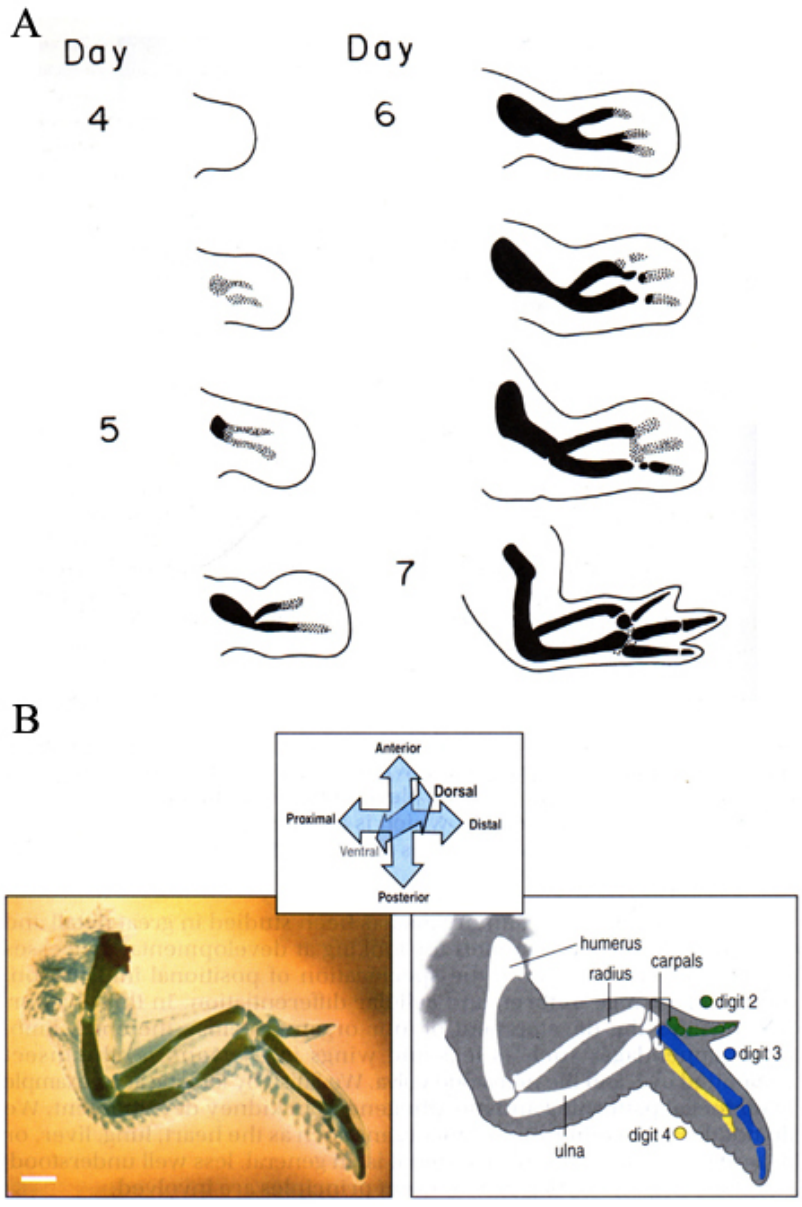

Figure 3.3: Embryonic limb development in chick. A) A-P–P-D sections of the developing limb at different times. B) The three developmental axes and the configuration of the three cartilage regions. See text for details. Adapted from: (A), figure 1 in [79] and (B), figure 10.2 in [124].

from external chemical gradients and differentiate accordingly. These differentiated cells can then form a particular spatial pattern in the tissue. Even though performing experiments to directly support the positional-information theory has proved very hard, and despite doubts about its validity, it remains a fundamental hypothesis of developmental biology.

Along the P-D axis, the embryonic chick limb forms three regions: the humerus at the proximal end (upper arm), radius and ulna in the middle (lower arm) and three digits at the distal end. In Wolpert's positional-information theory, underneath the AER, a band of undifferentiated cells, called the progress zone, proliferates at a high rate. The growth factors the AER secretes keep the progress-zone cells from differentiating (see figure 3.4). Continuous cell division in the progress zone pushes cells in the proximal region out of the progress zone. They then differentiate. Cells determine their positional information according to the time they spend in the progress zone. The longer the time mesenchymal cells stay in the progress zone, the more distal the region they will form.

Wolpert's model can explain why embryonic limbs truncated at different stages will develop different segments, *e.g.* the limb bud with the AER removed at an early time develops into a limb with only one cartilage element; the limb bud with the AER removed at a later time develops into a limb with one cartilage element in the proximal region and two cartilage elementss at the distal end. However, his model fails to explain why the chick limb has a 1-2-3 cartilage pattern in the P-D direction. Two studies [29, 111] in 2002 also seemed to contradict Wolpert's conceptual framework. Both [29, 111] suggest that cells do not acquire positional information from their time sequence of differentiation, but instead from their position in the early limb bud. The

selective multiplication of prespecified cohorts of cells is then time-dependent, with proximal cells prolifering earlier.

Also under debate is the specification of the limb's A-P axis. In chick, A-P axis specification happens long before the limb bud is recognizable [48]. Cells in the ZPA, when transplanted to the anterior side of another limb bud, double the number of digits of the resulting limb and the structures of the extra set of digits are mirror images of the normal structures (figure 3.7). The search for the molecule(s) conferring this polarizing activity on the limb bud identified Shh as the active agent of the ZPA [88, 70] (figure 3.6). However, how the ZPA specifies the A-P axis is still not clear. One model proposes that the tissue in the embryonic limb responds differently to different concentrations of the soluble morphogens, which the ZPA secretes [123, 112] (figure 3.7). However, Shh is not the soluble morphogen responsible for specifying the digits, since its active part (N-terminal region) cannot diffuse far from its source in the posterior limb bud [70].

3.1.2 Micromass Cell-Culture and *in vitro* Study of Cartilage Condensation During Embryonic Limb Development

In the developing vertebrate limb, precartilage mesenchymal condensation begins proximally, as the mesenchymal primordium of the *stylopod* (humerus or femur) begins to form. Condensation continues in the P-D direction to establish the mesenchymal template for the entire limb skeleton. Chondrogenesis follows this wave of condensation, replacing the mesenchymal template with a

cartilaginous one, which bone in turn, replaces in most vertebrate species.

Limb-bud precartilage cells growing in high density micromass cultures form nodular condensations (corresponding to the rods and nodules they form *in vivo*) that expand and converge, or remain spatially isolated, depending on species, limb type and growth-factor microenvironment [23, 27, 77]. In the embryo and in culture, limb precartilage condensation occurs in two phases [46, 47, 81]. First, cells accumulate in regions of prospective condensation, which are rich in the ECM glycoproteins fibronectin [39, 64, 113] and tenascin-C [72], giving rise to mesenchymal aggregates; second, cells produce cell-cell adhesion molecules such as N-CAM [82], N-cadherin [121] and cadherin-11 [60]. Once cells cluster, they epithelialize, undergo chondrogenesis, and separate as they produce cartilage-specific ECM. Neither tenascin-C [90] nor N-cadherin [17, 71] is essential for limb mesenchymal condensation or normal limb development.

How limb precartilage mesenchymal cells behave during the initial, aggregation phase of condensation is poorly understood. Several studies support a mechanism for condensation based on an extended version of the differential adhesion hypothesis (*DAH*) [103, 37], which Steinberg originally proposed to account for the sorting of epithelioid, not mesenchymal, cells. In this interpretation, random cell movements occurring in a tissue mass which has local patches of increased adhesivity (due to local fibronectin accumulation) drive cells to form higher-density aggregates [38, 39]. Test particles coated with the glycosaminoglycan heparin (similar to the heparan sulfate on the mesenchymal cells' surfaces [44]), mixed with limb mesenchymal cells, accumulate at sites of cell condensation *in vitro* in a fashion that depends on interactions of the particle surfaces with fibronectin [39]. Haptotaxis, a mechanism based on random

cell movement (or buffeting, in the case of particles), along with selective sticking to an adhesive substrate, is thus a plausible mechanism for the initial stages of condensation, and computational studies [61, 127, 128] have shown that it suffices to explain basic features of condensation.

Both older and more recent findings, however, suggest that this passive, haptotaxis-based picture of condensation initiation is oversimplified. For example, Ede and coworkers, using time-lapse films of a small sample of limb mesenchymal cells *in vitro*, reported that cells' speed of movement appeared to increase when they entered condensations [30]. Finally, limb precartilage cells round-up [120] in response to the mesenchyme-specific (B+A+) [40] splice variant of fibronectin, a behavior associated with both enhanced migration and condensation [120]. Indeed, exposure to progressively higher concentrations of fibronectin can increase, rather than decrease, cells' migration speed [24, 73, 100].

We therefore reexamined mesenchymal cell behavior at the initiation of condensation *in vitro* using higher resolution, automated, video tracking techniques, analysis of larger numbers of cells, and more comprehensive statistical methods than in earlier studies. We characterized the linear dimension and number of cells in condensations and found that cells within a precartilage condensation have smaller areas of surface contact with their substrate than peripheral cells. While cells inside and far outside the condensation have random speeds and directions of motion, cells in the periphery of a condensation tend to move towards the center of the condensation, as the simple haptotaxis model predicts. However, contrary to the predictions of the haptotaxis model, cells within the condensation move significantly faster than cells in the periphery.

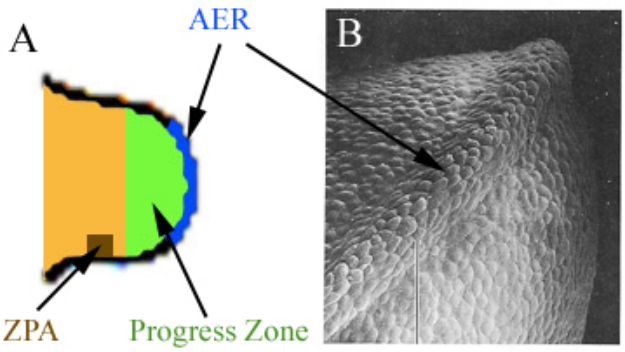

Figure 3.4: Progress-zone model. A) The AER secretes growth factors to keep a band of mesenchymal cells underneath from differentiating. B) Scanning electron micrograph of an early chick fore-limb bud showing the AER. (B) is adapted from figure 18.8 in [41]. The image size of (B) is approximately 220 μm across.

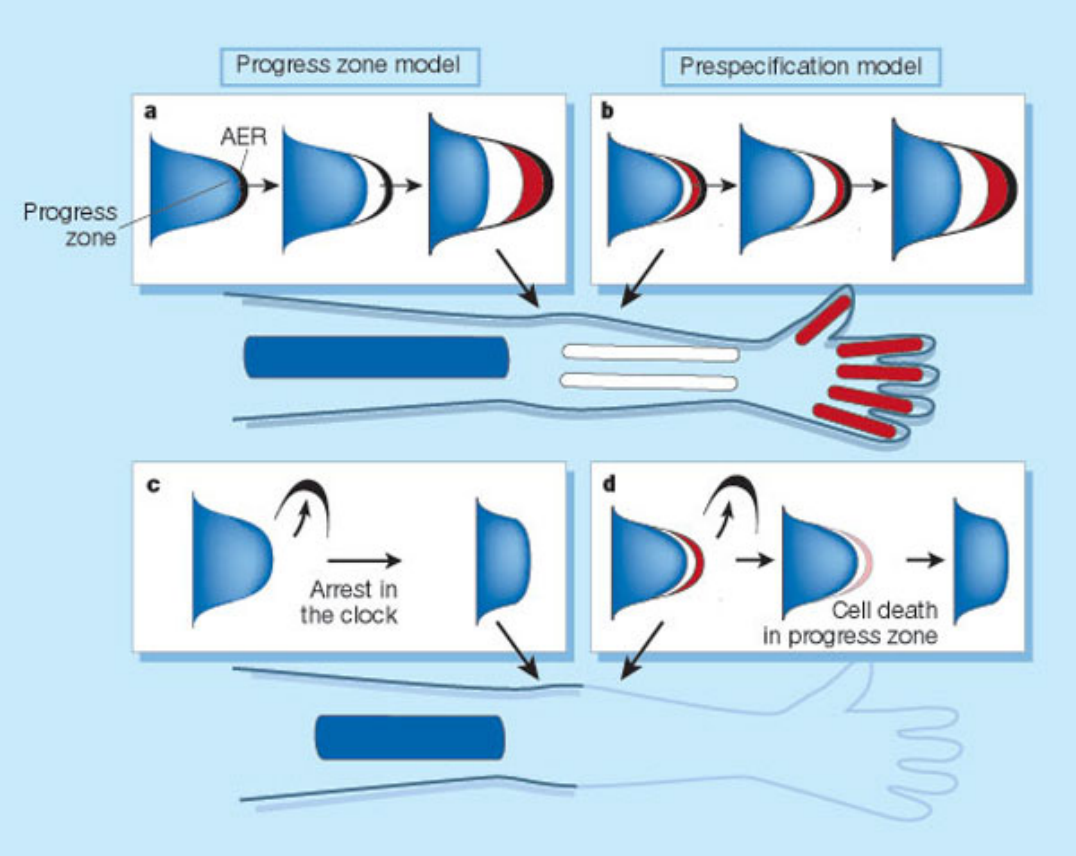

Figure 3.5: Two models of developing limbs. A) In the progress-zone model, the fate of proximal (blue) segments is specified before the fate of more distal segments as the limb bud grows. C) This model explains limb truncation experiments in which distal specification does not occur, since the cells in the progress zone stop proliferating once the AER is removed. B) In the prespecification model, P-D fates are specified early on and the oberved time sequence in skeletal development results from the selective expansion of these prespecified domains, along with cellular determination – the acquisition of definitive cell fates. D) This model also explains limb truncation experiments in which the distal domains is absent, because cells die after the removal of the AER. Adapted from figure 1 in [28].

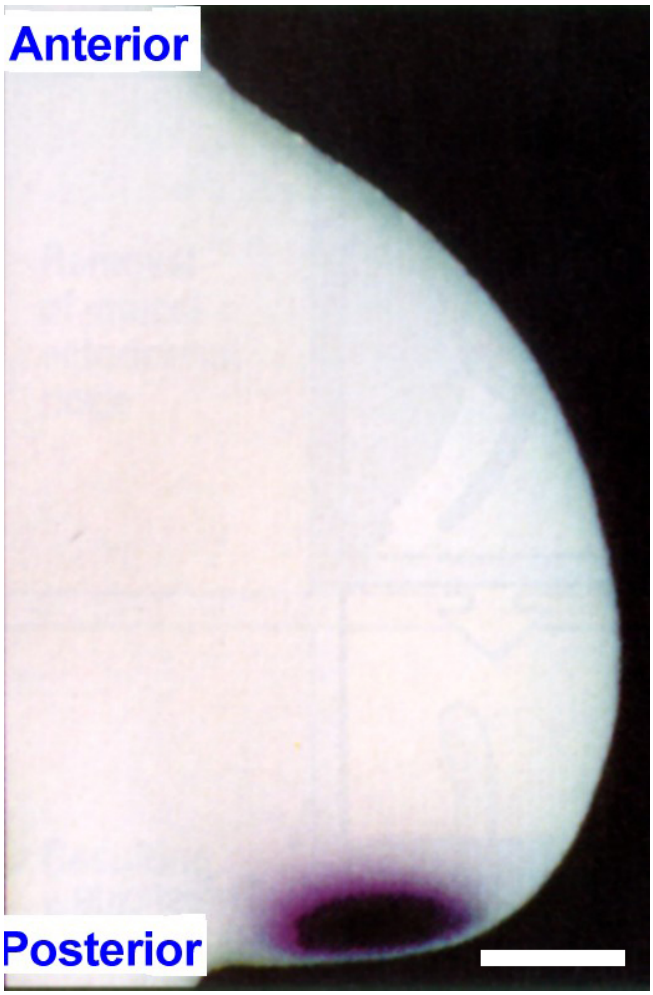

Figure 3.6: *In situ* hybridization for Sonic hedgehog (*Shh*) in embryonic chick limb shows that Shh is expressed at the posterior margin of the limb bud. Scale bar: 0.1 mm. Adapted from figure 10.8 in [124].

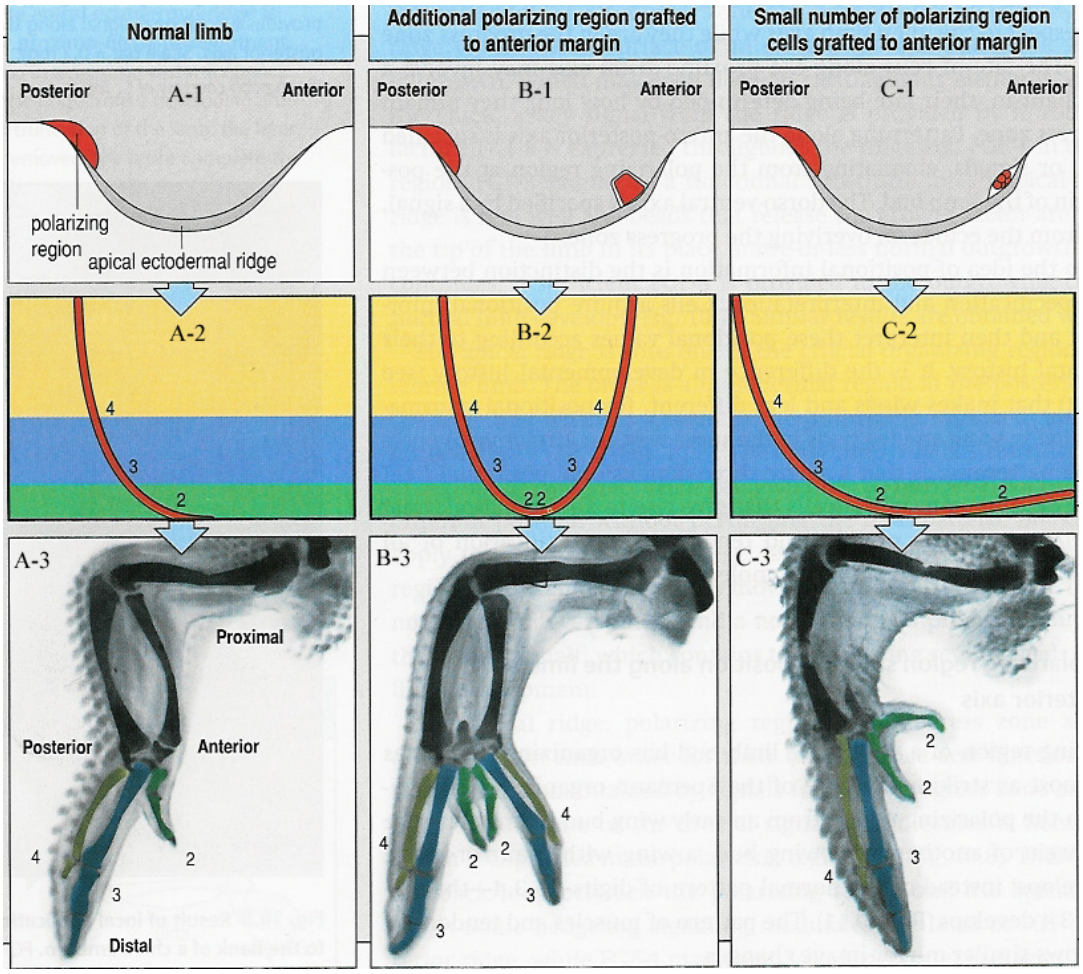

Figure 3.7: A-P axis specification of the embryonic chick limb: a morphogen model. A) In this model, the diffusing morphogen secreted from the posterior end of the limb diffuses across the whole limb and establishes a gradient field along the A-P axis. Mesenchymal cells at different places determine their positions from the concentration of the diffusing morphogen they encounter. B) When enough cells in the ZPA of one embryonic chick limb are transplanted into an anterior postion in another embryonic chick limb, the diffusing morphogen establishes a mirror-like gradient field. The resulting limb's digits are doubled and the extra set of digits is a mirror image of the normally-produced structures. C) Transplanting fewer ZPA cells results in fewer extra digits. Adapted from figure 10.11 in [124].

3.2 Materials and Methods

3.2.1 Cell-Culture

Section A.3 describes the micromass cell-culture technique. Here we briefly review our cell-culture technique.

We obtained fertile white Leghorn chicken eggs from Avian Services, Inc. (Frenchtown, NJ). We cut developing legs from HH-stage-25 chick embryos 0.3 mm from the distal end of the limb bud. This method excludes any cells from the ZPA. We used the tips, which have high concentrations of precartilage cells [80], to prepare cells for culture. We dissociated the cells in 1% trypsin-EDTA (Sigma), filtered them through Nytex 20-μm mono-filament nylon mesh (Tetko, Briarcliff Manor, NY), and resuspended them in defined medium (*DM* [86]) containing 10% fetal bovine serum with 2.0×10^7 cells/ml. Filtration removed most limb-bud ectoderm, which remained in sheets after trypsinization. We deposited one to three cell spots (10 μl each, containing 2.0×10^5 cells) in a 60 mm cell-culture dish (Corning 430166) and allowed the cells to adhere to the dish at 38.5°C in a 5% CO_2 atmosphere for 15 minutes before flooding the dish with serum-free DM. The initial cell-plating density is above confluency with this protocol, but with the addition of the full dish of medium at this step, the majority of remaining cells attach to the plastic, not to other cells, resulting in a tightly-packed monolayer. We returned the cell culture to the incubator for 24 hours, then sealed the lid of the culture dish with Parafilm to prevent dehydration during time-lapse photomicrography.

3.2.2 Microscopy and Image Acquisition

We placed the culture dish in a temperature-controlled Peltier warming device, maintained at 38.5°C on the stage of a Zeiss IM35 inverted microscope equipped with a 32x Planacromat, phase-contrast objective. Warm air blown across the dish lid prevented condensation on the lid's inner surface. A timer box turned the microscope's light source on and off in synchrony with the computer-controlled camera to minimize cells' exposure to light.

We took time-lapse images at intervals of 2 minutes at a resolution of 640×480 pixels. Of our eight experimental plates, three developed condensations near the center of the microscope's field of view and therefore permitted quantitative study. We chose one of these cultures for detailed analysis. The others developed at the same rate and had the same general morphology as the one we analyzed. We collected more than 350 individual images of the selected culture. Cells in frames 241-350 increasingly de-focused as differentiation to cartilage changed cell shapes and the culture thickened. In these frames we could not track individual cells, especially in the condensation center, so we processed and analyzed frames 1-240 (corresponding to the first 8 hours in culture).

We assumed that our two-dimensional images were sufficient because the cells formed a monolayer and rarely crawled over each other, though a few cells did detach from the substrate and other cells. However, information on the height of the cells would be extremely useful, since condensation correlates with vertical streching and polarization of the cells, while non-condensing cells spread over the substrate and become thinner.

3.2.3 Image Processing and Data Analysis

The resolution of the images was 0.285 μm/pixel, sufficient to track the 10 μm diameter cells' center-of-mass motion and to measure large-scale deformations of individual cells. With the aid of ImageJ software (`http://rsb.info.nih.gov/ij/`), which can play the sequence of images forward and backward, we hand-traced the boundaries between individual cells using Photoshop (Adobe). Cells moved much less ($< 10\%$) than one cell radius between frames, so we could unambiguously identify which cells in each image corresponded to the same experimental cell. We then used Photoshop and Matlab (MathWorks) to assign a district gray level to each experimental cell for display and tracking (figure 3.8).

We digitized the images, producing time series with different time intervals (see table 3.1). In image set I, we digitized every other image, processing 39 images. In image set I the interval between successive processed images is 4 minutes and the duration is 152 minutes. In image set II, we digitized every tenth image, processing 25 images. In image set II the interval between successive processed images is 20 minutes and the duration is 480 minutes. We used image set I to calculate the velocity autocorrelation $C(t)$ only and image set II for all other statistical measurements.

In both image sets, we labeled only cells lying completely within the field of view during the entire time series. We did not label or use cells which crossed the boundary of the field of view or which moved in or out of the field of view during the series. We observed 27 cell divisions during the 760 minute time-lapse series in a population of about 145 cells; 8 of 92 labeled cells divided during the first 480 minutes. When a cell divided, we randomly chose one of the daughter cells

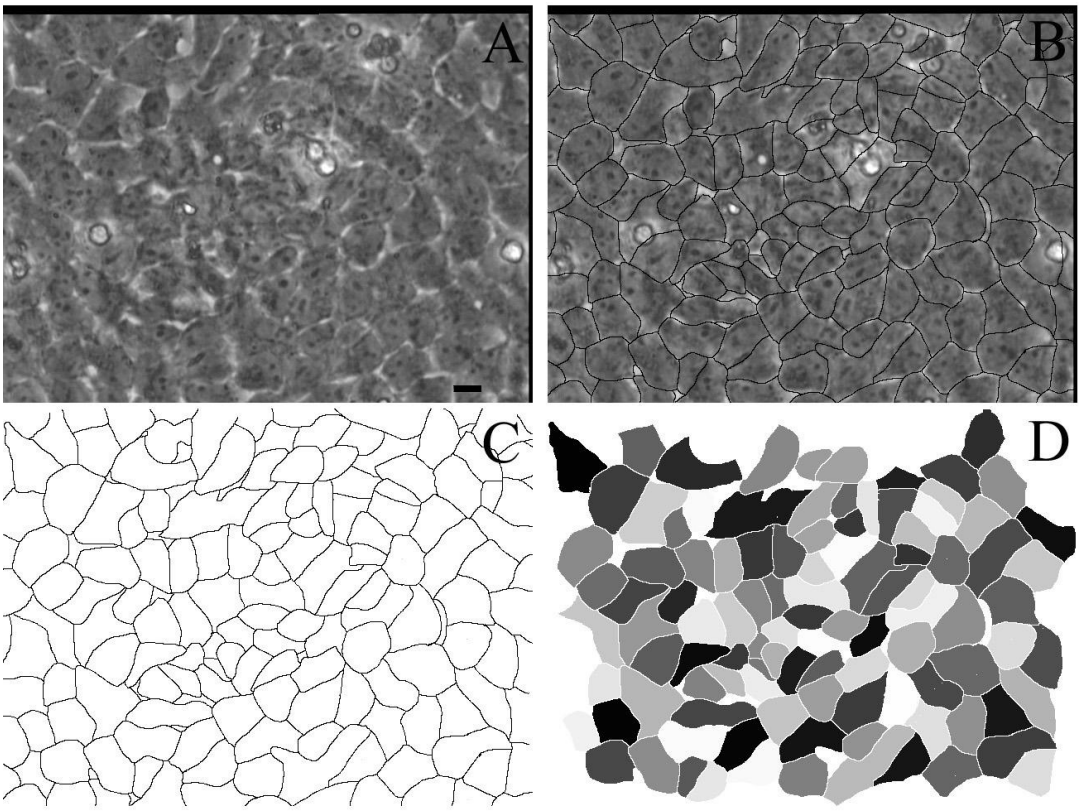

Figure 3.8: Digitization of images of a chick-leg embryonic (HH stage 25) mesenchymal micromass cell-culture. A) Original image. B) Image with boundaries drawn by hand in Photoshop. C) Tracked cell boundaries. D) Digitized image with gray-level-labeled cells. The scale bar in the bottom-right corner of (A) corresponds to 10 μm. White circular spots in (A) are cells which detached from the confluent cell layer during the experiment.

	Image Set I	Image Set II
Number of digitized images	39	25
Time interval	4 min	20 min
Number of cells labeled	89	92
Statistical measurements	Temporal auto-correlation of velocities	All others

Table 3.1: The two digitized image sets of cell movements during micromass culture of embryonic (HH stage 25) chick-leg mesenchymal cells.

and assigned it the mother cell's gray level. We used this daughter cell in our statistical measurements. We assigned the other daughter cell a new gray level and omitted it from our statistical measurements. By these criteria, image set I had 89 labeled and tracked cells and image set II had 92 labeled and tracked cells.

We used Matlab for image processing and data analysis. We recorded cell surface areas, which we interpreted as areas of contact with the underlying substrate, for all labeled cells. We used the two-dimensional coordinates of the center of mass $\vec{r}\,=(x_i,\, y_i)$ to analyze cell displacements. We approximated the velocity of cells at time t as $\vec{v}_{i(t)} = (\vec{r}_{i(t)} - \vec{r}_{i(t-\Delta t)})/\Delta t$, where Δt is 4 minutes in image set I and 20 minutes in image set II. To study cell deformations, we fitted the cells with ellipses (figure 3.9) and measured the eccentricity vector $\vec{e}$ which has magnitude equal to the eccentricity and inherits the direction of orientation of the major axis of the fitting ellipse (Matlab function 'imfeature'). The eccentricity vector $\vec{e}$ characterizes the cell's elongation.

3.2.4 Flatness of Distributions

We used the *Kolmogorov-Smirnov test* (*K-S test*) to see if a given distribution was statistically flat, or not. We converted the list of data points into an un-

biased estimator $S_N(x)$ of the *culmulative probability distribution* (*CPD*) from which we drew it. If the N events have values x_i, $i = 1,\ldots,N$, then $S_N(x)$ gives the fraction of data points to the left of x. For a flat distribution, we should find a straight line $S_N(x) = mx + b$ with $m = 1/|x_{max} - x_{min}|$. If the maximum difference between the CPD of a given distribution and the CPD of a flat distribution with the same range of x values is less than 5% (of 1.0), the distribution is *statistically flat*.

3.3 Experimental Results

3.3.1 Cell Movement and Deformation

After 24 hours of incubation in a CO_2 incubator, mesenchymal cells settled onto the substrate surface, flattened, and formed a continuous monolayer. During the experiment, cells in this monolayer moved, changed their relative positions, and deformed continuously. Cells divided occasionally (27 cells divided during 760 minutes in a population of about 145 cells and 8 of 92 labeled cells divided during the first 480 minutes). Figure 3.10 shows the center-of-mass positions of 17 cells at random, well-separated locations during the first 480 minutes. Some cells moved long distances, while others did not. Cells moved much less than their radius between frames, permitting movement and deformation analyses.

3.3.2 Decrease in Cell-Substrate Contact Area

Since the cells remained in a confluent monolayer and more cells migrated into than out of the field of view (*FOV*) (table 3.2), the average surface area of the

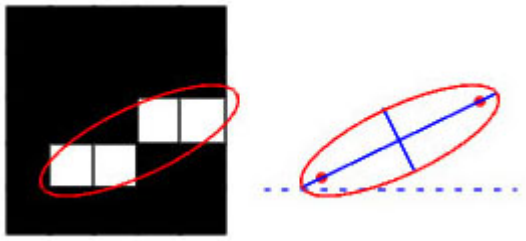

Figure 3.9: Cell fitting with an ellipse. The angle between the horizontal axis and the major axis of the ellipse defines the orientation of the cell. The eccentricity vector $\vec{e}$ has the magnitude of the eccentricity of the fitting ellipse and the direction of the orientation of the major axis of the fitting ellipse.

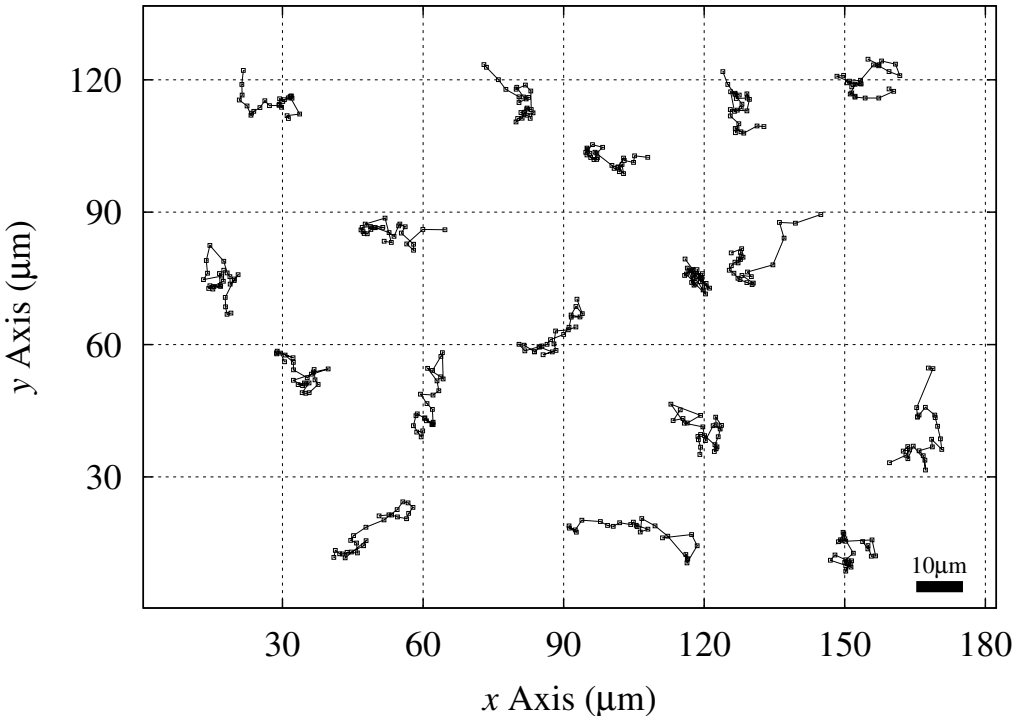

Figure 3.10: Trajectories of 17 embryonic (HH stage 25) chick-leg mesenchymal cells in micromass cell-culture over 8 hours, or 480 minutes. Dots indicate their center-of-mass positions at 20 minutes intervals. Scale bar: 10μm.

Class of Cells	Number of Cells
Cells present in all 25 digitized images	92
Cells moving into the FOV	23
Cells moving out of the FOV or disappearing	11

Table 3.2: Counts of cells moving into, out of, or remaining in the field of view (*FOV*) for image set II.

cells decreased (figure 3.11). The rate of decrease was about 0.030 μm^2/min and the average surface area of the cells decreased from about 171 to 157 μm^2.

3.3.3 Bulk Cell Movement

Figure 3.12 shows the center-of-mass trajectory averaged over all analyzed cells in image set II. The average center-of-mass stays within a 4μm×5μm box around its initial position, indicating a lack of coherent motion in the aggregate during the 8 hours of observation.

3.3.4 Cells Velocities and Orientations

Figure 3.13 shows that the mean cell speed decreases at the rate of 7.4×10^{-5} μm/min^2, or 0.018 μm/min (about 14%) in 4 hours. Figure 3.14 shows that the direction of cell movement is unbiased, again indicating the absence of bulk flows.

We used the K-S-test method (see section 3.2.4) to show that the distribution of cell movement directions is statistically flat (the maximum difference is 2.64%, see figure 3.15).

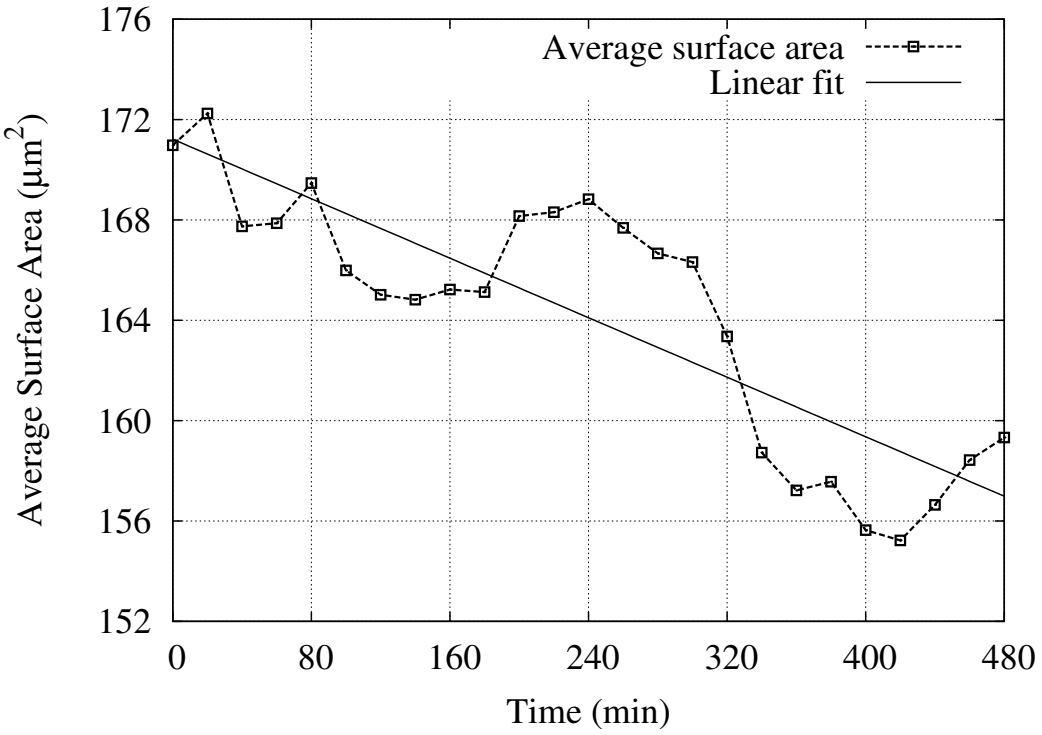

Figure 3.11: Average surface area of embryonic (HH stage 25) chick-leg mesenchymal cells in micromass cell-culture as a function of time, fitted to a straight line, area = $171.2 - 0.030t$ μm^2.

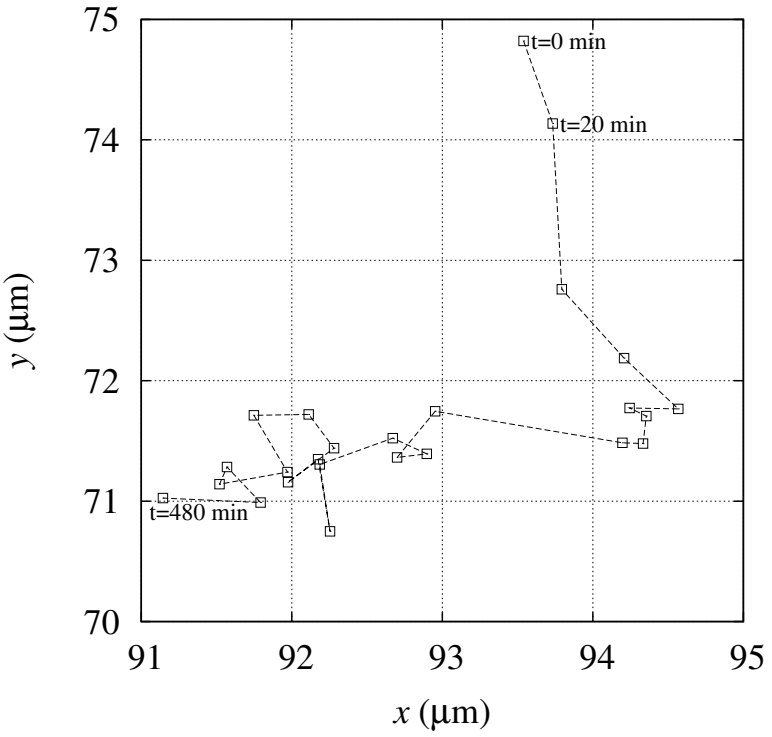

Figure 3.12: Trajectory of the average center-of-mass of all analyzed embryonic (HH stage 25) chick-leg mesenchymal cells in micromass cell-culture in image set II (8 hours).

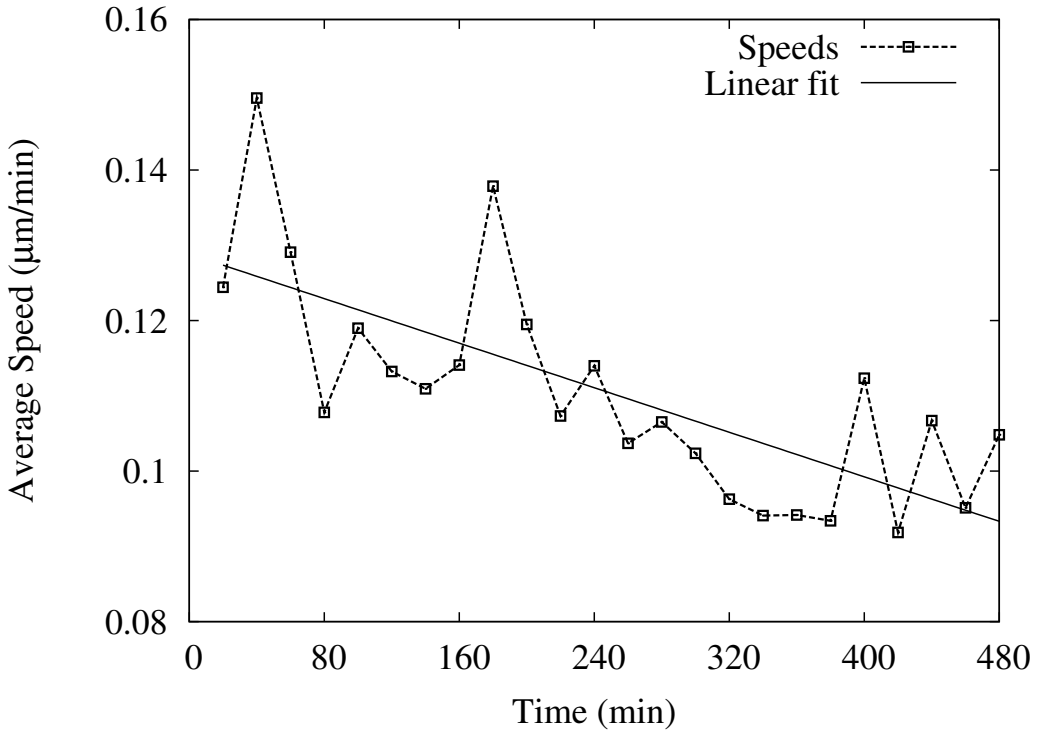

Figure 3.13: Average speed of embryonic (HH stage 25) chick-leg mesenchymal-cell movement in micromass cell-culture at different times in image set II.

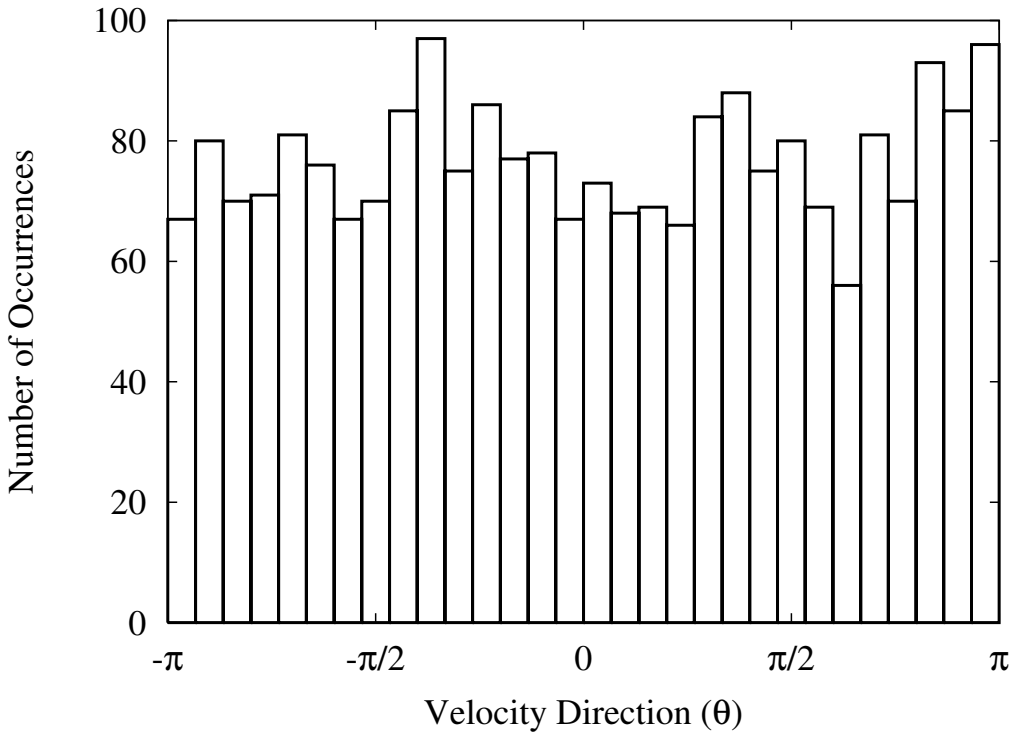

Figure 3.14: Distribution of movement directions of embryonic (HH stage 25) chick-leg mesenchymal cells in micromass cell-culture.

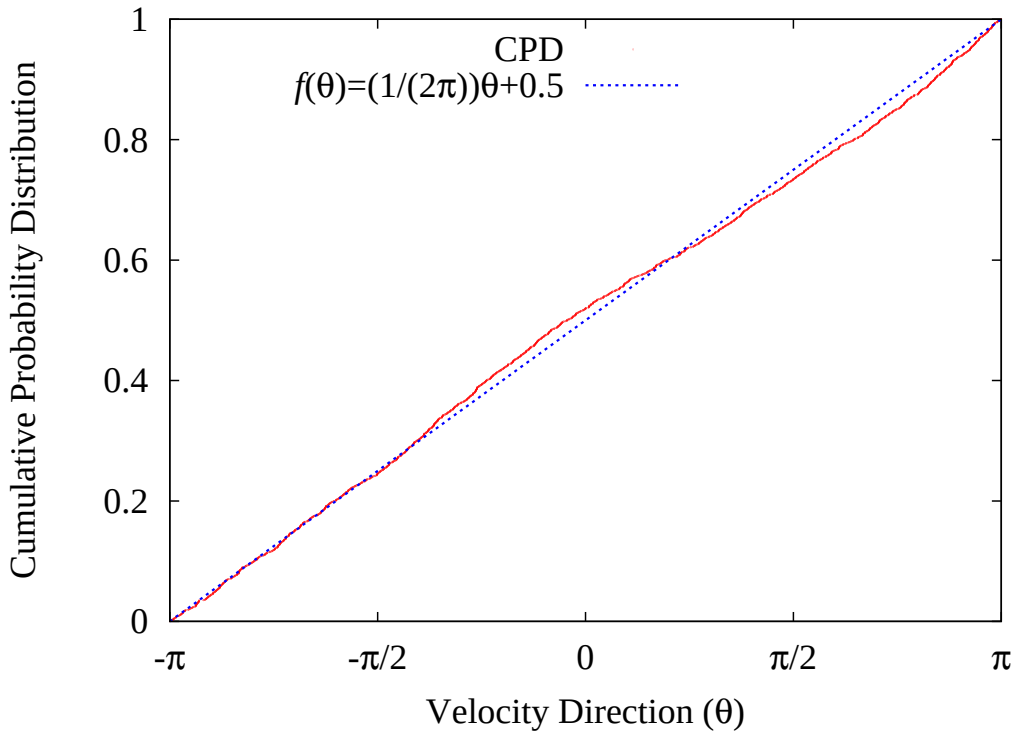

Figure 3.15: Cumulative probability distribution (*CPD*) of movement directions of embryonic (HH stage 25) chick-leg mesenchymal cells in micromass cell culture. The maximum difference is 2.64%. The distribution is statistically flat.

3.3.5 Cell Deformation, Cell Movement and Elongation Direction

We used the Matlab function 'imfeature', to fit the cell surfaces with ellipses as shown (figure 3.9) in order to find the cells' *elongation direction*, the angle between the major axis of the fitting ellipse and the horizontal axis. The *eccentricity* of the fitting ellipse is $e = \sqrt{1 - b^2/a^2}$, where a is the major axis and b is the minor axis and the eccentricity of a circle is 0. Figures 3.16 and 3.17 show that, at most times, most cells are elongated rather than isotropic with $<e>= 0.7388$.

Rietdorf *et al.* found that during late mound development, *Dictyostelium discoideum* cells show a pronounced correlation between their changes in velocity (movement) and shape (elongation) [89]. To relate cell elongation to movement, we histogram the angles between the eccentricity vectors $\vec{e}$ and velocity vectors $\vec{v}$ in image set II. We map the angles into the quadrant between 0 and $\pi/2$ because cell behavior is symmetrical along the axis of movement. We weighted the occurrence of an angle by counting that angle $|\vec{e}| \cdot |\vec{v}|$ times. If cells preferred to elongate at a particular angle θ_0 with respect to their direction of movement, we should see a peak in the histogram at this angle. However, the K-S test (figure 3.19) shows that the distribution of angles in figure 3.18 is statistically flat (the maximum difference is 1.42%, less than 5%), so the vector $\vec{e}$ does not lie at a preferred angle from $\vec{v}$. In other words, cells in micromass culture do not elongate in a particular direction with respect to their direction of movement.

Sometimes cells squeeze through small spaces between two neighboring cells in the monolayer and the substrate or crawl on top of the monolayer, either

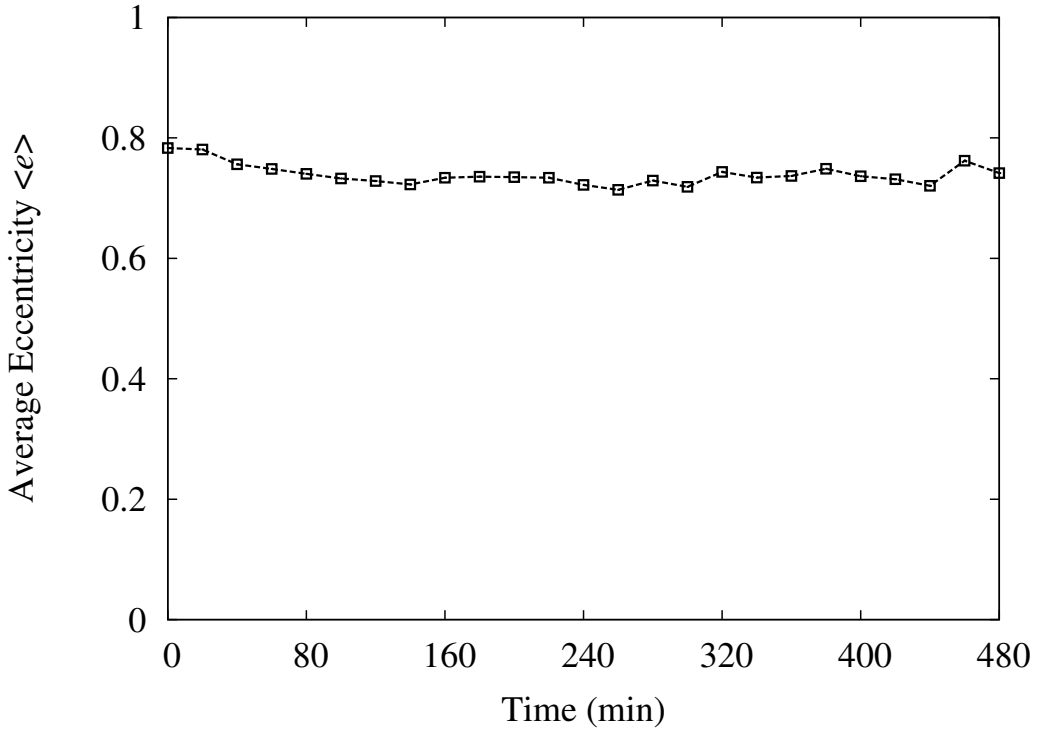

Figure 3.16: Average eccentricities of embryonic (HH stage 25) chick-leg mesenchymal cells in micromass cell-culture at different times in image set II.

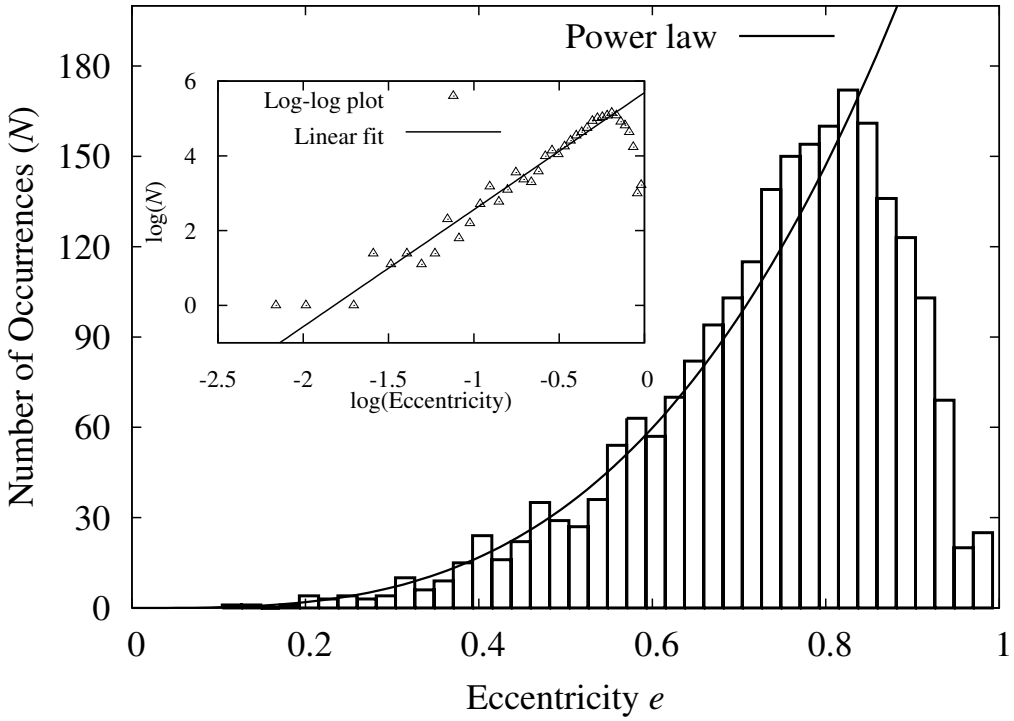

Figure 3.17: Distribution of eccentricities of fitting ellipses in the 25 images of image set II for 92 embryonic (HH stage 25) chick-leg mesenchymal cells in micromass cell-culture. Fitting functions are the exponential, $N = e^{6.61e}$, and power-law, $N = 296e^{3.13}$.

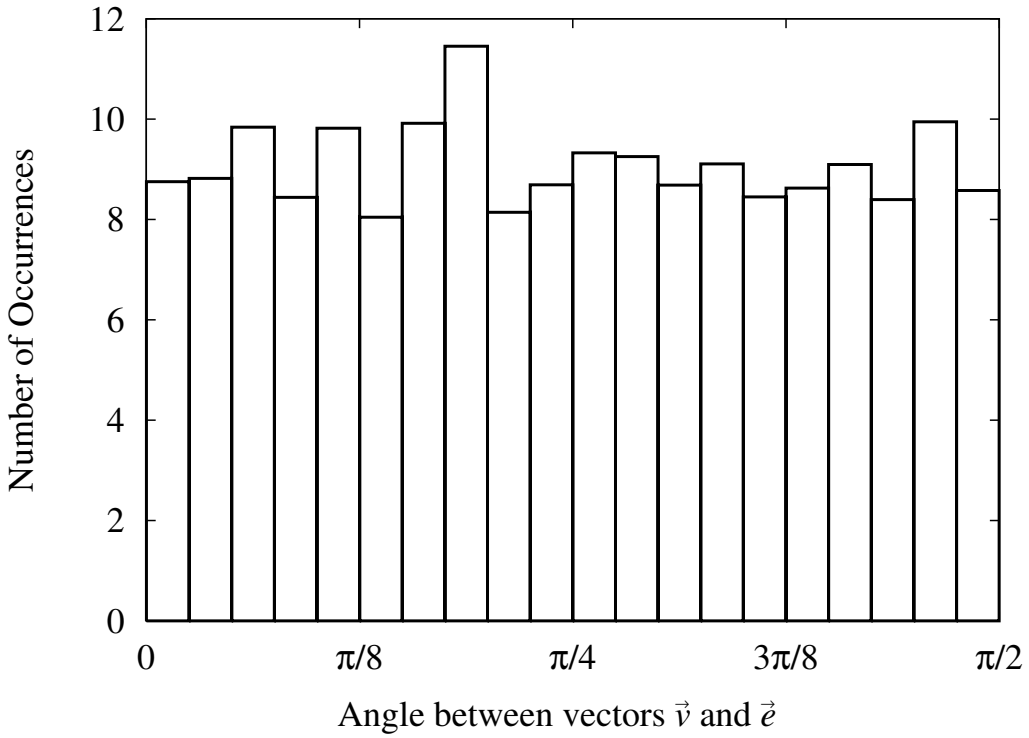

Figure 3.18: Histogram of the angles between the eccentricity vectors $\vec{e}$ and the velocity vectors $\vec{v}$ weighted by the factor $|\vec{e}| \cdot |\vec{v}|$ for embryonic (HH stage 25) chick-leg mesenchymal cells in micromass cell-culture.

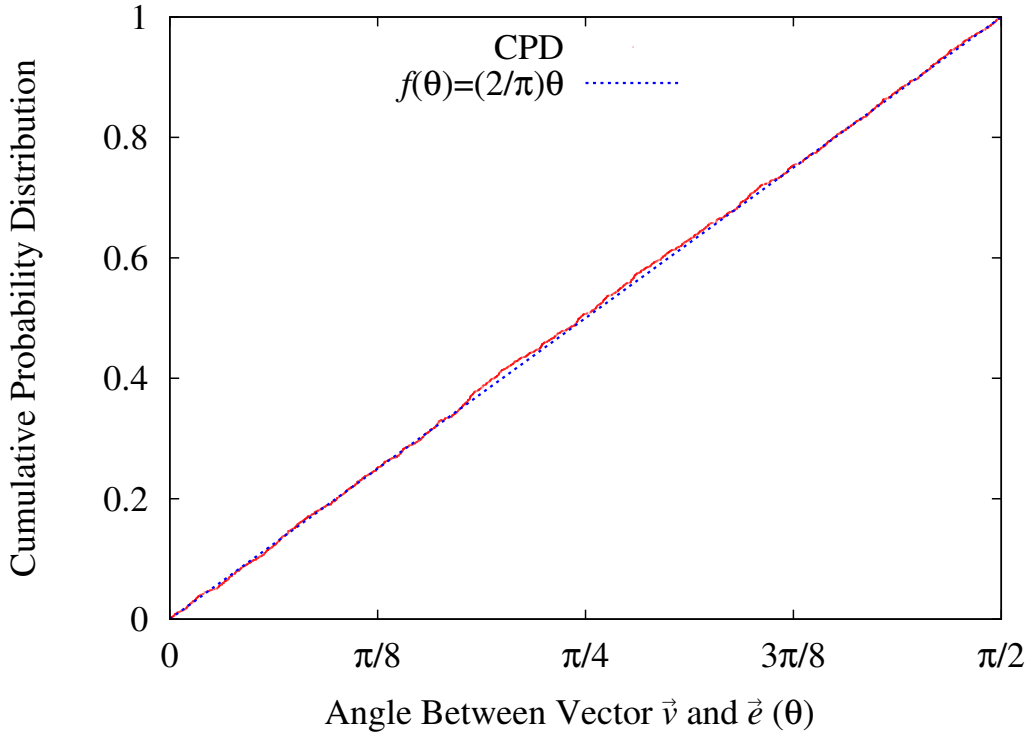

Figure 3.19: Cumulative probability distribution of angles (θ) between the eccentricity vectors $\vec{e}$ and the velocity vectors $\vec{v}$ weighted by the factor $|\vec{e}| \cdot |\vec{v}|$. Since the maximum difference is 1.42%, less than 5%, the distribution in figure 3.18 is statistically flat.

temporarily disappearing themselves or obscuring other cells. Since we cannot identify these obscured cells between frames we do not include them in our statistical measurements. Since only two cells disappeared and two cells appeared in the field of view during the experiment (480 minutes in image set II), this type of movement did not affect greatly our statistical results.

3.3.6 Auto-Correlation of Velocities

We used image set I to calculate the auto-correlation of velocity ($C(t)$) as a function of the time interval t for image set I (figure 3.20), which measures the persistence time of the velocity:

$$C(t) = \frac{Z(t)}{Z(0)}, \tag{3.1}$$

with,

$$Z(t) = \frac{1}{89}\sum_{i=1}^{89}(\vec{v}_i(t_0+t)\cdot\vec{v}_i(t_0)), \tag{3.2}$$

and,

$$Z(0) = \frac{1}{89}\sum_{i=1}^{89}|\vec{v}_i(t_0)|^2, \tag{3.3}$$

where $t{=}n\cdot\Delta t$, n=1,2,...,37 and Δt=4 min.

Since the correlation decays to zero within 4 minutes and remains near zero thereafter, the velocity auto-correlation time is less than 4 minutes.

3.3.7 Temporal Angular Correlation

We calculated the temporal angular correlation ($C'(t)$) as a function of the time interval t for image sets I and II (figure 3.21):

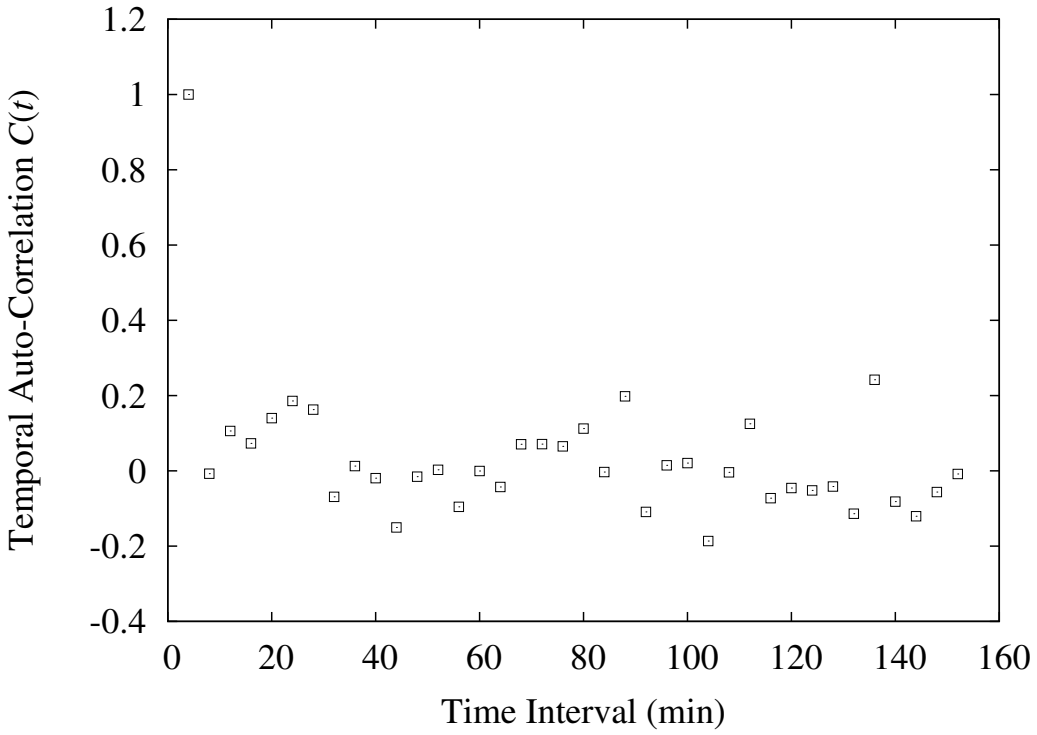

Figure 3.20: Temporal auto-correlation of the velocity *vs.* time interval, t, for image set I (see section 3.3.6) for embryonic (HH stage 25) chick-leg mesenchymal cells in micromass cell-culture. Time step Δt=4 min.

$$C'(t) = \frac{Z'(t)}{Z'(0)}, \tag{3.4}$$

with,

$$Z'(t) = \frac{1}{N}\sum_{i=1}^{N}(\theta(t_0 + t) \cdot \theta(t_0)), \tag{3.5}$$

and,

$$Z'(0) = \frac{1}{N}\sum_{i=1}^{N}(\theta(t_0)^2), \tag{3.6}$$

where N is the number of cells labeled in each image set (see table 3.1). For image set I, $t = n \cdot \Delta t$, $n = 1, 2, ..., 37$ and Δt is 4 minutes. We fitted the temporal angular correlation ($C'(t)$) to an exponential and found that the angular correlation time was 8.3 minutes.

3.3.8 Spatial Velocity Correlation

We assigned to all pixels in labeled cells the velocity vectors of their cells and calculated the spatial correlation of velocities in image set II ($C''(r)$) as a function of distance at different times:

$$C''(r) = \frac{1}{N}\sum_{i}\sum_{|\vec{r}_j - \vec{r}_i| = r}\frac{\vec{v}_i \cdot \vec{v}_j}{|\vec{v}_i|^2 \cdot |\vec{v}_j|^2}, \tag{3.7}$$

where i and j indicate pixels in labeled cells, r is the distance between the pixels, $\vec{v}_i$ and $\vec{v}_j$ are the velocities of the respective cells' centers-of-mass and N is the number of pixel pairs at a distance r. We used 5 pixel or 1.42 μm steps to calculate $C''(r)$. For example, we used all velocity pairs with distance $r = (0, 1.42]$ μm to calculate $C''(1.42\mu\text{m})$. Figure 3.22 shows a typical correlation

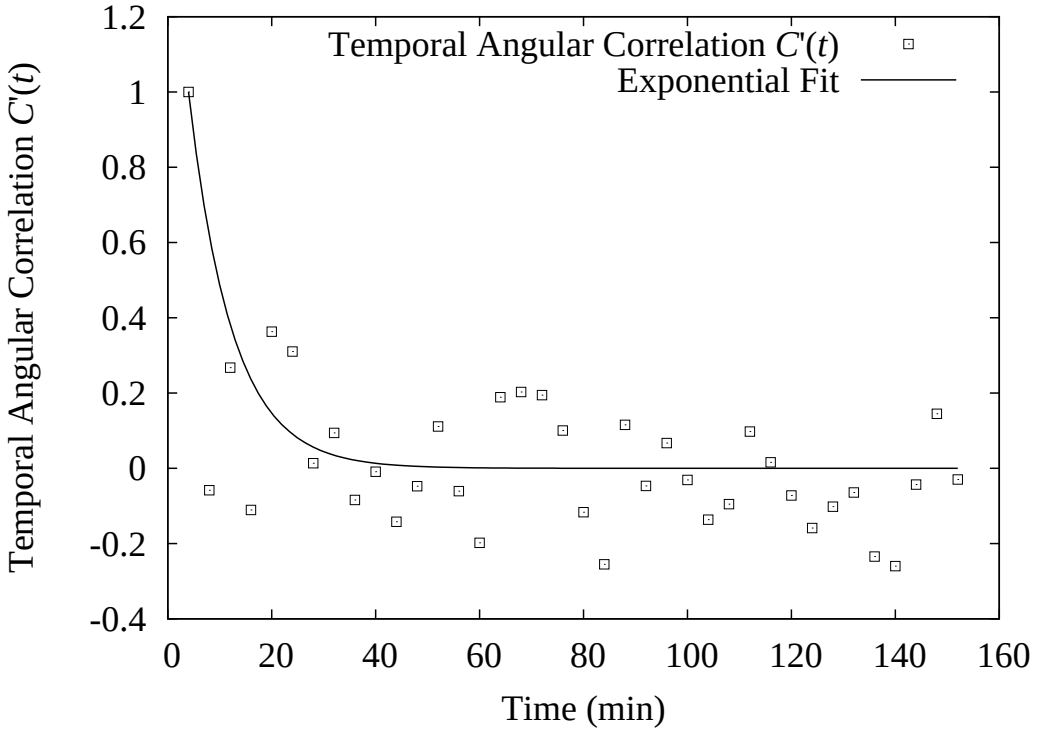

Figure 3.21: Temporal angular correlation of the velocity *vs.* time interval t for cells in image set I. Time step Δt=4 min. Fitting function is $f(t) = e^{(t-4)/8.3}$.

(for frame 2) and the correlation averaged over different times in image set II.

Figure 3.23 shows short-range spatial correlations in the cell velocities. The correlation length is on the order of 7 μm, which is about the radius of a cell.

3.3.9 Condensation Centers

In vivo we can identify precartilage condensation centers by their close-packed cells. In micromass cell-cultures, we can identify condensation centers by looking for patches of cells with smaller surface areas. At the magnification in our experiment, where we have about 100 cells and only one condensation center in the microscope's field of view, we can easily measure the cells' surface areas to find the condensation center. However, if we want to study the behavior of thousands of cells and several condensation centers and to track fluorescently-labeled cells, we need another way to identify condensation centers, because measuring individual cells' surface areas will be impractical.

For image set II we measured the surface area of each cell in each frame, then converted these values into a smooth color map (figure 3.24). We chose points at 25 pixel (or 7.1 μm) spacing in both $\hat{x}$ and $\hat{y}$ directions. The first such point has coordinates (20, 15) in pixels. For each point, we added the surface areas of all the cells whose center-of-mass lay within 150 pixels (or 42.6 μm) to calculate the average surface area for the point, for all 25 digitized images. So, each digitized image has a corresponding averaged area matrix. We then averaged these 25 matrices to generate an averaged surface-area matrix with dimension 19 by 25, resized it to the scale of the original images using two-dimensional linear interpolation and generated a color map in Matlab. The average surface

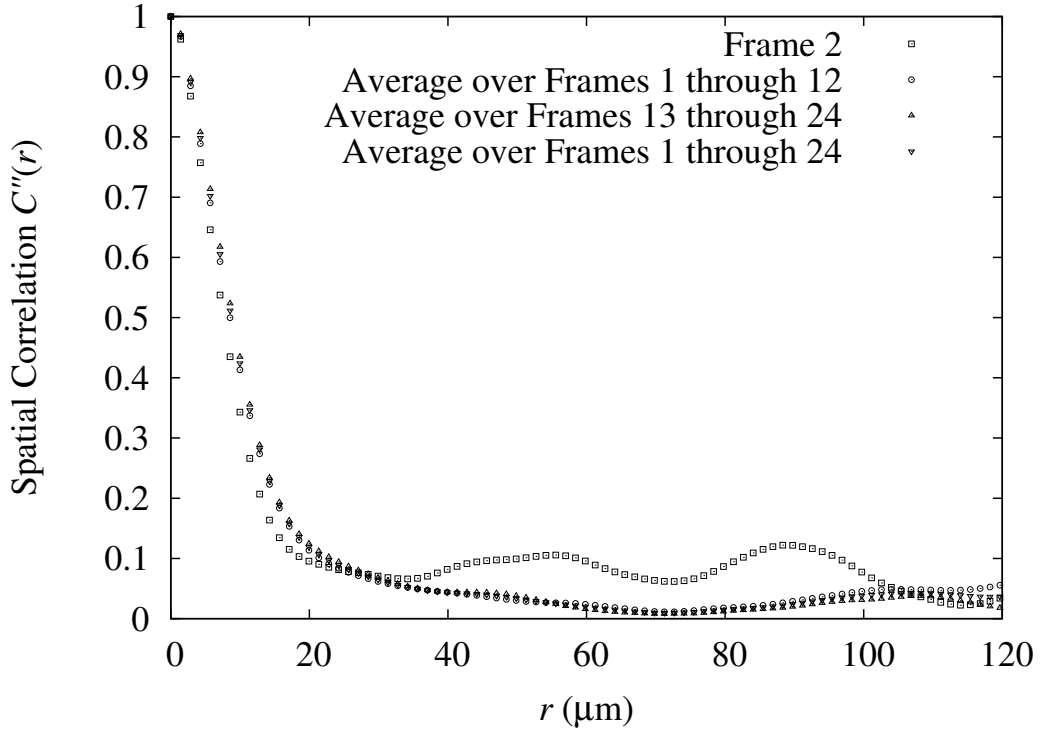

Figure 3.22: Spatial auto-correlation of velocities for frame 2 in image set II, and the spatial auto-correlation averaged over various frame intervals, also for image set II.

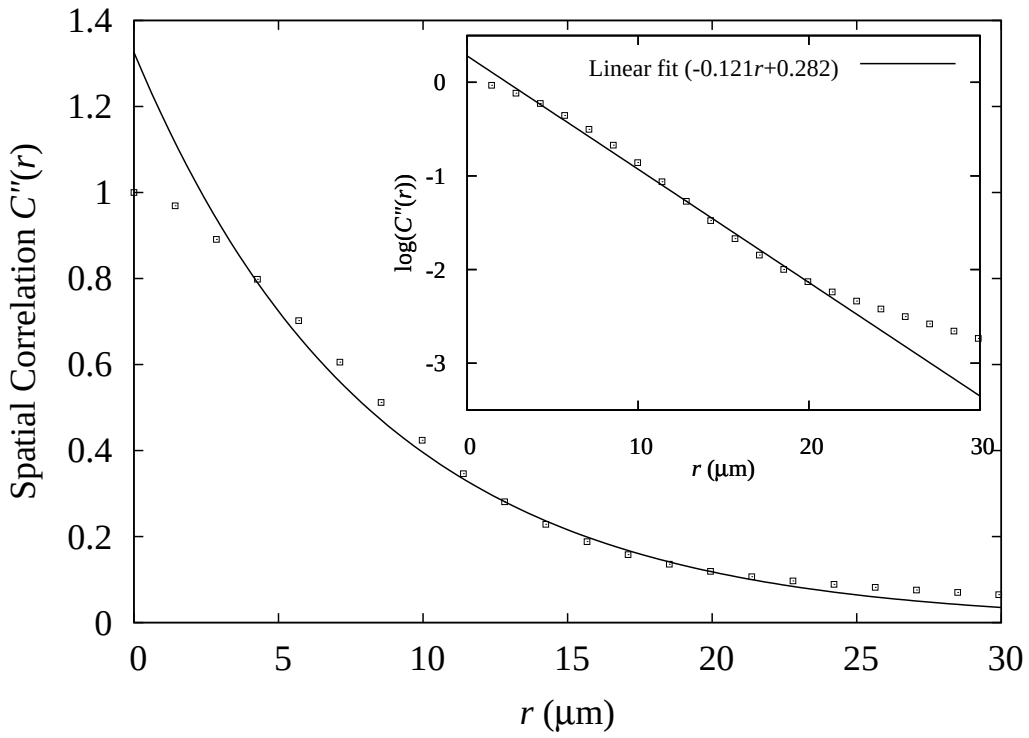

Figure 3.23: Exponential fit (line) to the spatial correlation (squares) averaged over frames 1 through 24 (see figure 3.22). The inset shows the linear fit (line) to a log plot of the data (squares).

area ranged between 120 μm^2 and 266 μm^2. We drew a contour line at an average surface area of 160 μm^2. To determine the center of the condensation (x_0, y_0), we averaged the position of all points inside the contour line, weighting each point (x_i, y_i) by its average surface area $s(x_i, y_i)$:

$$x_0 = \frac{\sum_{x_i,y_i}(x_i \cdot s(x_i, y_i))}{\sum_{x_i,y_i} s(x_i, y_i)}, \tag{3.8}$$

$$y_0 = \frac{\sum_{x_i,y_i}(y_i \cdot s(x_i, y_i))}{\sum_{x_i,y_i} s(x_i, y_i)}. \tag{3.9}$$

The cluster center was at (199.25, 331.36) pixels, or (56.77 μm, 94.40 μm).

3.3.10 Relative Cell Velocities

For image set II we measured the speed of each cell in each frame, then converted these values into a smoothed speed color map (figure 3.25). As for the average-area map, we chose points at 25 pixel (or 7.1μm) spacing in both the $\hat{x}$ and $\hat{y}$ directions. The first point has coordinates (20,15) pixels. For each point, we added the speeds of all the cells whose centers-of-mass lay within 150 pixels (or 42.6μm) to calculate the average speed for each point, for all 25 digitized images. We then averaged these 25 matrices to generate the average-speed matrix with dimensions 19 pixels by 25 pixels, and resized it to the scale of the original images using bilinear interpolation and generated a color map in Matlab.

Figures 3.24 and 3.25 correspond closely: cells near the center of condensation (330 pixels, 200 pixels) have smaller surface areas and move faster than cells in the periphery. To find the correlation between surface area and speed, we plotted average speed *vs.* average surface area for areas between 123.6μm^2

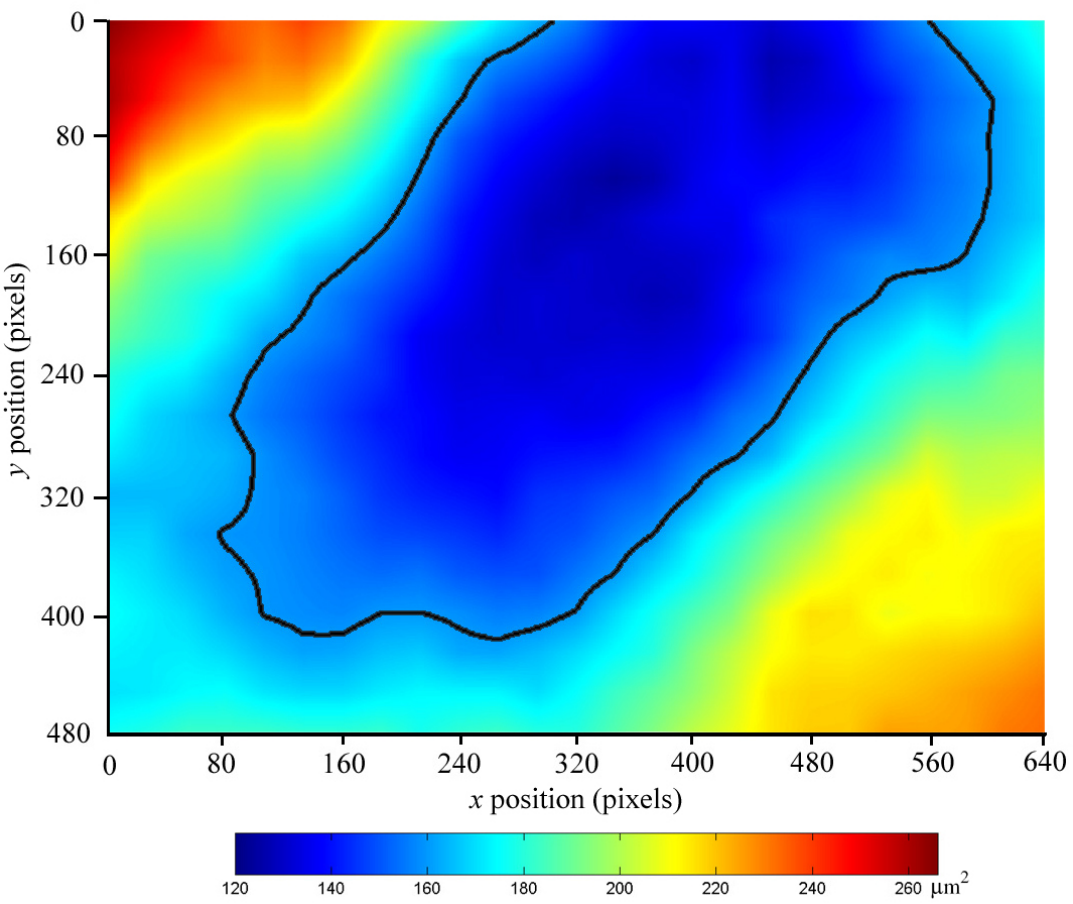

Figure 3.24: Color map of averaged cell surface area for cells in image set II. See text for details. Black line: contour line for area = 160 μm^2. The units of the $\hat{x}$ and $\hat{y}$ axes are pixels and the color bar is labeled in units of μm^2.

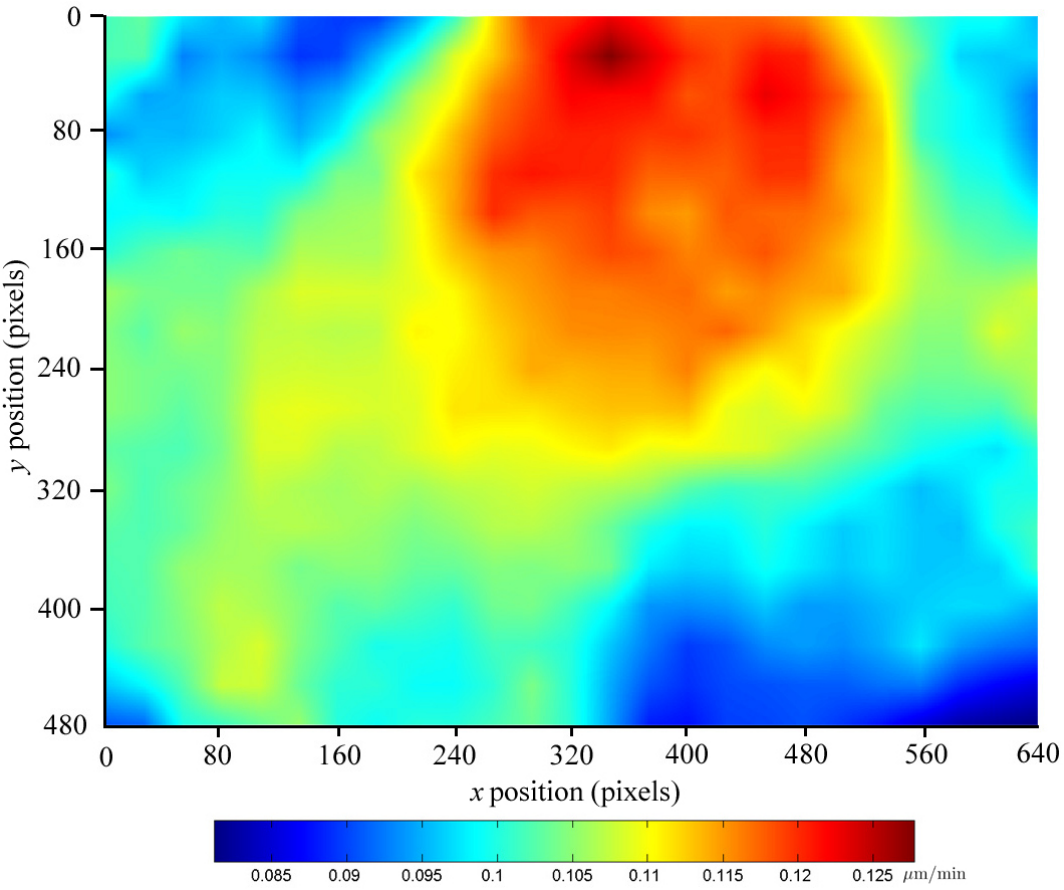

Figure 3.25: Color map of the average cell speed for cells in image set II. The units of the $\hat{x}$ and $\hat{y}$ axes are pixels and the color bar is labeled in units of μm/min.

and 265.1μm^2 with a bin width of 7.075μm^2. For example, all points with average surface area [123.6μm^2, 130.675μm^2) belong to the first bin. We averaged the speeds for points in each bin. Figure 3.26 shows that the average speed decreased linearly and monotonically with increasing surface area.

3.3.11 Cell Velocities

We plotted the cell-speed distribution inside and outside the condensation center for image set II (figure 3.27).

We used the first 1024 speeds for cells inside the condensation center and all (792) occurrences for cells outside the condensation center and performed a *Student's t-test* to determine if the two distributions had significantly different mean values. The Student's t is 4.01 and the probability of this result, assuming the null hypothesis that these two distributions' differences are due to chance, is less than 0.0001. So, the mean values of the two speed distributions indeed differ significantly and the average speed of cells inside the condensation center is significantly faster than that of cells outside.

3.3.12 Condensation-Center Radius

We drew 8 concentric bands centered on the center of condensation (94.0μm, 57.0μm) with a band width of 14.2 μm (see figure 3.28). To characterize the size of the condensation center, we plotted the flux of cells towards the condensation center in each band.

We defined the flux in a band as $v_r = \vec{v} \cdot \hat{r}$ averaged over all cells in the band over all 25 images in image set II, where $\hat{r}$ is the unit vector pointing from the

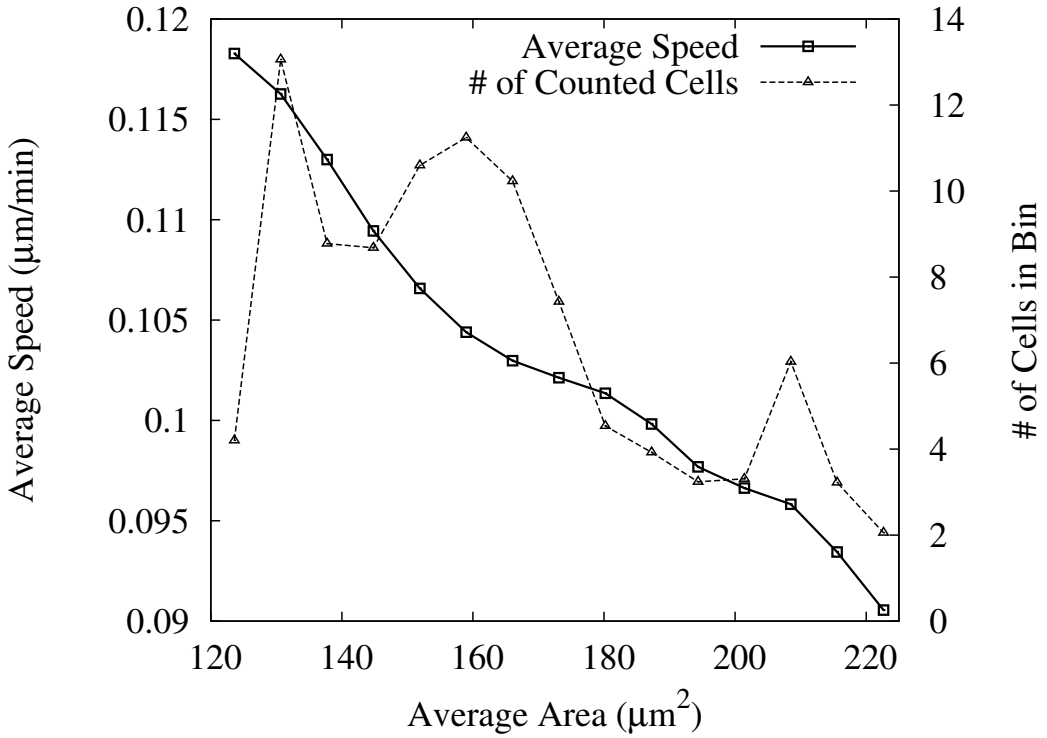

Figure 3.26: Average speed of cells (left $\hat{y}$ axis) and number of cells per bin (right $\hat{y}$ axis) as a function of average cell surface area in micromass cell-culture of embryonic (HH stage 25) chick-leg mesenchymal cells. We omitted the average speeds for surface areas larger than 220 μm^2 because the number of cells per bin was less than 3.

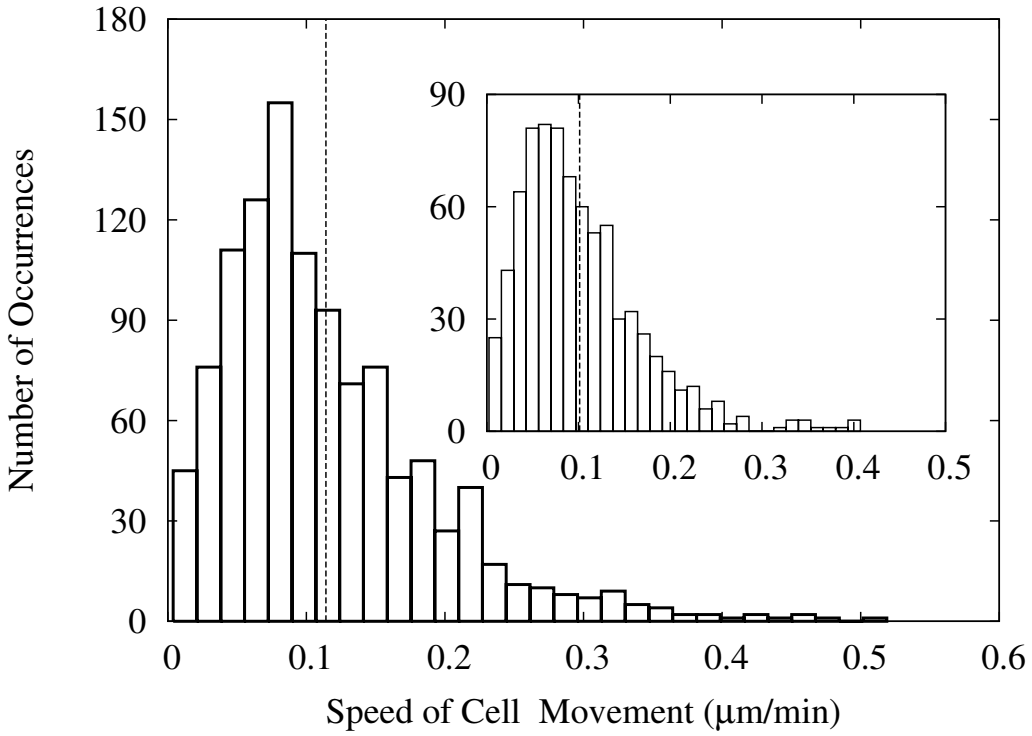

Figure 3.27: Histograms of speeds for cells staying inside (main graph) and outside (inset) the condensation center in image set II with the center-of-mass movement of all cells and drift of cells outside the condensation center subtracted for micromass cell-culture of embryonic (HH stage 25) chick-leg mesenchymal cells. The dashed line in the main graph indicates that the average speed of cells staying inside the condensation center was 0.1141 μm/min, and the dashed line in the inset indicates that the average speed of cells staying outside the condensation center was 0.1012 μm/min.

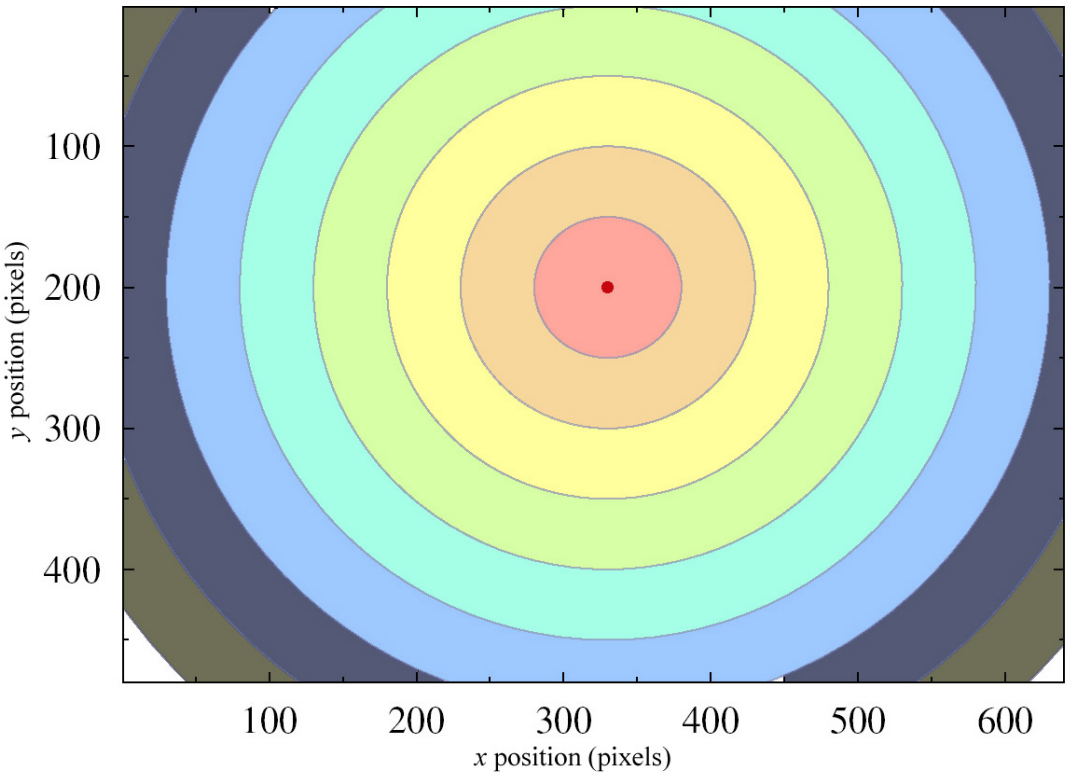

Figure 3.28: Concentric bands centered at the center of condensation (330, 200) with a band width of 50 pixels.

center-of-mass of the cell to the center of condensation, and $\vec{v}$ is the velocity of the cell. So, in a particular band, if v_r is greater than zero, the cells in that band, on average, move towards the center of condensation. On the other hand, if v_r is less than zero in a band, the cells in that band, on average, move away from the center of condensation. In figure 3.29, cell fluxes are around zero in bands 3, 4 and 5 (42.6μm, 56.8μm, 71.0μm from the center of condensation), while cell fluxes are positive in bands 6, 7 and 8 (85.2μm, 99.4μm and 113.6μm from the center of condensation) indicating that most cells in these bands move towards the center of condensation. Figure 3.29 shows a monotonic increase of the average flux with distance from the condensation center. So we could characterize the size of the condensation center by measuring where the flux is zero. The radius of the condensation center in our experiment was about 57.0μm with the center of condensation at (94.0μm, 57.0μm).

We also plotted the average speeds in the bands in figure 3.29, again showing that cells in the condensation center moved faster than cells in the periphery (confirming the result in section 3.3.10).

3.3.13 Changes in Cell Diffusion Rates

To rule out the possibility that the apparent change of diffusion constant of cells inside the condensation center resulted from center-of-mass movement of the whole aggregate or drift of cells outside the condensation center towards the center of condensation, we calculated the mean-squared displacement (*MSD*) for cells inside and outside the condensation center and for all cells (with the center-of-mass movement of the whole aggregate and drift of cells outside the

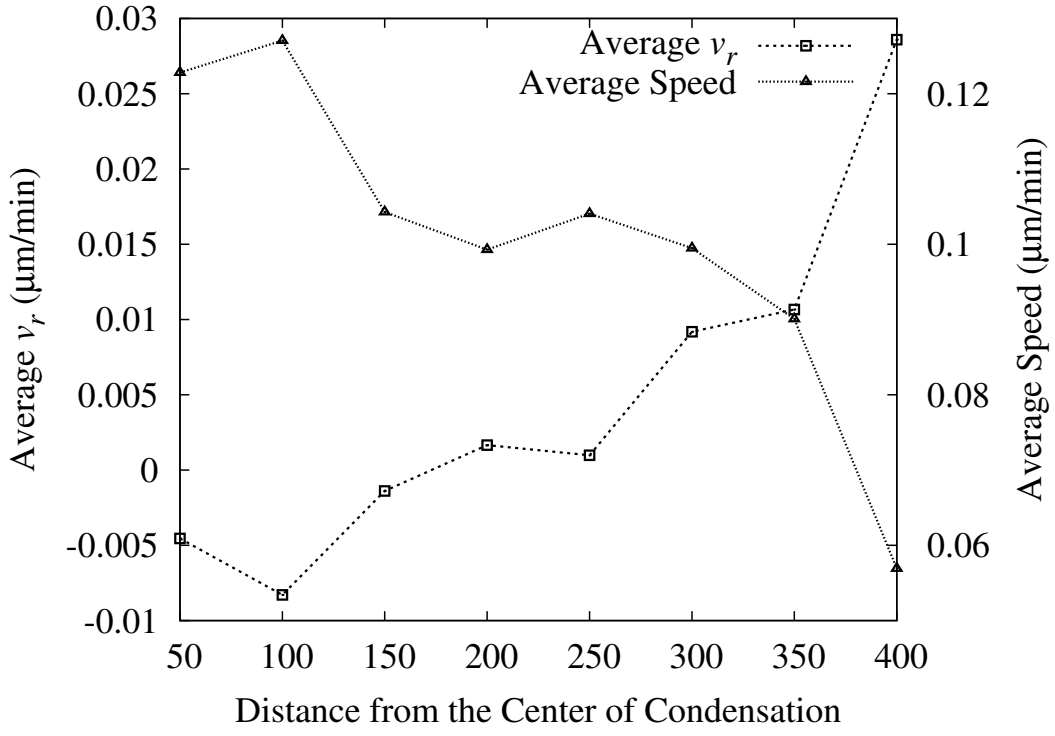

Figure 3.29: Cell flux towards the center of condensation at (330 pixels, 200 pixels) and average cell speed as a function of distance from the center of condensation in micromass cell-culture of embryonic (HH stage 25) chick-leg mesenchymal cells.

condensation center subtracted) during the periods 0-240 minutes (figure 3.30) and 240-480 minutes (figure 3.31). Using the result for a two-dimensional random walk,

$$<r^2>= 4Dt, \tag{3.10}$$

we found that the diffusion coefficient $D = 0.136 \pm 0.002\mu\text{m}^2/\text{min}$ between 0 and 240 minutes and $D = 0.083 \pm 0.004\ \mu\text{m}^2/\text{min}$ between 240 and 480 minutes. Between 0 and 240 minutes the diffusion coefficient $D = 0.157 \pm 0.002\ \mu\text{m}^2/\text{min}$ for cells inside the condensation center and $D = 0.116 \pm 0.002\ \mu\text{m}^2/\text{min}$ for cells outside the condensation center, between 240 and 480 minutes inside $D = 0.078 \pm 0.003\mu\text{m}^2/\text{min}$ and outside $D = 0.093 \pm 0.003\mu\text{m}^2/\text{min}$. Thus all cells gradually slow in time, while cells inside the condensation center move faster than cells outside at early times. The result is surprising, since we would expect cells bound to fibronectin in the substrate to diffuse more slowly than the weakly-bound cells outside. However, our data also suggest that cells inside the condensation center will move slower than cells outside at late times (smaller diffusion constant for cells inside the condensation center than for cells outside the condensation center as shown in figure 3.33), which is experimentally correct at later stages in the micromass culture.

3.3.14 Directed Cell Movement

Cell movement velocity consists of two components: a directed-cell-movement velocity $\vec{v}_{directed}$ and a random-cell-movement velocity $\vec{v}_{random}$:

$$\vec{v} = \vec{v}_{directed} + \vec{v}_{random}. \tag{3.11}$$

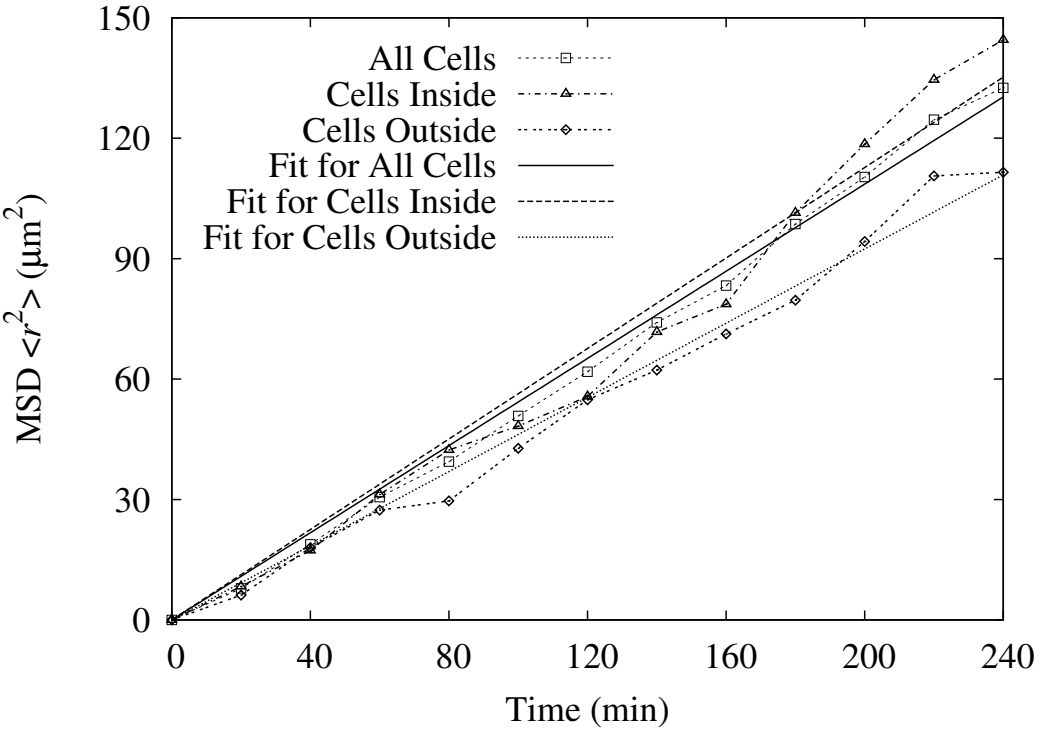

Figure 3.30: Mean-squared displacement between 0 and 240 minutes for all cells, cells inside the condensation center and cells outside the condensation center, with center-of-mass movement of all cells and drift of cells outside the condensation center subtracted.

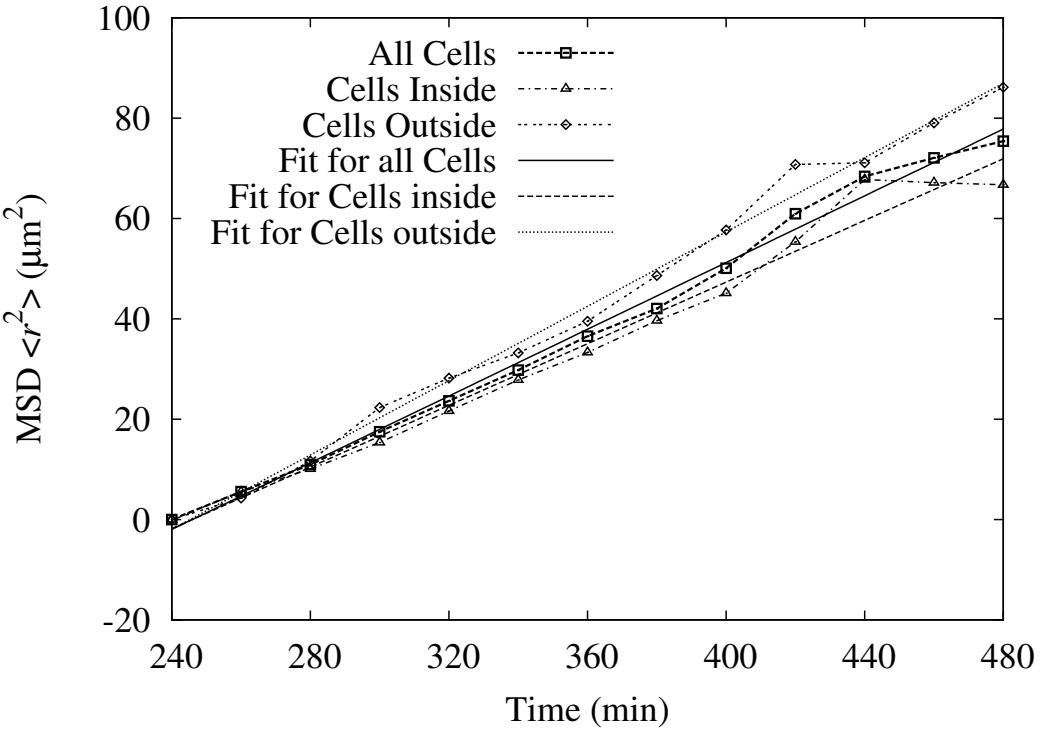

Figure 3.31: Mean-squared displacement between 240 and 480 minutes for all cells, cells inside the condensation center and cells outside the condensation center, with center-of-mass movement of all cells and drift of cells outside the condensation center subtracted.

Since $<\vec{v}_{random}>= 0$ and $<2 \cdot \vec{v}_{directed} \cdot \vec{v}_{random}>= 0$, we have:

$$<\vec{v}^2> = <\vec{v}^2_{directed} + 2 \cdot \vec{v}_{directed} \cdot \vec{v}_{random} + \vec{v}^2_{random}> \quad (3.12)$$

$$= <\vec{v}^2_{directed}> + <\vec{v}^2_{random}>, \quad (3.13)$$

$$<\vec{v}>^2 = <\vec{v}_{random}>^2 + <\vec{v}_{directed}>^2 \quad (3.14)$$

$$= <\vec{v}_{directed}>^2 . \quad (3.15)$$

We calculated the average kinetic ratio ($<\vec{v}>^2$ / $<\vec{v}^2>$) as:

$$R = \frac{<\vec{v}>^2}{<\vec{v}^2>} = \frac{<\vec{v}_{directed}>^2}{<\vec{v}^2_{directed}> + <\vec{v}^2_{random}>}, \quad (3.16)$$

from which we can determine how much directed cell movement contributes to overall cell movement. We did so for all cell-movement velocities and the radial and the azimuthal cell-movement velocity components in different bands (figure 3.28) and found that directed cell movement contributed less than 6% in all three cases (see figure 3.32).

3.4 Discussion

3.4.1 Cell Behavior Changes in Time

Cells in micromass cell-culture may behave differently at different times. At early times, as shown in our experiment, cells in micromass culture random walk with little directed cell movement and cells in the condensation center diffuse (statistically) significantly faster than cells outside. Since cells in the condensation deposit more fibronectin than cells outside and since mesenchy-

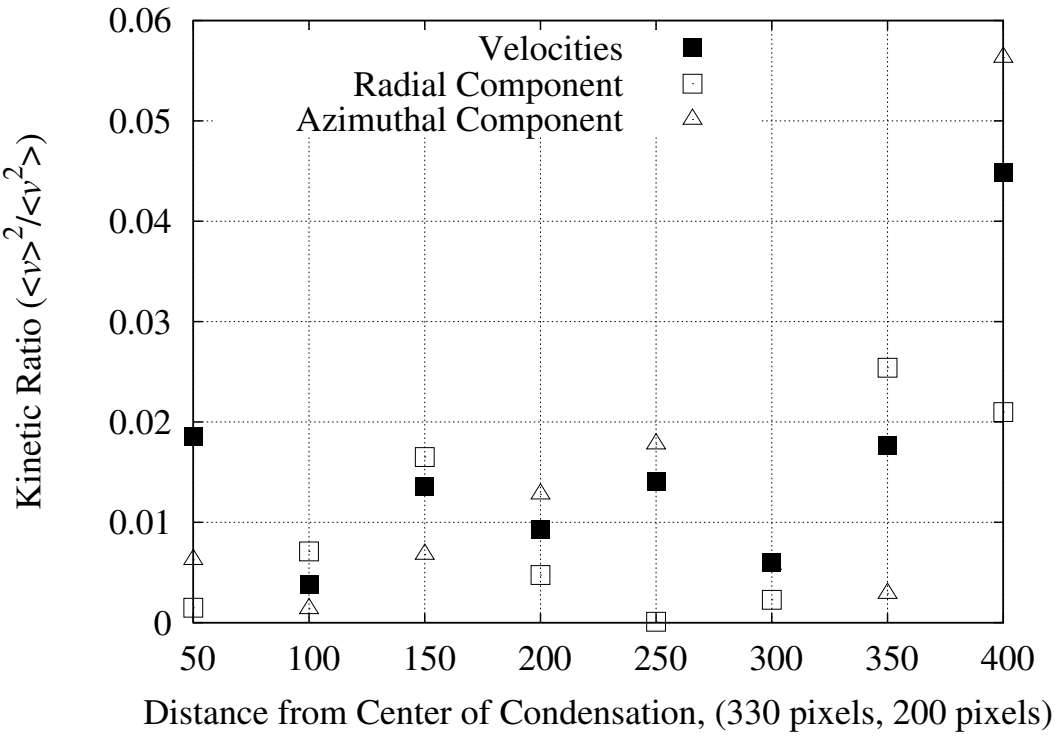

Figure 3.32: Kinetic ratio ($<\vec{v}>^2$ / $<\vec{v}^2>$). See text for details.

mal cells tend to move up the gradient of fibronectin [100], cells outside the condensation center drift towards the center, creating a net inward flux. As more fibronectin is deposited in the condensation center, we expect to see that directed cell movement contributes more in later stages. In later stages of micromass cell-culture, as cells secrete more extracellular matrix (such as collagen type II and sulfated proteoglycans), we found that cells in the condensation center rounded up and exhibited very little relative cell movement.

If cells behaved identically and moved up fibronectin gradients because they stuck more strongly, we would expect them to slow in regions of high fibronectin, like the condensation center. Our analysis and studies of cell movement on fibronectin-coated substrates [100] showed that cells moved faster when they were exposed to more fibronectin at early stages. Thus cell-substrate adhesion cannot be the only factor determining cell velocities in micromass cell-culture.

3.4.2 Possible Mechanisms

In micromass cell-culture, cells bind to each other (by adhesion molecules on the cell-membrane surface) and to the substrate. Cells produce and deposit fibronectin, some between the cell layer and the substrate. So, in terms of adhesion energy, we need to consider three components: cell-cell adhesion (σ_c), cell-substrate adhesion in the absence of fibronectin (σ_s) and adhesion between cells and substrate with fibronectin (σ_s'). If cells stick more to fibronectin than to bare substrate we would expect the cell area to increase in condensation centers if the cell-cell adhesion remained the same, and the cells in the condensation center to move slower. Our study showed that cells in the condensation center

had smaller contact-surface areas and moved faster, which indicates that:

1. Cells stick more to fibronectin so that they can move up the fibronectin gradient.

2. Fibronectin can induce cells to produce more cadherins, or other cell-cell adhesion molecules. Thus cells stick more to each other, reducing the cell-substrate contact area,

3. Fibronectin can promote cytoskeletal activity, hence increasing the rate of cell movement.

3.4.3 Cell Diffusion and Haptotaxis

The average mean-squared displacement over 480 minutes (figure 3.33) increased linearly at short times, indicating that cells executed a random walk. Unlike a normal random walk, in which MSD always increases linearly, the MSD of all cells in image set I first increased linearly, then flattened between 280 and 360 minutes, after which it increased again as before. Grima, Sanguansin and Newman (paper in preparation) have recently shown that in a model in which cells interact with each other by chemotaxing to secreted molecules which have low diffusivity and low decay, the MSD of the cells grows linearly in time for short and long times and flattens at intermediate times, as in our experiments (figure 3.33). This model applies particularly well to haptotaxis, since the surface binding of the fibronectin ensures low diffusivity and decay. The decrease in effective cell movement at intermediate times is due to a temporary self-localization of the cells due to buildup of the adhesive chemical. Random fluctuations in cell position (due, for example, to physical interactions with other

cells) enable a cell to eventually escape the 'barrier' caused by the adhesive chemical buildup; in the flat MSD region, self-interaction of a cell with its own chemical secretion is larger than the interaction with the chemical generated by other cells. At short times, chemical production might not be too large so self-interaction will not be dominant, hence the linear growth of the MSD with time.

An alternative mechanism could accout for our results. In chemotaxis, the chemotactic response increases linearly with the local chemical gradient for small concentrations but saturates for large chemical concentrations [11]. If such saturation effects occur for haptotaxis (possible, since receptors tend to saturate for large concentrations - this mechanism is quite general), then at short times the cells experience significant gradients with small total concentrations, leading to random-walk behaviour biased in the gradient direction. At longer times, due to chemical buildup, the concentration increases and the cells correspondingly move less in response to similar gradients. The cell will eventually delocalize; although the chemical concentration will grow larger, the left or right gradients also grow larger, so small perturbations in the position will cause the cell to escape its temporary barrier.

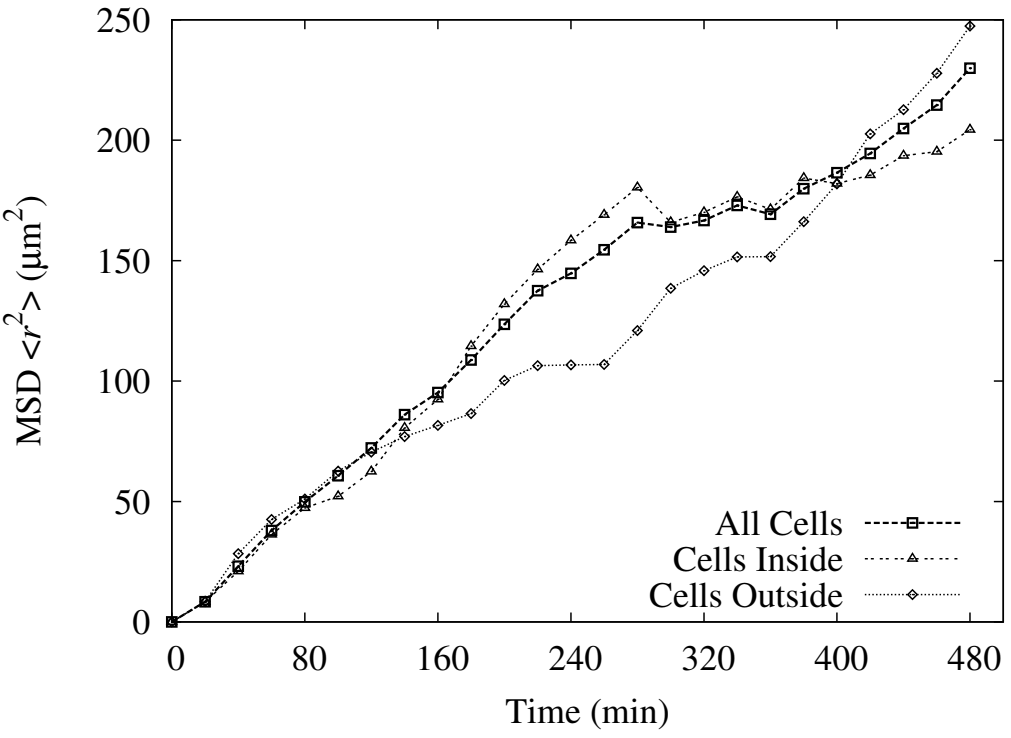

Figure 3.33: Mean-squared displacement of all cells, cells which remained inside the condensation center at all times and cells which remained outside the condensation center at all times, with the center-of-mass movement of all cells and the drift of cells outside the condensation center removed.

Chapter 4

Whole-Mount Culture of Chick Embryos Between HH Stages 13 and 22

The key goals of *in vitro* culture of whole-mount chick embryos are to provide continuous access, manipulation and monitoring in the most natural conditions over the broadest possible range of developmental stages. This chapter describes an *EEC* (*Extended EC*) culture method which uses a filter-paper ring to culture chick embryos from HH stage 13 to HH stage 22 (figure 4.1). Some embryos remain viable up to HH stage 24 (figure 4.2).

4.1 Introduction

The chick embryo has long been one of the most widely used animals in the study of vertebrate development simply because fertile chick eggs are cheap and readily available, and the chick's development resembles in many ways that of mammals.

Researchers with different scientific objectives have developed many corresponding experimental methods to culture chick embryos after explanting them from the yolk. These methods differ in the developmental stage at explant and the period over which the explanted embryos remain viable. For example, Chapman and coworkers [13] developed an improved method for whole-embryo chick culture using a filter-paper carrier, which allowed culture of chick embryos from EG stage X [31] to HH stage 10. Similarly, Flamme and coworkers [34] developed a method to culture chick embryos from HH stage 13 to HH stage 25 using two different culture media in succession. However, these procedures do not serve well experiments requiring easy access to the embryo for micro-surgical manipulations and continuous microscope observation. Our EEC culture method, which we developed in Prof. Newman's laboratory at New York Medical College, Valhalla, New York, offers a number of advantages over other culture methods, see section 4.3, including the possiblity to manipulate and reorient the embryo.

4.2 Experimental Procedures and Results

We adapted this protocol from the EC culture method described in [13] with minor modifications. The EC culture method is easier and less time-consuming

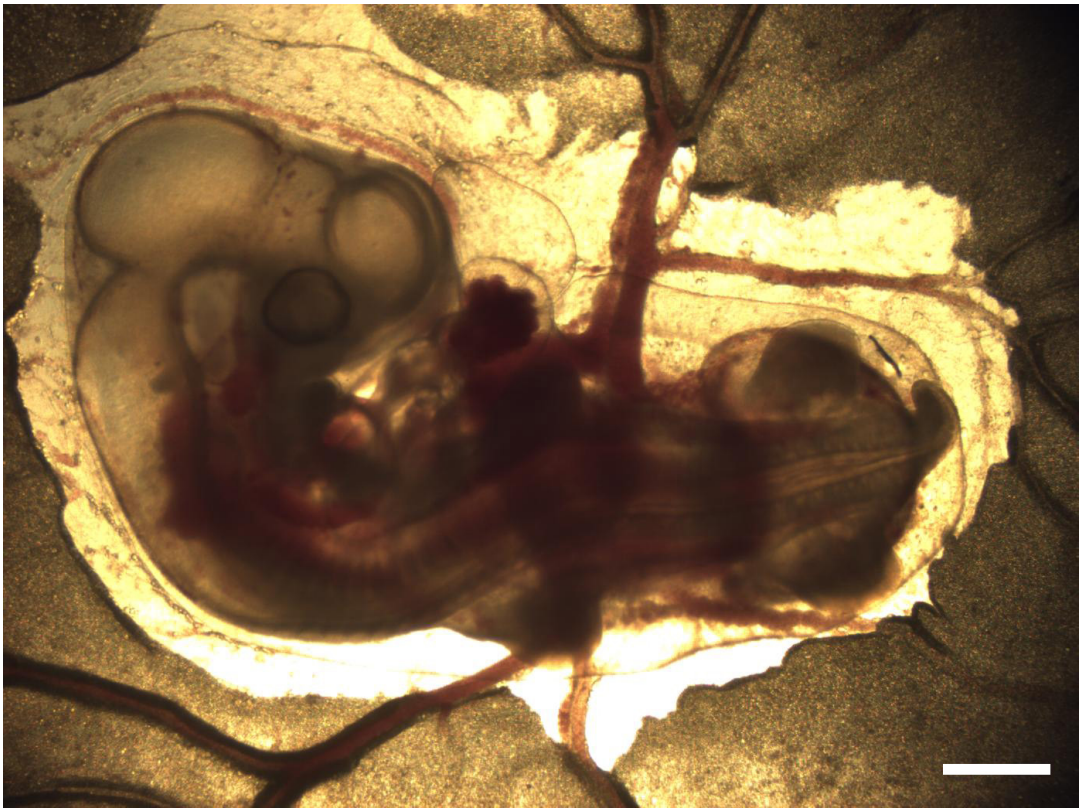

Figure 4.1: Photograph of a chick embryo cultured using the EEC (Extended EC) method. The cultured embryo is shown at HH stage 21-22. Scale bar: 0.4 mm.

than New's method which was developed in the 1950s, so that it is more productive. The original paper [13] cultured the embryos ventral side up. However, we found that we could culture the embryos dorsal side up and that the embryos developed as well, if not better.

4.2.1 Protocol for Preparing Agar-Albumen Culture Dishes

Instruments and Media/Chemicals

1. 35 mm Petri dishes (Falcon 351008).
2. 245 x 245 mm square Bio-Assay dish (Corning 431272).
3. Beakers (250 ml).
4. 500 ml flask.
5. 10 ml serological pipette (Falcon 357551).
6. 2 dozen fresh eggs.
7. 120 ml of simple saline, autoclaved (7.91 g NaCl dissolved in 1 l distilled water).
8. 0.72 g Bacto-Agar (Difco).
9. Penicillin/Streptomycin (Gibco BRL 15140-148).

Steps

1. Heat the water bath to 49°C.

2. Add the saline to a sterile 500 ml flask and put on hot plate/stirrer.

   Bring saline solution to boiling while stirring. Add the agar gradually.

   Wait until the agar dissolves fully, then transfer it to the preheated water bath.

3. Allow the dissolved agar to equilibrate at 49°C for about 20 minutes.

4. Collect 120 ml of thin albumen from fresh eggs into a 250 ml beaker.

5. On a flat surface, lay out 80, 35mm Petri dishes with their lids off.

6. Put the beaker containing 120 ml of thin albumen into the water bath for 5 minutes.

7. Add the the dissolved agar to the beaker containing the thin albumen.

   Add the Penicillin/Streptomycin to this mixture, 100 units/ml.

   Mix by swirling for 30-60 seconds.

8. Using a sterile 10 ml serological pipette and a mechanical pipette pump, aliquot 2.5 ml of the mixture into each Petri dish without introducing air bubbles.

9. Put the lids on the Petri dishes and leave the dishes for several hours or overnight at room temperature to dry.

10. Place dishes in 245 x 245 mm square Bio-Assay dishes. Store in a refrigerator at 4°C for up to one week.

4.2.2 Protocol for Preparing Cultured Chick Embryos

Instruments

1. Blunt-end forceps (Fisherbrand 10-295).
2. Fine-tip forceps (Dumont #5 inox).
3. Surgical fine-tip scissors (Fisherbrand 08-940).
4. 10 cm extra-deep dishes (Fisherbrand 08-757-11Z).
5. Monoject, plastic 6cc syringe with plastic Luer-lock tip (Monoject 516937).
6. Precision-glide 18G 1.5 inch needle (BD 305196).
7. Autoclaved filter-paper rings (Whatman #3, ID: 26 mm, OD: 33 mm).
8. Tissue wipes (Kimberly-Clark No. 05511-20).

Steps

1. Hold prepared agar-albumen-substrate Petri dishes at room temperature for 1 hour before experiment starts.

   Put a paper towel on the bottom of a 245 x 245 mm Bio-Assay square dish, moisten with distilled H_2O and place the dish in a 37°C tissue-culture incubator.

2. Remove the incubated fertile eggs (50-65 hours, as desired) from the egg incubator. Allow them to cool for 10 minutes.

   Spray 70% ethanol on eggs.

3. Fill one 10 cm extra-deep dish with autoclaved simple saline plus 100 units/ml Penicillin/Streptomycin.

   Collect some (~10 ml) thin albumen from the fresh fertile (white or red Leghorn) eggs.

4. Place one egg in the lid of a 10 cm extra-deep Petri dish with the egg's long axis oriented horizontally and remove 10-12 ml albumen from the pointed end of the egg using the syringe.

5. Use the lid of the packing container of the syringe as an egg holder. Put the egg vertically in the egg holder with its blunt end up.

   Use the blunt-end forceps to crack open the egg and to remove any egg shell and outer shell membrane above the egg's air space.

   Carefully remove the inner shell membrane. Using the forceps to make a hole at the boundary of the remaining egg shell, grab and tear all of the shell membrane without allowing any part of it to fall inside the egg.

   Use the forceps to remove more egg shell to half the height of the egg. Use the syringe to take out extra albumen if necessary.

6. Pour the yolk and remaining albumen into a 10 cm extra-deep dish.

   Try to keep the embryo upright in the dish. If it is not, use a tissue wipe to adjust its position.

7. Use a tissue wipe to remove extra albumen on top of or around the chick embryo and the *area vasculosa*.

Use the fine-tip forceps to put a filter-paper ring on top of the yolk, centering the embryo in the middle of the hole in the ring.

8. Apply a drop of the freshly-collected thin albumen (0.5 ml) to the agar-albumen substrate.

9. Carefully excise the vitelline membrane around the filter-paper ring using the surgical fine-tip scissors.

   Use fine-tip forceps to transfer the filter-paper ring together with the vitelline membrane and embryo into the dish containing the simple saline.

   Shake the filter-paper ring gently to remove the attached yolk from the embryo.

   After washing the embryo, remove the filter paper from the saline and dab an edge on a piece of tissue paper to absorb any extra liquid.

   Place the filter-paper ring with the vitelline membrane and attached embryo either dorsal side up or ventral side up onto a prepared embryo-culture dish covered with agar-albumen substrate.

   Try to avoid introducing air bubbles under the vitelline membrane.

10. Put the Petri dish with the cultured embryo into the 245 x 245 mm Bio-Assay square dish in the tissue-culture incubator.

    The embryos should grow and develop normally for 36 to 48 hours. Some can survive for more than 55 hours up to HH stage 22.

4.3 Discussion

4.3.1 Advantages of the EEC Method Compared to Other Methods

Other whole-mount culture methods for chick embryos include:

- The methods New [78] and Chapman [13] developed to culture chick embryos from HH stage 1 or earlier to HH stage 10.
- Stern's [107] modified New culture method, which allowed culture of chick embryos up to HH stage 20.
- Flamme's [35] two-phase method to culture chick embryos from HH stages 13-15 up to HH stages 20-25. Kucera [66] used a method very similar to Flamme's.

Compared with these methods, the EEC method we have developed is better for micro-manipulation and video-microscopy because:

1. It is easier to set up.
2. It permits easier access to the embryo. In Stern's method, the embryo is ventral side up, while in Flamme's method, the embryo is ventral side up during the first phase and dorsal side up during the second phase.

   Our ECC method permits the embryo to be either ventral side up or dorsal side up. The experimenter can change the orientation easily at any time during the experiment.

A Petri dish contains the entire culture and its supporting components, allowing access at any time.

3. The embryo is more stable. In both Stern's and Flamme's methods, the embryo rests on fluid, either albumen or a combination of albumen and yolk. Because of water evaporation, the embryo tends to 'sink' during culture, which can cause problems for video-microscopy as the area of interest goes gradually out of focus.

   However, in our ECC method, since the embryo rests on a semi-solid agar-albumen substrate and the filter-paper ring maintains the tension of the vitelline membrane to be the same as *in ovo*, the embryo tends not to move around and the vibration caused by the heart beat is minimal.

4.3.2 Larger Filter-Paper Rings Allow Cultured Embryos to Live Longer

With the EEC method described in the previous sections, which uses a small (ID: 26 mm, OD: 33mm) filter-paper ring (see page 112), we found that the cultured embryo could develop from basically any early stage up to HH stages 20 or 21. For some studies, such as a study of the origin of the vascular smooth muscle cells around the two merging dorsal aortae in chick embryo [54], chick embryos cultured up to HH stage 21 suffice.

However, some studies require cultured embyros to develop past HH stage 21. For example, when we studied the limb-tip deformation when we removed the AER, we wanted the chick embryo to develop in culture as long as possible. We then determined the oldest stage to which the cultured chick embryo could

develop. Previous studies and our own experiments showed that cultured chick embryos normally died because of heart bleeding. Usually the expansion of the *area vasculosa* stopped when it reached the inner rim of the filter-paper ring. However, hematopoiesis continued, causing polycythemia. Our video observations showed that polycythemia and thus increased blood viscosity eventually led to heart insufficiency, bleeding from the heart and later embryo death.

In order to culture using a bigger filter-paper ring, we incubated fertile chick eggs for 50 hours. At this time, the chick embryos reach HH stage 17, the yolks are looser and expand maximal in the extra-deep dish. Only at this time could we use large filter-paper rings with ID: 40 mm and OD: 55 mm in the EEC culture method we described in the last section, using a bigger Petri dish (60 mm, Falcon 351007). This method allows cultured embryos to survive and grow up to HH stages 24-25 (figure 4.2).

4.3.3 Is Dorsal Side Up, or Ventral Side Up Better?

The optimum orientation of the chick embryo in the agar-albumen-substrate Petri dish depends on the objective of the experiment.

However, a dorsal-side-up embryo can develop more normally than a ventral-side-up embryo in the following ways:

1. Embryos cultured dorsal side up develop at almost the same rate as embryos *in ovo*, while embryos cultured ventral side up develop slower.

2. During chick-embryo development, the body of the embryo rotates clockwise 90° along the A-P axis, starting from the head and continuing gradually to the tail. Ventral-side-up culture blocks rotation when it reaches a

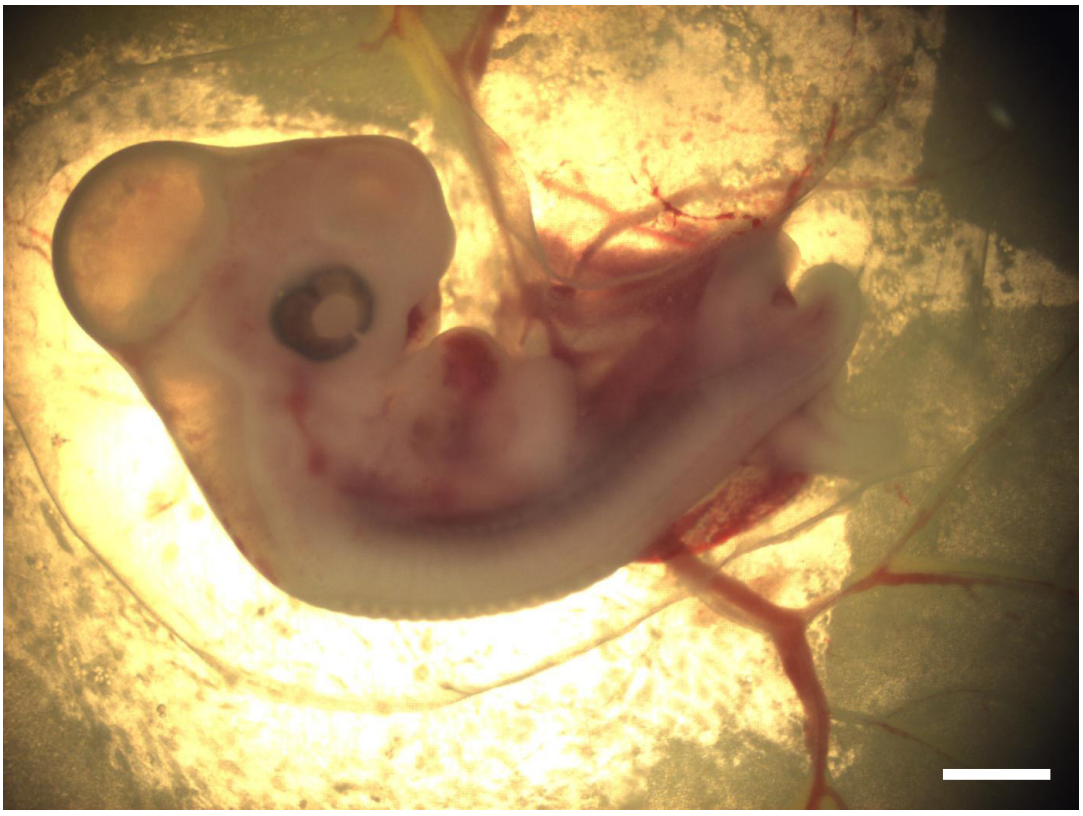

Figure 4.2: Chick embryo cultured using a bigger filter-paper ring and a bigger culture dish following our EEC protocol. The photograph shows the cultured embryo at HH stage 24-25. Scale bar: 0.5 mm.

zone between the forelimb and the hindlimb. The embryonic body remains twisted, with the posterior dorsal side up and the anterior ventral side up. The dorsal-side-up embryo completes its rotation and the embryonic body has the same orientation as *in ovo*.

3. In a ventral-side-up embryo, the *area vasculosa* layer is uppermost, which could make micro-manipulation of the embryo more difficult since it requires penetrating the *area vasculosa* layer. Severed blood vessels can cause blood loss, which, in excess, can lead to the embryo's death. In dorsal-side-up culture, the vitelline membrane is uppermost. It will reseal if micro-manipulation creates a slit or hole. Thus, dorsal-side-up culture is generally more reliable and convenient.

4.4 Conclusion

Our *in vitro* EEC (Extended EC) culture method allows chick embryos to develop from HH stage 13 up to HH stages 22-25, the period when cells differentiate and organs form. Our EEC method allows direct study of development at the cell level *in situ* in the embryo throughout this key period.

Chapter 5

Transplantation of Embryonic Chick Limbs

5.1 Introduction

Developing chick limbs are a widely-used model for the study of cell differentiation, cell-cell and cell-extra cellular matrix (*ECM*) interactions, pattern formation and developmental mechanisms. Previous studies, either worked directly with limbs *in situ* in developing embryos or transplanted limbs from donors onto the chorioallantoic membrane (*CAM*), flanks, or somites of the hosts. The researchers then sealed the eggs and checked several days later how the manipulated limbs had developed. This protocol did not permit monitoring the grafted limbs' development continuously. Other methods cut off limbs and maintain them either in defined culture medium, or on a semi-solid substrate containing medium which supplies the limbs with nutrients. These methods allow examination of the influence of different chemicals or growth factors on the explanted

limbs. However, without a direct blood supply, the explanted limbs grow in an abnormal way, sometimes leading to ambiguous experimental results. This chapter describes our new method to graft limb buds from HH stage 21-23 donors to the flank site posterior to the left or right vitelline artery, or the somites, of HH stage 15-16 host embryos in Petri-dish culture. The grafted limbs can then continue to grow for another 35-40 hours. Since we can micro-manipulate the explanted limbs before grafting, *e.g.* by AER-removal, micro-injection or electroporation, then monitor the growth of grafted limbs continuously using video-microscopy, we can study how the micro-manipulations affect individual cells' behaviors.

5.2 Experimental Protocols for Limb Grafting

5.2.1 Prepare Cultured Chick Embryos as Hosts

Incubate fertile eggs for 2.5 days until the embryos reach HH stage 15. Use the method we described in chapter 4 to culture chick embryos in Petri dishes either dorsal or ventral side up. Continue incubation in an incubator at 37°C. These cultured embryos will serve as hosts for chick limb grafts.

5.2.2 Explant Chick Limb Buds from Donor Embryos and Graft to the Host's Flank

Instruments and Media/Chemicals

1. 10 cm extra-deep dishes (Fisherbrand 08-757-11Z).

2. Fine-tip forceps (Dumont #5 inox).

3. Etched tungsten micro-needle (Fine Science Tools 10130-10).

4. Autoclaved Ringer's solution (Dissolve 9.0 g NaCl, 0.25 g $CaCl_2$ and 0.42 g KCl in 1000 ml distilled and deionized H_2O [95]).

5. Penicillin/Streptomycin (Gibco BRL 15140-148) solution (100 units/ml in Ringer's solution).

Steps

1. Incubate (red or white Leghorn) fertile eggs for 3.5-4.5 days until embryos reach HH stages 21-24.

2. Crack open eggs and transfer chick embryos into 10 cm extra-deep dishes containing Ringer's solution.

3. Use fine-tip forceps to remove any extra-embryonic membrane and transfer the embryos into a new dish containing Ringer's solution.

4. Use one fine-tip forceps to press the embryo body near the limb to prevent the embryo from floating away and cut off the limb bud using another fine-tip forceps.

5. Transfer the cut-off limb buds to a new dish containing Ringer's solution.

6. Repeat to excise all limb buds.

7. Use an etched tungsten micro-needle to cut through the vitelline membrane and make a small slit (a little bit smaller than the cross-sectional

antero-posterior length of the excised limb buds) along the flank of the host embryos parallel to the main body midline immediately posterior to the left or right vitelline artery.

8. Transfer an explanted limb bud near the slit and use fine-tip forceps to push the explanted limb bud into the slot with the cut-off cross section inside the slit and the limb-bud tip outside the slit. Both sides of the flank can serve as sites for grafts.

9. Apply a drop or two of Penicillin/Streptomycin solution to the transplantation site in order to prevent infection. The cut-through vitelline membrane will heal in several hours.

5.2.3 Advantages of Grafting Chick Limb Buds to the Flanks of Earlier-Stage Hosts

While we could operate on limbs *in situ* after explanting an embryo into Petri-dish culture, transplanting limbs from donors to earlier-stage hosts has several advantages:

- Since cultured embryos normally die at HH stages 23-25 we cannot observe subsequent limb development *in situ*. Limb transplantation can remedy this problem. Transplanting chick limb buds from later-stage donors (HH stages 20-23) onto flanks of hosts at HH stages 15-16 allows the grafted limbs to develop up to HH stages 25-26 or further.

- We can modify part or all of the limb bud, *e.g.* by electroporation, or AER removal, then transplant it into the flank of an unmodified host so that

we can monitor cell movement in the grafted limb for an extended period of time.

- We can orient and position the grafted limb bud for better microscopy.
- The grafted limb grows outside the vitelline membrane, facilitating monitoring of cell movement.

Figure 5.1 shows the development of a limb (from a HH stage 21 donor embryo) grafted onto a host's left flank (the host was ventral side up at HH stage 15).

5.3 Application: Chick Limb Buds Grafted to Both Flanks of a Host

5.3.1 Motivation and Introduction

The limb transplantation protocol described in section 5.2 provides a way to manipulate and monitor limb development directly under the microscope. This section introduces an application of this protocol in which we transplanted limb buds to both flanks of a host, with one limb bud's AER removed.

Figure 5.2 shows two chick limb buds from an older donor transplanted to the host's flanks. One limb bud's AER was removed and the other left untouched.

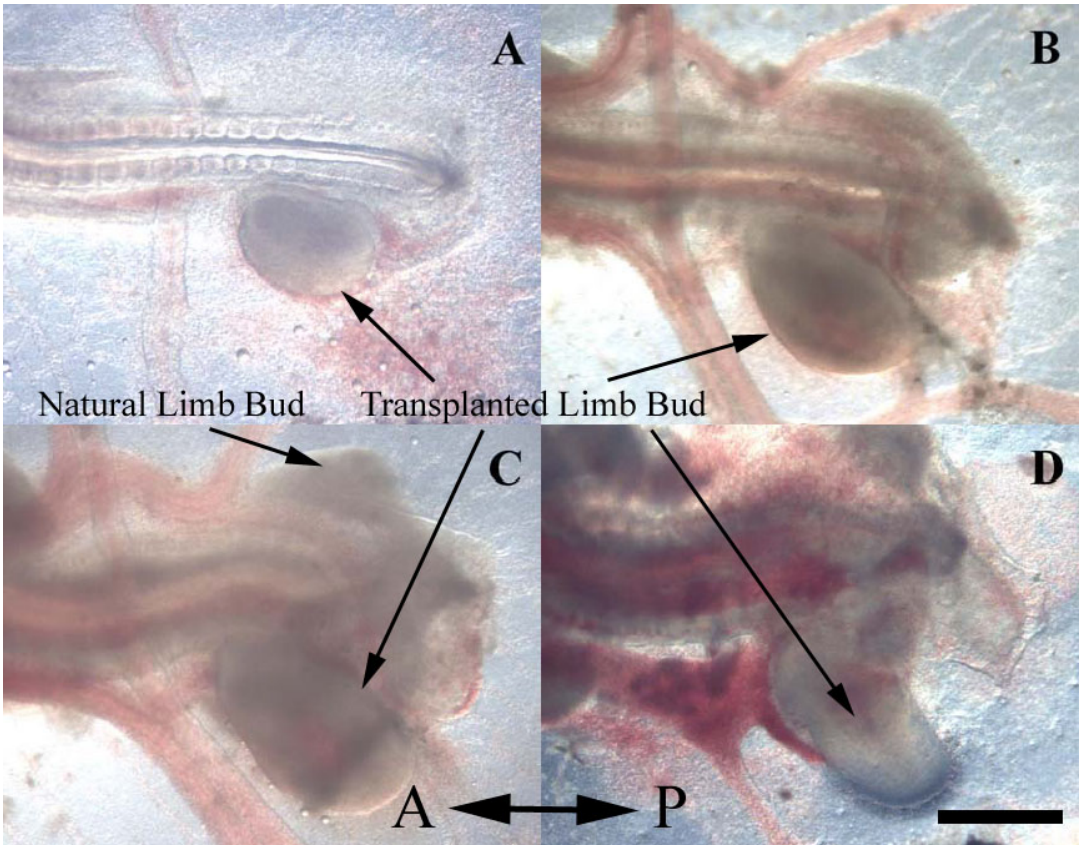

Figure 5.1: Flank transplantation of an embryonic chick limb. Times after transplantation: A) 0.5 hrs, B) 17 hrs, C) 26 hrs, D) 43 hrs. In (D), the grafted chick limb reached HH stage 26 and the host embryo was at HH stage 21. Scale bar: 0.5 mm.

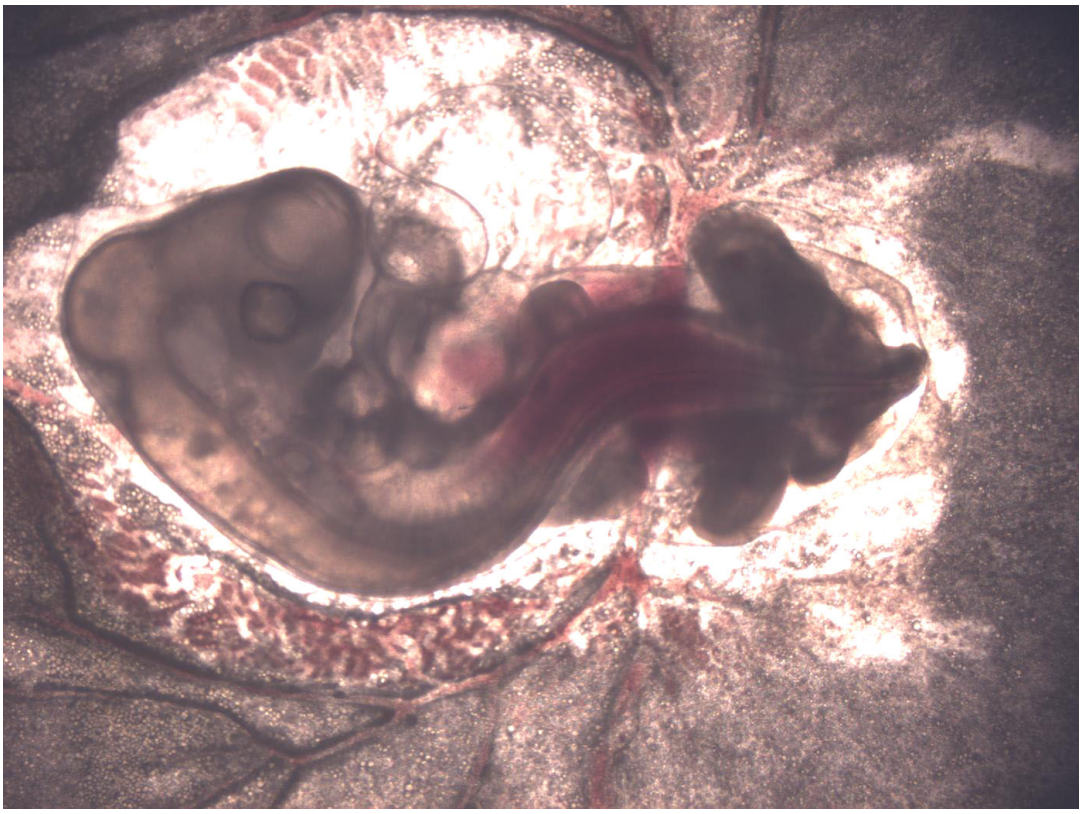

Figure 5.2: Two limbs from donors at HH stage 20 were transplanted onto a host at HH stage 15. The host reached HH stage 20/21, and the grafted limbs reached HH stage 24/25. The AER of the lower grafted limb bud was removed before transplantation. The lower, grafted, limb bud is smaller than the upper, intact, limb bud.

5.3.2 Transplantation of Limbs with AER Removed

A great advantage of operating directly on natural limbs is that the operator can compare directly the operated limb to the other untouched limb. HH stage 17 chick embryos are cultured dorsal side up. Normally, operating on the hind limbs is easier because they are easier to see than forelimbs. Use an etched tungsten micro-needle (Fine Science Tools 10130-10) to cut an opening through the vitelline membrane and the extra-embryonic membrane underneath it to expose the hind limb. Use the micro-needle to cut the AER off while leaving the underlying mesoderm cells and other ectoderm cells untouched. Apply several drops of Penicillin-Streptomycin solution to prevent contamination.

In our experiments in which we removed the AERs, the operated limbs continued to grow at almost the same rate as the intact limbs. However, the operated limbs were broader both at the base and at the tip than the intact limbs.

We propose two possible explanations:

1. Without the mechanical tension exerted by the AER the limb could not maintain the curved shape of the tip of a normal limb.

2. The AER supplies FGFs to underlying mesenchymal cells to maintain the cells' mechanical properties. With the AER removed, the mesenchymal cells' mechanical properties changed and the cells became less cohesive and expanded more, broadening both the base and the tip of the limb.

Micromass cell-culture would provide some helpful information to test these two ideas, such as how the cells move when they receive different growth factors. However, the chemical and mechanical role of the AER in limb development is

still not clear. The most promising way to understand the AER's role is to monitor how the cells behave directly in the developing limb. We can label cells with DiI and monitor their movements using high-magnification fluorescence, or confocal microscopy. The techniques used by Kulesa and Fraser [67] could be particular helpful.

5.4 Conclusion

Cultured chick embryos in Petri dishes provide good hosts for grafted chick limbs from later-stage donors. Both the grafted chick limbs and the cultured chick embryos can survive in a 37°C environment for up to 45 hours. During this time, the grafted chick limbs grow in the same way as natural limbs and can be monitored using video-microscopy until the host dies. The most important advantage of this method is that the operator can manipulate the explanted chick limb before grafting it onto the host. Operating on intact limbs of cultured chick embryos in a Petri dish is also possible. In both methods, since the embryo lies on a semi-solid agar-albumen substratum, the embryo or limb does not move much during development. These methods permit investigation of cell movement in either grafted or intact limbs using epi-fluorescence or confocal microscopy.

Chapter 6

Conclusions and Suggestions for Future Work

The main object of our research has been the study of cell and tissue motion using time-lapse microscopy, based on our belief that cell and tissue motion can reveal some aspects of developmental mechanisms. As in any other scientific work, the work in this dissertation advanced our knowledge of development, but, at the same time, raised new questions. In the past several years, new technologies have made the chick embryo a better model than ever, mainly because up-regulating (using DNA constructs) and down-regulating (using double-stranded RNA and morpholino antisense oligos) protein production at desired developmental stages and positions is now possible. In this chapter, we discuss the implications of our work and propose some future studies of chick embryonic development.

6.1 Gastrulation

We studied cell and tissue motion in early gastrulating chick embryos and found that cells in the epiblast layer of the blastoderm moved in two counter-rotating vortices. By analyzing cell-division patterns and by applying cell-division inhibitors, we showed that cell division was not required for primitive streak initiation, but indispensible for maintaining the counter-rotating tissue flow pattern and the elongation of the primitive streak. However, we still do not understand what mechanism initiates the primitive streak or how the primitive streak elongates.

6.1.1 Initiation of the Primitive Streak

During primitive streak initiation, cells in the epiblast layer accumulate at the posterior region of the *area pellucida* and undergo an epithelial-mesenchymal transition (*EMT*): cells originally move together in one sheet, then lose their adhesion to each other and move individually. The EMT seems to be the key to the initiation of the primive streak. Direct evidence shows that Wnt and TGF-β can activate LEF-1 production in cells and induce an EMT [51, 59]. Since the LEF-1 virus is able to induce the EMT directly, we propose to apply this virus to another region of the blastoderm to see if it can induce an ectopic primitive streak without additional intervention.

6.1.2 Primitive-Streak Elongation

To study primitive-streak elongation, the mechanisms of which are a major question in gastrualtion, we will need to follow cells' movements when they

migrate into the streak. With proper spatial and temporal resolution, and *in vivo* electroporation (see section 6.3), we should be able to track the cells' movements, deformations (by transfecting cells with pCAGGS-GFP plasmid) and division cleavage-plane orientation inside the streak. With this method we can design and perform experiments to answer the following questions related to primitive-streak elongation:

- How long do cells stay inside the streak?
- Do some cells stay inside the streak significantly longer than other cells?
- Do cells intercalate once they move into the streak?
- Does cell-division orientation correlate with the streak elongation direction?
- How do the primitive-streak cells deform and does deformation accompany intercalation in the streak?

6.1.3 Individual Cell Movement in the Epiblast

Now that we understand that the cell-movement pattern during gastrulation resembles two counter-rotating vortices at the tissue level, we should investigate how the cells in the epiblast move individually. Some of our movies showed that not all the cells followed the counter-rotating-vortex path. Some cells moved towards the boundary between the *area pellucida* and the *area opaca*. We should label the nuclei of epiblast cells fluorescently (electroporating the embryo with H2B-GFP plasmid) and follow their movements using time-lapse microscopy to

clarify the movement patterns and identify the subpopulations of cells and the reasons for their divergent movements.

6.2 Embryonic Limb Development

We characterized cell movement in the early stages of chondrogenic nodule formation in micromass cell-cultures of embryonic chick-limb mesenchyme and found that cells inside condensation centers moved faster than cells outside condensation centers even though the condensation centers had more deposited fibronectin. We also provided a way to identify condensation centers using the cells' velocity vectors. These studies make possible large-scale analysis of cell movement during condensation in micromass cell-culture, in which hundreds or even thousands of cells form multiple condensation centers within the field of view. However, since we cannot identify individual cells at this large scale (which requires lower magnification), we will need to label cells fluorescently. One way is to use a virus which can transfect cells in culture so they produce (H2B) GFP after about 12 hours of incubation. Another way would be *in ovo* or *in vivo* electroporation of embryonic limb bud at the desired stage, followed by dissection to use these cells in micromass cell-culture.

Our whole-mount culture of late-stage chick embryos (between HH stage 15 and HH stage 22) and transplantation of embryonic chick limbs from older embryos (HH stage 21, or 22) to younger hosts (HH stage 16) would permit us to track cell movement and cell division inside a developing embryonic limb bud if we could label the limb precursor cells (lateral-plate mesoderm cells) at an early stage (HH stage 16). This experiment should answer some very funda-

mental questions about early embryonic limb development. Other experiments would involve mechanical manipulation (such as AER removal) and regulation of protein production in particular regions of the embryonic limb by *in ovo* or *in vitro* electroporation (see section 6.3), then following cells' movements.

6.3 *In vivo* Electroporation

While DiI can only label groups of cells, making following individual cells' movements difficult, *in vivo* electroporation of cells to label nuclei fluorescently can help reveal individual cell's movements explicitly. Our preliminary studies showed that *in vivo* electroporation can label many cells in the epiblast at the same time and that the labeled embryo can develop normally up to HH stage 11 (figure 6.1) [21]. Labeling lateral-plate mesoderm (*LPM*) cells fluorescently by electroporation and following cells' movements in a developing chick limb up to HH stage 25 should also be possible.

With electroporation, we could not only label many cells at the same time, but also label specific types of cells, such as precursors of vascular endothelial cells using a DNA plasmid with the flk-1 promoter. Now, after the complete mapping of the chick genome, we could theoretically insert any gene into a DNA plasmid using a generic promoter, such as pCAGGS, then transfect a particular group of cells, such as endodermal cells between HH stage 5 and HH stage 10 in a quail embryo. This technique will be very useful in investigating cell lineage and cell motion during gastrulation using avian embryos as a model. One example concerns the lineage of mesodermal cells in avian embryos. Most people believe that in avian embryos all mesodermal cells arise from the epiblast cells which

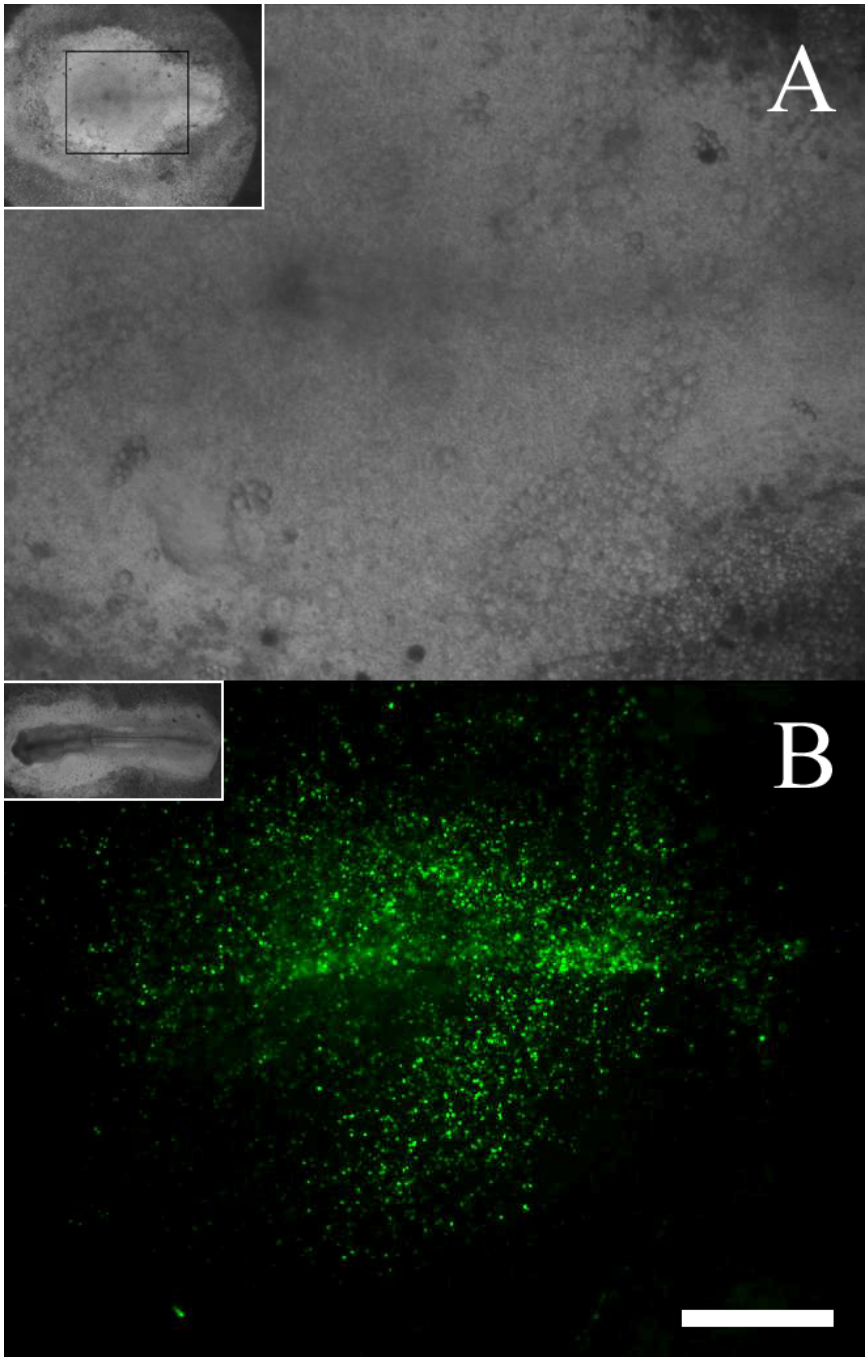

Figure 6.1: *In vivo* electroporation of a quail embryo. A) Brightfield image of a HH stage 4 quail embryo 20 hours after electroporation. B) Fluorescent image of the same embryo. Many cells in all three germ layers were labeled. (A) and (B) show enlarged images of the region inside the black rectangle in the inset figure in (A). The inset figure in (B) shows the same embryo after 50 hours of incubation at HH stage 11. At that time, many cells in the main body, including the two cell layers of the embryonic heart were labeled. Scale bar: 0.5 mm.

ingress through the primitive streak. However, by labeling epiblast cells in the *area opaca*, our preliminary results showed that some mesodermal cells in both the intra- and extra-embryonic regions arise from epiblast cells which did not ingress through the streak. Another goal would be a more detailed fate map for the cells forming organs, such as the heart. Our preliminary data showed that some cells labeled at HH stage 1 gave rise to cells in both endocardium and myocardium layers of the heart at HH stage 10. A third project would be following cells' movement in the epiblast between HH stage 1 and HH stage 4 (when the primitive steak extends to its full length) at higher magnification so that we can track individual cells' movements. This experiment should be able to determine whether cells have individual movement beside the large-scale tissue motion we discussed in chapter 2, and whether cell intercalation causes primitive-streak elongation?

If we insert a gene into a DNA plasmid using a specific promoter, we should be able to cause a particular type of cell to produce more of a specific protein. In this way, we should be able to up-regulate specific protein production in a desired region, or in a desired type of cell. Delivering ds-RNA (or siRNA), or morpholino antisense oligos into cells by electroporation should also enable us to down-regulate the product of certain proteins in a desired region of tissue (such as the endoderm, ectoderm, posterior marginal zone, ZPA or the ectodermal cells surrounding the limb bud). We have not performed any experiments to promote or down-regulate specific proteins in avian embryos. However, if we could, we could test the hypothesis that the initiation of the primitive streak results from Wnt signaling in the PMZ inducing an EMT in the epiblast cells anterior to the PMZ, by ectopically producing Wnt molecules to see if they can

induce another streak, and/or down-regulating the production of Wnt molecules in PMZ cells to see if lowered Wnt production can inhibit the initiation of the primitive streak.

Appendix A

Experimental Protocols

A.1 Chick Whole-Embryo Culture Using a Filter-Paper Carrier

We adapted this protocol from the EC culture method described in [13] with minor modifications. Compared to New's method which was developed in the 1950s, EC culture is easier, less time-consuming, and more productive. The original paper [13] cultured the embryos ventral side up. However, we found that the embryos can also be cultured dorsal side up and develop as well, if not better.

A.1.1 Protocol for Preparing Agar-Albumen Culture Dishes

The protocol for preparing agar-albumen culture dishes is the same as in section 4.2.1.

A.1.2 Protocol for Preparing EC Cultures

Instruments

1. Fine-tip forceps (Dumont #5 inox).
2. Surgical fine-tip scissors (Fisherbrand 08-940).
3. 10 cm extra-deep dishes (Fisherbrand 08-757-11Z).
4. Filter paper (Whatman No. 5, or Whatman No. 52).
5. Blunt-tip forceps (Fisherbrand 10-295).
6. Tissue wipes (Kimberly-Clark No. 05511-20).
7. Corning 245 x 245 mm Bio-Assay square dish (Fisherbrand 07-200-600).

Steps

1. Incubate eggs to the desired embryonic stage.
2. Allow the eggs to cool to room temperature for 15 minutes. Then spray 70% Ethanol on the eggs.
3. Crack the egg shell, hold the egg horizontally in a 10 cm extra-deep dish, open the egg and remove the egg shell. In most cases, the blastoderm should be positioned uppermost and roughly centered on the yolk.
4. Use a plastic pipette to remove the thick and thin albumen, then use a piece of tissue wipe to remove the remaining albumen on the yolk.

5. Place a peice of filter paper with a 6-8 mm central aperture (Figure A.1) gently onto the vitelline membrane with the embryo in the center of the aperture.

6. Use scissors to cut around the filter paper and the vitelline membrane.

7. Use fine-tip forceps to pull the filter paper away from the yolk in an oblique direction (not vertically upward). The embryo is attached to the vitelline membrane.

8. Use blunt-end forceps to remove any attached yolk. Then wash the culture gently in simple saline (or EPBS). Remove as much attached yolk as possible.

9. Put the washed culture into a Petri dish either ventral side up or dorsal side up, depending on the objective of the experiment.

10. Put the EC culture dishes into the Corning 245 mm Bio-Assay square dish (Figure A.2), with moistened tissue paper lining the base. Embryos in EC culture can develop for 36 hours, with some surviving up to 72 hours.

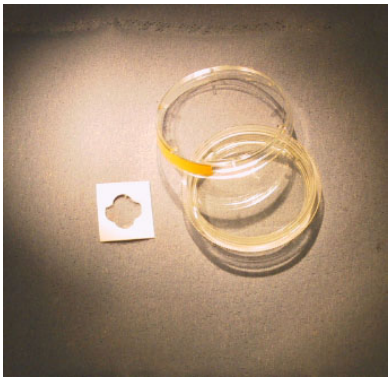

Figure A.1: Filter paper ring and 35 mm dish with substrate.

Figure A.2: Embryo culture dishes are kept in a 245 x 245 mm Bio-Assay square dish with moistened tissue lining the base.

A.2 Protocol for Whole-Mount BrdU Incorporation

We used 5-bromo2'-deoxy-uridine (*BrdU*) incorporation to measure cell proliferation rates in different regions and developmental stages of early chick embryos. Incubating early chick embryos in BrdU solution (at room temperature) causes BrdU to incorporate into DNA in place of thymidine during cell-cycle S-phase. We can then detect cells which have incorporated BrdU into their DNA using a monoclonal antibody against BrdU.

The following protocol is that used in the Weijer laboratory, which Prof. Weijer adapted from the standard protocol which PharMingen supplied with their BrdU.

A.2.1 Solutions

10 μM BrdU

PharMingen, Cat. # 2420KC, diluted with PBS.

PBS 10x

To make 1000 ml 10x PBS, dissolve 80.0 g NaCl, 2 g KCl, 14.4 g Na_2HPO_4, and 2.4 g KH_2PO_4 in 800 ml millipore H_2O. Adjust the pH to 7.4. Add H_2O to 1000 ml. Sterilize by autoclaving. Store at room temperature. Dilute to 1x with millipore H_2O before use.

4% Paraformaldehyde

To make 500 ml 4% Paraformaldehyde, dissolve 20 grams (4% $\times$ 500 ml) Paraformaldehyde powder in 500 ml PBS solution. Heat at 60-70°C, stirring continuously until the solution becomes clear again, in a safety hood. Wait for the solution to cool to 20°C. Use NaOH to adjust the pH to 7.40. Store in a refrigerator at 4°C.

TBST

TBST is 0.1% Tween20 in TBS. To make TBST 10x, dilute 1.0% Tween 20 in TBS 10x. For use, dilute TBST 10x stock solution to 1x by diluting with millipore H_2O.

TBS 10x Stock Solution

To make 1000 ml TBS 10x stock solution, dissolve 80.0 g NaCl, 2.0 g KCl, and 30.0 g Tris base ($C_4H_{11}NO_3$) in 800 ml millipore H_2O. Adjust the pH to 8.0 with 1M HCl. Adjust the volume to 1000 ml. Dispense in convenient volumes and sterilize by autoclaving. Store at room temperature.

2N HCl

Stock HCl: 1.18/37%, *i.e.* 1180 grams of HCl in 1 litre of H_2O produces a concentration of HCl of 37%. To calculate the concentration of HCl in M (mol/l), use:

$$0.37 \times 1180(g/l) = 436.6(g/l), \tag{A.1}$$

$$\frac{436.6(g/l)}{36.5g/mol} = 11.96(mol/l) = 11.96M \simeq 12M. \tag{A.2}$$

The final concentration of HCl should be 2N, *i.e.* the concentration of H^+ ions is 2M. To make 500 ml 2N HCl, add $500 \times \frac{1}{6}$ =83.3 ml 12M HCl to $500 \times \frac{5}{6}$ =416.7 ml distilled H_2O. Always add acid to water when diluting acid.

Anti-BrdU

PharMingen, Cat. # 555627. Centrifuge stock anti-BrdU for 5 seconds at 10,000 rpm. The concentration of the stock anti-BrdU is 0.5 mg/ml. Before use, add 5 μl stock anti-BrdU to 495 μl of 1% BAS/PBS to make 500 μl diluted anti-BrdU antibody.

1% BSA/PBS

Add 0.1 g Bovine Serum Albumin (*BSA*) to 10 ml PBS. Vortex until the BSA has dissolved. Store at -20°C in a freezer.

Secondary Antibody, Anti-Mouse

Anti-mouse IgG (H+L), HRP conjugate, Promega, Cat. #W4021. The concentration of stock anti-mouse is 1 mg/ml. To make 500 μl diluted anti-mouse secondary-antibody solution, add 1 μl stock anti-mouse antibody to 500 μl of 1% BSA/PBS solution.

DAB/Tris

Store the DAB tablets at $-20°$C. Dissolve 1 DAB tablet in 15 ml of 0.1 M Tris buffer (pH 7.4) and vortex hard to dissolve the tablet. Filter with a 0.2 millipore filter before use.

DAB/Tris+H_2O_2

Add 1 μl of 30% H_2O_2 for every 1 ml of DAB/Tris.

Tris/Glycerine

Combine 20% Tris/HCl (pH8.0) with 80% Glycerine.

A.2.2 Procedures

Process at room temperature unless specified otherwise. We used a collection of chick embryos before HH stage 4.

1. Expose embryos to 10 μM BrdU by applying 100 μl 10 μM BrdU to the top of the blastoderm. Then incubate embryos at 37°C for 2 to 4 hours.
2. Fix embryos with 4% Paraformaldehyde at 4°C overnight.
3. Wash and keep fixed embryo in TBST for 30 minutes.
4. Place embryos in 2N HCl for 60 minutes (to denature the chromosomes).
5. Wash embryos with TBST two or three times, leaving embryos on a shaker for 1 hour each time.
6. Incubate embryos in diluted primary antibody (anti-BrdU) for 24 hours at 4°C.
7. Wash embryos with TBST two or three times, leaving embryos on a shaker for 1 hour each time.
8. Incubate embryos in diluted secondary antibody (anti-mouse, 2 μM) for 15 to 24 hours at 4°C.
9. Wash embryos with TBST two or three times, leaving embryos on a shaker for 1 hour each time.
10. Wash embryos with PBS, leaving embryos on a shaker for 20 minutes.
11. Incubate with DAB/Tris for 30 minutes at room temperature in a dark environment (a drawer).
12. Replace DAB/Tris with new DAB/Tris+H_2O_2 and hold for 5 minutes.
13. Wash with PBS+NaN_3 (Sodium Azide), or PBS, to stop the color reaction.

14. Wash with TBST three times. Keep in TBST overnight at room temperature.

15. Mount embryos on slides with glass covers. Use Tris/glycerine to keep the embryos moist. Store at 4°C, in a dark environment.

A.2.3 Special Notes

Wearing Gloves and Disposing of Solutions Containing DAB

Since DAB is highly carcinogenic, wearing gloves when working with DAB is essential. Inactivate waste DAB solution by pouring into a beaker containing 3% $KMnO_4$ and 2% Na_2CO_3 in distilled water. Dispose of inactivated DAB down sink.

Working with Paraformaldehyde

Paraformaldehyde is highly toxic. Work only in a safety hood when dissolving. Do not keep stock Paraformaldehyde solution in a refrigerator used for live samples or chemicals used with live samples since Paraformaldehyde can contaminate them.

A.3 Protocol for Micromass Chick Limb Cell-Cultures

A.3.1 Materials and Instruments

Fertile Chicken Eggs: We obtained fertile white Leghorn chicken eggs from Avian Services, Inc. (Frenchtown, NJ).

Extra-Deep Dishes: Fisherbrand extra-deep stackable 100 x 20 mm dishes, Fisher Cat. # 08-757-11Z.

Fine-Tip Forceps: Dumont #5 inox forceps, Fine Science Tools, Inc.

15 ml Centrifuge Tubes: Fisher Cat. # 14-959-49B, or Falcon 352097.

Nylon Filters: Nytex 20-μm mono-filament nylon mesh, 13mm in diameter. TETKO, 333 South Highland Ave, Briarcliff Manor, Tel: 914-941-7767, or 1-800-995-0531.

Gaskets: Millipore swinnex 13. Millipore Cat. # SX0001300.

3 ml Syringes: BD No. 309585, Fisher Cat. # 14-823-40.

18 G Needles: BD No. 305196, Fisher Cat. # 14-826-5D.

Corning 24-Well Cell-Culture Plates: Corning No. 3526, Fisher Cat. # 09-761-146.

Corning 60 mm Cell-Culture Dishes: Corning No. 430166, Fisher Cat. # 08-772-21.

A.3.2 Media

EBSS with Ca^{2+} and Mg^{2+} (1 liter)

Combine 1 pack of Modified Earle's Balanced Salts (Sigma E6132) and 2.20 g Sodium Bicarbonate ($NaHCO_3$). Dilute to 1 liter with distilled H_2O.

EBSS without Ca^{2+} and Mg^{2+}

Gibco BRL Cat. # 14155-063.

EDTA

Fisher Cat. # BP120-500, 0.5M, pH 8. Use directly.

Trypsin

Gibco BRL Cat. # 15400-054. Use directly.

DMEM (1 liter)

Combine 1 pack of Dulbeccos Modified Eagles Medium (Gibco BRL Cat. # 12100-046, or 11971-025) and 3.70 g Sodium Bicarbonate ($NaHCO_3$). Dilute to 1 liter with distilled H_2O.

F-12 (Ham) with L-Glutamine and Sodium Bicarbonate (1 liter)

Combine 1 pack of F-12 (Gibco BRL Cat. # 21700-075) and 1.18 g Sodium Bicarbonate ($NaHCO_3$). Dilute to 1 liter with distilled H_2O.

DM (1 liter)

Combine the following solutions to make 1 liter of DM:

F-12	600 ml,
DMEM	400 ml,
10X Transferrin	500 μl,
10X Ascorbic Acid	500 μl,
10X Insulin	500 μl,
1X Hydrocortisone	100 μl,
Penicillin-Streptomycin	10 ml.

Fetal Bovine Serum (*FBS*)

HyClone Cat. # SH30071.01. Use directly.

DMS (100 ml)

Combine 90 ml DM with 10 ml FBS (HyClone Cat. # SH30071.01) to make 100 ml DMS.

Transferrin 10 mg/ml in DM (10X)

Dissolve 200.0 mg Transferrin (Sigma C0880, or C7786) in 20 ml DM (60 ml F-12 + 40 ml DMEM).

Ascorbic Acid (Vitamin C) 100 mg/ml (10X)

Dissolve 2.0 g Ascorbic Acid (Sigma A4403) in 20 ml DM.

Insulin 10 mg/ml (10X)

Dissolve 10 mg/ml Insulin (Sigma I1882) in 0.01N HCl (5 μl 12N HCl in 6 ml distilled H_2O).

Hydrocortisone (1X)

Dissolve Hydrocortisone (Sigma H0135) in distilled H_2O to 1 mM.

Penicillin-Streptomycin

Invitrogen 15140-148. Use directly.

A.3.3 Procedures

Collect Limb Tips

1. Incubate 5 dozen fertile chicken eggs for 5 days. Spray 70% ethanol on eggs.

2. Open the eggs and remove the embryos into an extra-deep dish containing EBSS with $Ca^{2+}$and Mg^{2+}.

3. Remove the outer membranes around the embryos and transfer them to a new extra-deep dish containing EBSS with Ca^{2+} and Mg^{2+}.

4. Use fine-tip forceps to cut off the limb tips, 0.3 mm from the distal end and put them into a new dish containing EBSS with $Ca^{2+}$and Mg^{2+}.

5. Collect tips and put them into a 15 ml centrifuge tube.

Removal of Ectoderm with EDTA Treatment

1. Centrifuge at 1500 x G for about 2 minutes to pellet.
2. Use a pipette to remove EBSS with $Ca^{2+}$and Mg^{2+}.
3. Add 5 ml of EBSS without Ca^{2+}or Mg^{2+} and 100 μl EDTA solution. Use a pipette to generate gentle flows inside the medium to dissociate the pellet.
4. Incubate for 20 minutes at 37°C (5% CO_2). Do not close the lid of the 15 ml centrifuge tube too tight.
5. Centrifuge at 1500 x G for about 2 minutes to pellet.
6. Use a pipette to remove the medium.
7. Add 5 ml of fresh EBSS without Ca^{2+}or $Mg^{2+}$and 100 μl of Fetal Bovine Serum (FBS) to stop the EDTA reaction.
8. Gently pipette up and down six to ten times to remove ectoderm. Be careful to avoid introducing air bubbles into the solution.
9. Transfer tips to a clean dish. Use a microscope to check that cells from the ectoderm are absent.
10. Pick out large pieces of mesenchyme with forceps to use in the following steps.

Preparation of Mesenchyme Cells for Incubation

1. Add 4.5 ml EBSS without Ca^{2+} or Mg^{2+} and 500 μl Trypsin.

2. Incubate 15-20 minutes at 37°C (5% CO_2). Loosen the lid of the 15 ml centrifuge tube a little bit. Warm about 5 ml DMS to 37 °C for later use. Set up a filter unit by putting a clean nylon filter into the gasket.

3. After trypsinizing the limb-bud tips, close the tube tightly. Centrifuge at 1500 x G for 5 mins to pellet.

4. Use a pipette to remove the medium in the 15 ml centrifuge tube.

5. Add 2.5 ml fresh, pre-warmed DMS to the 15 ml centrifuge tube containing the pellet.

6. Put a 18 G needle on a 3 ml syringe and pipette in the tube up and down twenty times to dissociate the cells. Be careful to avoid introducing air bubble into the solution.

7. Suck cells into the syringe.

8. Remove the 18 G needle, replace it with the filter unit and gently push the solution through the filter unit into a clean 15 ml centrifuge tube.

9. Take 10 μl of the cell suspension for cell counting.

10. Place the 15 ml tube in a centrifuge and centrifuge at 1500 x G for 15 minutes to pellet.

11. Remove as much DMS from the 15 ml tube as possible. We will assume that 20 μl of medium remains. Dilute with DMS to the desired cell density, typically 1.6-2.0$\times 10^5$ cells/10μl. The amount of DMS (in μl) to be added is:

$$V = \frac{x * y}{z} - 20, \tag{A.3}$$

where x is the number of cells in 0.1mm^3 (one bigger chamber) in a bright-line Hemocytometer, y is the volume of the cell suspension in ml and z is the target cell concentration ($\times 10^5$).

12. Use a micropipette to pipette up and down five to ten times. Be careful not to introduce air bubbles into the solution.

13. Put 10 μl of cell suspension into each well of a Corning 24-well cell-culture plate, or into a Corning 60 mm cell-culture dish, and culture in an incubator at 37°C with 5% CO_2.

14. Warm enough DMS at 37 °C to flood the cell-culture wells.

15. After 30-40 minutes, flood each well with 0.5 ml or 1 ml of fresh, pre-warmed DMS to remove unattached cells.

16. Change the DMS medium each day (if flooded with 0.5 ml DMS) or every other day (if flooded with 1 ml DMS). Normally the cells will live for up to 7 days.

A.3.4 Special Notes

Protocol for F-12 and DMEM Media

Add (F-12 or DMEM) powder and other necessary chemicals to a beaker with a stir bar inside. Add 800 ml distilled water and stir for 5 minutes or until chemicals fully dissolve. Add more distilled water to 1000 ml and stir for 1 minute. In a sterile hood, filter the medium through a bottle-top filter kit (Millipore Steritop Sterile Vacuum Bottle-Top Filters, PVDF, 0.22 μm pore

size, with 500 ml or 1000 ml funnel) into an autoclaved bottle. Note: the thread size of the bottle-top filter kit may differ (33 or 45mm) depending on the bottle used.

Protocol for Cleaning Nylon Filters and Filter Holders (Gaskets)

The nylon filters and filter holders are reusable after each experiment. To clean a nylon filter, rinse with deionized water or distilled water, put in ethanol (70%) for 4-6 hours and expose to UV light overnight. To clean a filter holder, rinse with deionized water and expose to UV light overnight.

Bibliography

[1] Aristotle. The history of animals, book VI, part one of nine. Written in 350 B.C.

[2] Y. Azar and H. Eyal-Giladi. Interaction of epiblast and hypoblast in the formation of the primitive streak and the embryonic axis in chick, as revealed by hypoblast-rotation experiments. *J. Embryol. Exp. Morphol.*, 61: 133–144, 1981.

[3] R. K. Baker, A. K. Vanderboom, G. W. Bell, and P. B. Antin. Expression of the receptor tyrosine kinase gene EphB3 during early stages of chick embryo development. *Mech. Dev.*, 104: 129–132, 2001.

[4] R. K. Baker and P. B. Antin. Ephs and ephrins during early stages of chick embryogenesis. *Dev. Dyn.*, 228: 128–142, 2003.

[5] B. I. Balinsky. *An Introduction to embryology, Fourth Edition.* W. B. Saunders Company, Philadelphia, 1975.

[6] R. Bellairs. Studies on the development of the foregut in the chick blastoderm. 1. The presumptive foregut area. *J. Embryol. Exp. Morphol.*, 1: 115–124, 1953.

[7] P. Berge. Raleigh Bénard convection as an introduction to the physics of hydrodynamic instabilities: Experimental aspects. In *Von Karman Inst. for Fluid Dyn. Nat. and Free Convection: Theory and Expt*, Commissariat a l'Energie Atomique, Saclay (France), 1982.

[8] C. Bertet, L. Sulak, and T. Lecuit. Myosin-dependent junction remodelling controls planar cell intercalation and axis elongation. *Nature*, 429: 667–671, 2004.

[9] F. Bertocchini and C. D. Stern. The hypoblast of the chick embryo positions the primitive streak by antagonizing nodal signaling. *Dev. Cell*, 3: 735–744, 2002.

[10] F. Bertocchini, I. Skromne, L. Wolpert, and C. D. Stern. Determination of embryonic polarity in a regulative system: evidence for endogenous inhibitors acting sequentially during primitive streak formation in the chick embryo. *Development*, 131: 3381–3390, 2004.

[11] D. A. Brown and H. C. Berg. Temporal stimulation of chemotaxis in *Escherichia coli*. *Proc. Natl. Acad. Sci. USA*, 71: 1388–1392, 1974.

[12] M. Callebaut, F. Harrisson, and H. Bortier. Effect of gravity on the interaction between the avian germ and neighbouring ooplasm in inverted egg yolk balls. *Eur. J. Morphol.*, 39: 27–38, 2001.

[13] S. C. Chapman, J. Collignon, G. C. Schoenwolf, and A. Lumsden. Improved method for chick whole-embryo culture using a filter paper carrier. *Dev. Dyn.*, 220: 284–289, 2001.

[14] S. C. Chapman, F. R. Schubert, G. C. Schoenwolf, and A. Lumsden. Analysis of spatial and temporal gene expression patterns in blastula and gastrula stage chick embryos. *Dev. Biol.*, 245: 187–199, 2002.

[15] C. M. Chuong. The making of a feather: homeoproteins, retinoids and adhesion molecules. *Bioessays*, 15: 513–521, 1993.

[16] M. L. Concha and R. J. Adams. Oriented cell divisions and cellular morphogenesis in the zebrafish gastrula and neurula: a time-lapse analysis. *Development*, 125: 983–994, 1998.

[17] H. Cremer, R. Lange, A. Christoph, M. Plomann, G. Vopper, J. Roes, R. Brown, S. Baldwin, P. Kraemer, and S. Scheff. Inactivation of the N-CAM gene in mice results in size reduction of the olfactory bulb and deficits in spatial learning. *Nature*, 367: 455–459, 1994.

[18] A. Czirok, B. J. Rongish, and C. D. Little. Extracellular matrix dynamics during vertebrate axis formation. *Dev. Biol.*, 268: 111–122, 2004.

[19] C. Cui, X. Yang, M. Chuai, J. A. Glazier, and C. J. Weijer. Analysis of tissue flow patterns during primitive streak formation in the chick embryo. *Dev. Biol.*, In press.

[20] C. Cui, J. A. Glazier, T. Glimm, and S. A. Newman. Precartilage mesenchymal condensation involves undirected migration and trapping of cells with increase, rather than decrease, in their rate of movement. Submitted to *Developmental Dynamics*.

[21] C. Cui, M. Filla, B. J. Rongish, R. Lansford, and C. D. Little. Labeling specific cells using *in vivo* electroporation of avian embryos. In preparation.

[22] L. A. D'Amico and M. S. Cooper. Morphogenetic domains in the yolk syncytial layer of axiating zebrafish embryos. *Dev. Dyn.*, 222: 611–624, 2001.

[23] A. M. DeLise and R. S. Tuan. Electroporation-mediated DNA transfection of embryonic chick limb mesenchymal cells. *Methods Mol. Biol.*, 137: 377–382, 2000.

[24] P. A. DiMilla, J. A. Stone, J. A. Quinn, S. M. Albelda, and D. A. Lauffenburger. Maximal migration of human smooth muscle cells on fibronectin and type IV collagen occurs at an intermediate attachment strength. *J. Cell Biol.*, 122: 729–737, 1993.

[25] N. M. Le Douarin and M. A. Teillet. The migration of neural crest cells to the wall of the digestive tract in avian embryo. *J. Embryol. Exp. Morphol.*, 30: 31–48, 1973.

[26] N. M. Le Douarin. The ontogeny of the neural crest in avian embryo chimaeras. *Nature*, 286: 663–669, 1980.

[27] S. A. Downie and S. A. Newman. Morphogenetic differences between fore- and hind-limb precartilage mesenchyme: relation to mechanisms of skeletal pattern formation. *Dev. Biol.*, 162: 195–208, 1994.

[28] D. Duboule. Making progress with limb models. *Nature*, 418: 492–493, 2002.

[29] A. T. Dudley, M. A. Ros, and C. J. Tabin. A re-examination of proximodistal patterning during vertebrate limb development. *Nature*, 418: 539–544, 2002.

[30] D. A. Ede, O. P. Flint, O. K. Wilby, and P. Colquhoun. *Vertebrate limb and somite morphogenesis, British Society for Developmental Biology, Symposium 3*, chapter, The development of pre-cartilage condensations in limb bud mesenchyme *in vivo* and *in vitro*. Pages 161–179. Cambridge University Press, Cambridge, 1977.

[31] H. Eyal-Giladi and S. Kochav. From cleavage to primitive streak formation: a complementary normal table and a new look at the first stages of the development of the chick. I. General morphology. *Dev. Biol.*, 49: 321–337, 1976.

[32] H. Eyal-Giladi, A. Debby, and N. Harel. The posterior section of the chick's *area pellucida* and its involvement in hypoblast and primitive streak formation. *Development*, 116: 819–830, 1992.

[33] R. Farooqui and G. Fenteany. Multiple rows of cells behind an epithelial wound edge extend cryptic lamellipodia to collectively drive cell-sheet movement. *J. Cell Sci.*, 118: 51–63, 2005.

[34] I. Flamme. Prolonged and simplified *in vitro* culture of explanted chick embryos. *Anat. Embryol.* (*Berl.*), 176: 45–52, 1987.

[35] I. Flamme, K. Albach, S. Muller, B. Christ, and H. J. Jacob. Two-phase *in vitro* culture of explanted chick embryos. *Anat. Rec.*, 229: 427–433, 1991.

[36] A. C. Foley and C. D. Stern. Evolution of vertebrate forebrain development: how many different mechanisms? *J. Anat.*, 199: 35–52, 2001.

[37] G. Forgacs, R. A. Foty, Y. Shafrir, and M. S. Steinberg. Viscoelastic properties of living embryonic tissues: a quantitative study. *Biophys. J.*, 74: 2227–2234, 1998.

[38] D. A. Frenz, S. K. Akiyama, D. F. Paulsen, and S. A. Newman. Latex beads as probes of cell surface-extracellular matrix interactions during chondrogenesis: evidence for a role for amino-terminal heparin-binding domain of fibronectin. *Dev. Biol.*, 136: 87–96, 1989.

[39] D. A. Frenz, N. S. Jaikaria, and S. A. Newman. The mechanism of precartilage mesenchymal condensation: a major role for interaction of the cell surface with the amino-terminal heparin-binding domain of fibronectin. *Dev. Biol.*, 136: 97–103, 1989.

[40] A. L. Gehris, S. A. Oberlender, K. J. Shepley, R. S. Tuan, and V. D. Bennett. Fibronectin mRNA alternative splicing is temporally and spatially regulated during chondrogenesis *in vivo* and *in vitro*. *Dev. Dyn.*, 206: 219–230, 1996.

[41] S. F. Gilbert. *Developmental Biology*. Sinauer Associates, Inc., Sunderland, Massachusetts, 1997.

[42] N. S. Glickman, C. B. Kimmel, M. A. Jones, and R. J. Adams. Shaping the zebrafish notochord. *Development*, 130: 873–887, 2003.

[43] Y. Gong, C. Mo, and S. E. Fraser. Planar cell polarity signalling controls cell division orientation during zebrafish gastrulation. *Nature*, 430: 689–693, 2004.

[44] S. E. Gould, W. B. Upholt, and R. A. Kosher. Syndecan 3: a member of the syndecan family of membrane-intercalated proteoglycans that is expressed in high amounts at the onset of chicken limb cartilage differentiation. *Proc. Natl. Acad. Sci. USA*, 89: 3271–3275, 1992.

[45] L. Gräper. Die primitiventwicklung des hühnchens nach stereokinematischen untersuchungen, kontrolliert durch vitale farbmarkierung und verglichen mit der entwicklung anderer wirbeltiere. *Wilhelm Roux Arch. Entwmech. Org.*, 116: 382–429, 1929.

[46] B. K. Hall and T. Miyake. Divide, accumulate, differentiate: cell condensation in skeletal development revisited. *Int. J. Dev. Biol.*, 39: 881–893, 1995.

[47] B. K. Hall and T. Miyake. All for one and one for all: condensations and the initiation of skeletal development. *Bioessays*, 22: 138–147, 2000.

[48] V. Hamburger. Morphogenetic and axial self-differentiation of transplanted limb primordia of 2-day chick embryos. *J. Exp. Zool.*, 77: 379–400, 1938.

[49] V. Hamburger and H. L. Hamilton. A series of normal stages in the development of the chick embryo. *J. Morphol.*, 88: 49–92, 1951.

[50] Y. Hatada and C. D. Stern. A fate map of the epiblast of the early chick embryo. *Development*, 120: 2879–2889, 1994.

[51] E. D. Hay. The mesenchymal cell, its role in the embryo, and the remarkable signaling mechanisms that create it. *Dev. Dyn.*, 233: 706–720, 2005.

[52] L. W. Hillier, *et al.* Sequence and comparative analysis of the chicken genome provide unique perspectives on vertebrate evolution. *Nature*, 432: 695–716, 2004.

[53] C. R. Hume and J. Dodd. Cwnt-8c: a novel wnt gene with a potential role in primitive streak formation and hindbrain organization. *Development*, 119: 1147–1160, 1993.

[54] J. E. Hungerford, G. K. Owens, W. S. Argraves, and C. D. Little. Development of the aortic vessel wall as defined by vascular smooth muscle and extracellular matrix markers. *Dev. Biol.*, 178: 375–392, 1996.

[55] H. Karabagli, P. Karabagli, R. K. Ladher, and G. C. Schoenwolf. Comparison of the expression patterns of several fibroblast growth factors during chick gastrulation and neurulation. *Anat. Embryol.* (*Berl.*), 205: 365–370, 2002.

[56] R. Keller and P. Tibbetts. Mediolateral cell intercalation in the dorsal, axial mesoderm of *Xenopus laevis*. *Dev. Biol.*, 131: 539–549, 1989.

[57] R. Keller, L. Davidson, A. Edlund, T. Elul, M. Ezin, D. Shook, and P. Skoglund. Mechanisms of convergence and extension by cell intercalation. *Philos. Trans. Roy. Soc. London, B. Biol. Sci.*, 355: 897–922, 2000.

[58] R. Keller, L. A. Davidson, and D. R. Shook. How we are shaped: the biomechanics of gastrulation. *Differentiation*, 71: 171–205, 2003.

[59] K. Kim, Z. Lu, and E. D. Hay. Direct evidence for a role of beta-catenin/LEF-1 signaling pathway in induction of EMT. *Cell Biol. Int.*, 26: 463–476, 2002.

[60] Y. Kimura, H. Matsunami, T. Inoue, K. Shimamura, N. Uchida, T. Ueno, T. Miyazaki, and M. Takeichi. Cadherin-11 expressed in association with mesenchymal morphogenesis in the head, somite, and limb bud of early mouse embryos. *Dev. Biol.*, 169: 347–358, 1995.

[61] M. A. Kiskowski, M. S. Alber, G. L. Thomas, J. A. Glazier, N. B. Bronstein, J. Pu, and S. A. Newman. Interplay between activator-inhibitor coupling and cell-matrix adhesion in a cellular automaton model for chondrogenic patterning. *Dev. Biol.*, 271: 372–387, 2004.

[62] V. Knezevic and S. Mackem. Activation of epiblast gene expression by the hypoblast layer in the prestreak chick embryo. *Genesis*, 30: 264–273, 2001.

[63] S. Kochav and H. Eyal-Giladi. Bilateral symmetry in chick embryo determination by gravity. *Science*, 171: 1207–1029, 1971.

[64] R. A. Kosher, K. H. Walker, and P. W. Ledger. Temporal and spatial distribution of fibronectin during development of the embryonic chick limb bud. *Cell Differ.*, 11: 217–228, 1982.

[65] C. E. Krull. A primer on using *in ovo* electroporation to analyze gene function. *Dev. Dyn.*, 229: 433–439, 2004.

[66] P. Kucera and M. B. Burnand. Routine teratogenicity test that uses chick embryos *in vitro*. *Teratog. Carcinog. Mutagen.*, 7: 427–447, 1987.

[67] P. M. Kulesa and S. E. Fraser. Cell dynamics during somite boundary formation revealed by time-lapse analysis. *Science*, 298: 991–995, 2002.

[68] A. Lawson and G. C. Schoenwolf. Cell populations and morphogenetic movements underlying formation of the avian primitive streak and organizer. *Genesis*, 29: 188–195, 2001.

[69] M. Levin, R. L. Johnson, C. D. Stern, M. Kuehn, and C. Tabin. A molecular pathway determining left-right asymmetry in chick embryogenesis. *Cell*, 82: 803–814, 1995.

[70] A. López-Martínez, D. T. Chang, C. Chiang, J. A. Porter, M. A. Ros, B. K. Simandl, P. A. Beachy, and J. F. Fallon. Limb-patterning activity and restricted posterior localization of the amino-terminal product of Sonic hedgehog cleavage. *Curr. Biol.*, 5: 791–796, 1995.

[71] Y. Luo, I. Kostetskii, and G. L. Radice. N-cadherin is not essential for limb mesenchymal chondrogenesis. *Dev. Dyn.*, 232: 336–344, 2005.

[72] E. J. Mackie, I. Thesleff, and R. Chiquet-Ehrismann. Tenascin is associated with chondrogenic and osteogenic differentiation *in vivo* and promotes chondrogenesis *in vitro*. *J. Cell Biol.*, 105: 2569–2579, 1987.

[73] G. Maheshwari, A. Wells, L. G. Griffith, and D. A. Lauffenburger. Biophysical integration of effects of epidermal growth factor and fibronectin on fibroblast migration. *Biophys. J.*, 76: 2814–2823, 1999.

[74] F. Marlow, J. Topczewski, D. Sepich, and L. Solnica-Krezel. Zebrafish rho kinase 2 acts downstream of wnt11 to mediate cell polarity and effective convergence and extension movements. *Curr. Biol.*, 12: 876–884, 2002.

[75] W. M. Michael and J. Newport. Coupling of mitosis to the completion of S phase through Cdc34-mediated degradation of Wee1. *Science*, 282: 1886–1889, 1998.

[76] E. Mitrani, T. Ziv, G. Thomsen, Y. Shimoni, D. A. Melton, and A. Bril. Activin can induce the formation of axial structures and is expressed in the hypoblast of the chick. *Cell*, 63: 495–501, 1990.

[77] M. Z. Moftah, S. A. Downie, N. B. Bronstein, N. Mezentseva, J. Pu, P. A. Maher, and S. A. Newman. Ectodermal FGFs induce perinodular inhibition of limb chondrogenesis *in vitro* and *in vivo* via FGF receptor 2. *Dev. Biol.*, 249: 270–282, 2002.

[78] D. A. T. New. A new technique for the cultivation of the chick embryo *in vitro*. *J. Embryol. Exp. Morphol.*, 3: 320–331, 1955.

[79] S. A. Newman, H. L. Frisch. Dynamics of skeletal pattern formation in developing chick limb. *Science*, 205: 662-668, 1979.

[80] S. A. Newman, M. P. Pautou, and M. Kieny. The distal boundary of myogenic primordia in chimeric avian limb buds and its relation to an accessible population of cartilage progenitor cells. *Dev. Biol.*, 84: 440–448, 1981.

[81] S. A. Newman and J. J. Tomasek. *Extracellular Matrix Molecular Components and Interactions, volume 2*, chapter, Morphogenesis of connective tissues. Pages 335–369. Harwood Academic Publishers, Amsterdam, 1996.

[82] S. A. Oberlender and R. S. Tuan. Expression and functional involvement of N-cadherin in embryonic limb chondrogenesis. *Development*, 120: 177–187, 1994.

[83] B. Pain, P. Chenevier, and J. Samarut. Chicken embryonic stem cells and transgenic strategies. *Cells Tissues Organs*, 165: 212–219, 1999.

[84] K. J. Painter, P. K. Maini, and H. G. Othmer. A chemotactic model for the advance and retreat of the primitive streak in avian development. *Bull. Math. Biol.*, 62: 501–525, 2000.

[85] I. Palmeirim, D. Henrique, D. Ish-Horowicz, and O. Pourquié. Avian hairy gene expression identifies a molecular clock linked to vertebrate segmentation and somitogenesis. *Cell*, 91: 639–648, 1997.

[86] D. F. Paulsen and M. Solursh. Microtiter micromass cultures of limb-bud mesenchymal cells. *In Vitro Cell Dev. Biol.*, 24: 138–147, 1988.

[87] L. A. Pennacchio. Insights from human/mouse genome comparisons. *Mamm. Genome*, 14: 429–436, 2003.

[88] R. D. Riddle, R. L. Johnson, E. Laufer, and C. Tabin. Sonic hedgehog mediates the polarizing activity of the ZPA. *Cell*, 75: 1404–1416, 1993.

[89] J. Rietdorf, F. Siegert, and C. J. Weijer. Analysis of optical density wave propagation and cell movement during mound formation in *Dictyostelium discoideum*. *Dev. Biol.*, 177: 427–438, 1996.

[90] Y. Saga, T. Yagi, Y. Ikawa, T. Sakakura, and S. Aizawa. Mice develop normally without tenascin. *Genes Dev.*, 6: 1821–1831, 1992.

[91] E. J. Sanders, M. Varedi, and A. S. French. Cell proliferation in the gastrulating chick embryo: a study using BrdU incorporation and PCNA localization. *Development*, 118: 389–399, 1993.

[92] J. J. Sanz-Ezquerro and C. Tickle. Fgf signaling controls the number of phalanges and tip formation in developing digits. *Curr. Biol.*, 13: 1830–1836, 2003

[93] J. W. J. Saunders. The proximo-distal sequence of origin of parts of the chick wing and the role of the ectoderm. *J. Exp. Zool.*, 108: 363–404, 1948.

[94] J. W. J. Saunders and M. T. Gasseling. *Epithelial-Mesenchymal Interactions*, chapter, Ectodermal-mesenchymal interactions in the origin of limb symmetry, Pages 78–97. Williams & Wilkins, Baltimore, 1968.

[95] J. W. J. Saunders. *Methods in Avian Embryology*, volume 51, chapter, Operations on limb buds of avian embryos. Pages 125–144. Academic Press, New York, 1996.

[96] E. A. Seleiro, D. J. Connolly, and J. Cooke. Early developmental expression and experimental axis determination by the chicken Vg1 gene. *Curr. Biol.*, 6: 1476–1486, 1996.

[97] S. B. Shah, I. Skromne, C. R. Hume, D. S. Kessler, K. J. Lee, C. D. Stern, and J. Dodd. Misexpression of chick Vg1 in the marginal zone induces primitive streak formation. *Development*, 124: 5127–5138, 1997.

[98] F. Siegert, C. J. Weijer, A. Nomura, and H. Miike. A gradient method for the quantitative analysis of cell movement and tissue flow and its application to the analysis of multicellular *Dictyostelium* development. *J. Cell Sci.*, 107: 97–104, 1994.

[99] I. Skromne and C. D. Stern. Interactions between Wnt and Vg1 signalling pathways initiate primitive streak formation in the chick embryo. *Development*, 128: 2915-2927, 2001.

[100] J. T. Smith, J. K. Tomfohr, M. C. Wells, T. P. Beebe, T. B. Kepler, and W. M. Reichert. Measurement of cell migration on surface-bound fibronectin gradients. *Langmuir*, 20: 8279–8286, 2004.

[101] N. T. Spratt and H. Haas. Integrative mechanisms in development of the early chick blastoderm. I. Regulative potentiality of separated parts. *J. Exp. Zool.*, 145: 97–137, 1960.

[102] M. S. Steinberg. Reconstruction of tissues by dissociated cells. Some morphogenetic tissue movements and the sorting out of embryonic cells may have a common explanation. *Science*, 141: 401–408, 1963.

[103] M. S. Steinberg. Cell-cell recognition in multicellular assembly: levels of specificity. *Symp. Soc. Exp. Biol.*, 32: 25–49, 1978.

[104] C. D. Stern and D. R. Canning. Gastrulation in birds: a model system for the study of animal morphogenesis. *Experientia*, 44: 651–657, 1988.

[105] C. D. Stern and D. R. Canning. Origin of cells giving rise to mesoderm and endoderm in chick embryo. *Nature*, 343: 273–275, 1990.

[106] C. D. Stern. Mesoderm induction and development of the embryonic axis in amniotes. *Trends Genet.*, 8: 158–163, 1992.

[107] C. D. Stern. Avian embryo. In C. D. Stern and P. W. H. Holland, editors, *Essential Developmental Biology: A Practical Approach*, Pages 45–54. IRL Press at Oxford University Press, Oxford, 1993.

[108] C. D. Stern. The chick embryo–past, present and future as a model system in developmental biology. *Mech. Dev.*, 121: 1011-1013, 2004.

[109] C. D. Stern. The chick; a great model system becomes even greater. *Dev. Cell*, 8: 9–17, 2005.

[110] A. Streit, K. J. Lee, I. Woo, C. Roberts, T. M. Jessell, and C. D. Stern. Chordin regulates primitive streak development and the stability of induced neural cells, but is not sufficient for neural induction in the chick embryo. *Development*, 125: 507–519, 1998.

[111] X. Sun, F. V. Mariani, and G. R. Martin. Function of FGF signalling from the apical ectodermal ridge in limb development. *Nature*, 418: 501-508, 2002.

[112] C. Tickle. The number of polarizing region cells required to specify additional digits in the developing chick wing. *Nature*, 289: 295–298, 1981.

[113] J. J. Tomasek, J. E. Mazurkiewicz, and S. A. Newman. Nonuniform distribution of fibronectin during avian limb development. *Dev. Biol.*, 90: 118–26, 1982.

[114] A. M. Turing. The Chemical Basis of Morphogenesis. *Phil. Trans. Roy. Soc. London, B*, 237: 37–72. 1952.

[115] C. Viebahn, C. Stortz, S. A. Mitchell, and M. Blum. Low proliferative and high migratory activity in the area of brachyury expressing mesoderm progenitor cells in the gastrulating rabbit embryo. *Development*, 129: 2355–2365, 2002.

[116] J. B. Wallingford, S. E. Fraser, and R. M. Harland. Convergent extension: the molecular control of polarized cell movement during embryonic development. *Dev. Cell*, 2: 695–706, 2002.

[117] J. Walshe and I. Mason. Expression of FGFR1, FGFR2 and FGFR3 during early neural development in the chick embryo. *Mech. Dev.*, 90: 103–110, 2000.

[118] L. Wei, W. Roberts, L. Wang, M. Yamada, S. Zhang, Z. Zhao, S. A. Rivkees, R. J. Schwartz, and K. Imanaka-Yoshida. Rho kinases play an

obligatory role in vertebrate embryonic organogenesis. *Development*, 128: 2953–2962, 2001.

[119] Y. Wei and T. Mikawa. Formation of the avian primitive streak from spatially restricted blastoderm: evidence for polarized cell division in the elongating streak. *Development*, 127: 87–96, 2000.

[120] D. G. White, H. P. Hershey, J. J. Moss, H. Daniels, R. S. Tuan, and V. D. Bennett. Functional analysis of fibronectin isoforms in chondrogenesis: Full-length recombinant mesenchymal fibronectin reduces spreading and promotes condensation and chondrogenesis of limb mesenchymal cells. *Differentiation*, 71: 251–261, 2003.

[121] R. B. Widelitz, T. X. Jiang, B. A. Murray, and C. M. Chuong. Adhesion molecules in skeletogenesis: II. neural cell adhesion molecules mediate precartilaginous mesenchymal condensations and enhance chondrogenesis. *J. Cell Physiol.*, 156: 399–411, 1993.

[122] P. Wilson and R. Keller. Cell rearrangement during gastrulation of *Xenopus*: direct observation of cultured explants. *Development*, 112: 289–300, 1991.

[123] L. Wolpert. Positional information and the spatial pattern of cellular differentiation. *J. Theor. Biol.*, 25: 1–47, 1969.

[124] L. Wolpert, R. Beddington, J. Brockes, T. M. Jessell, P. Lawrence, and E. Meyerrowitz. *Principles of Development*. Oxford University Press, London, 1998.

[125] X. Yang, D. Dormann, A. E. Munsterberg, and C. J. Weijer. Cell movement patterns during gastrulation in the chick are controlled by positive and negative chemotaxis mediated by FGF4 and FGF8. *Dev. Cell*, 3: 425–437, 2002.

[126] J. A. Zallen and E. Wieschaus. Patterned gene expression directs bipolar planar polarity in drosophila. *Dev. Cell*, 6: 343–355, 2004.

[127] W. Zeng, G. L. Thomas, S. A. Newman, and J. A. Glazier. *Mathematical Modelling and Computing in Biology and Medicine, 5th ESMTB Conference 2002*, chapter, A novel mechanism for mesenchymal condensation during limb chondrogenesis *in vitro*. Pages 80–86, 2003.

[128] W. Zeng, G. L. Thomas, and J. A. Glazier. Non-Turing stripes and spots: a novel mechanism for biological cell clustering. *Physica A*, 341: 482–494, 2004.

Cheng Cui

CONTACT INFORMATION

Dept. of Anatomy and Cell Biology
WHW 1008
University of Kansas Medical Center
3901 Rainbow Blvd.
Kansas City, KS 66160 USA

Tel: (913) 588-1857
Fax: (913) 588-2710
Email: ccui@kumc.edu

CITIZENSHIP

China

RESEARCH INTERESTS

In-vivo electroporation,*in-vivo*/*in-vitro* cell tracking, image processing and analysis of cell movement, developmental mechanisms, chick development, modeling and simulation of development.

EDUCATION

Indiana University, Bloomington, Indiana, USA

Ph.D. Candidate, Major in Biophysics, Outside Minor in Molecular and Developmental Biology. (expected graduation date: July 2005).

- Dissertation Topic: "Dynamics of Cell And Tissue Motion in Gastrulation And Micromass Cell Culture".
- Advisor: Prof. James A. Glazier

University of Notre Dame, Notre Dame, Indiana, USA

M.S., Physics, May 2002.

Jilin University, Changchun, Jilin, China

B.A., Physics, May, 1997.

HONORS AND FELLOWSHIPS

BaoSteel Corp. National Undergraduate Student Fellowship, Jilin University, China, 1996.
Summer Grant Writing Fellowship, University of Notre Dame, U.S., 2002.

ACADEMIC EXPERIENCE

University of Notre Dame, Notre Dame, Indiana, USA

M.S. **August, 1998 - May, 2002**

Includes current Ph.D. research, Ph.D. and Masters level coursework and research projects.

University of Dundee, Dundee, Scotland, UK

Visiting Student **September, 2001 - March, 2002**

Visited Prof. Cornelis Weijer at the Wellcome Trust Biocenter. Worked on cell tracking in gastrulating chick embryo before HH stage 2.

Indiana University, Bloomington, Indiana, USA

Graduate Student **August, 2002 - Present**

Includes current Ph.D. research, Ph.D. level coursework in biophysics and molecular and developmental biology.

New York Medical College, Valhalla, New York, USA

Visiting Student **November, 2002 - March, 2003**

Visited Prof. Stuart A. Newman. Worked on cell tracking in condensing micromass

cell culture of mesenchymal cells from embryonic chick limb.

Kansas University Medical Center, Kansas City, Kansas, USA

Visiting Student **June, 2004**

Visited Prof. Charles D. Little. Worked on labelling mesenchymal cells from embryonic chick limb by using DiI and fluorescent quantum dots and cell tracking using advanced image acquisition facilities.

Kansas University Medical Center, Kansas City, Kansas, USA

Postdoctoral Fellow **January, 2005 - Present**

Working under the leadship of Prof. Charles D. Little and Prof. Brenda J. Rongish on studying cell and tissue movement during vasculogenesis.

Publications

C. Cui, X. Yang, M. Chuai, J. A. Glazier, C. J. Weijer. Analysis of tissue flow patterns during primitive streak formation in the chick embryo. *Dev. Biol.*, In Press, 2005.

C. Cui, J. A. Glazier, T. Glimm, S. A. Newman. Precartilage mesenchymal condensation involves undirected migration and trapping of cells with increase, rather than decrease, in their rate of movement. Submitted to *Dev. Dyn.*

C. Cui, S. A. Newman, T. Glimm, J. A. Glazier. Analysis of cell movement in two dimensional micromass cell mono-layer. In Preparation.

Conference Presentations

Oral Presentation – C. Cui, J. A. Glazier, C. J. Weijer. "Cell tracking in gastrulating chick embryo using fluorescent dye," at *Biocomplexity II: Structure and Function of the Cytoskeleton*. University of Notre Dame, South Bend, IN, November, 2001.

Poster – C. Cui, S. A. Newman, J. A. Glazier. "Whole-mount chick embryo culture from HH stage 15 to HH stage 23 and limb transplantation," at *Biocomplexity V, Multiscale Modeling in Biology*. University of Notre Dame, South Bend, IN, August, 2003.

Poster – C. Cui, S. A. Newman, J. A. Glazier. "Study of cell movement in micromass cell culture," at *44th Annual Midwest Regional Developmental Biology Meeting and Singer Symposium*. Kansas City, MO, June, 2004.

Experimental Skills

- Whole-mount chick embryo culture in Petri dish from HH stage 1 to 23.
- Chick-limb micromass cell culture method.
- Cell labeling with fluorescent dyes.
- *In-vivo* electroporation to label cells in avian embryo.
- BrdU incorporation.
- Micro-injection of fluorescent dye, DiI.
- Micro-manipulation of gastrulating chick embryos on separate germ layers and chick limb (AER removal).
- Spinning-disk confocal microscopy.

Computer Skills

- Monte Carlo simulations using the Cellular Potts Model.
- C++.
- Image processing and programming using Matlab.
- Parallel computation using MPI (Message Passing Interface).